FINAL REPORT

Underwater Advanced Time-Domain Electromagnetic System

ESTCP Project MR-201313

APRIL 2019

Steve Saville
CH2M HILL

ESTCP

Page Intentionally Left Blank

Page Intentionally Left Blank

REPORT DOCUMENTATION PAGE

Form Approved
OMB No. 0704-0188

1. REPORT DATE *(DD-MM-YYYY)*	2. REPORT TYPE	3. DATES COVERED *(From - To)*
04-26-2019	ESTCP Final Report	Oct 2013 – Apr 2019

4. TITLE AND SUBTITLE

Underwater Advanced Time-Domain Electromagnetic System

5a. CONTRACT NUMBER
W912HQ-13-C-0048

5c. PROGRAM ELEMENT NUMBER

6. AUTHOR(S)

Saville, Steve (Principal Investigator); Bancroft, Stuart; Bell, Thomas; Odlum, Nick; Steinhurst, Daniel

5d. PROJECT NUMBER
MR-201313

5e. TASK NUMBER

5f. WORK UNIT NUMBER

7. PERFORMING ORGANIZATION NAME(S) AND ADDRESS(ES)

CH2M HILL
2411 Dulles Corner Park
Suite 500
Herndon, VA 20171

8. PERFORMING ORGANIZATION REPORT NUMBER

MR-201313

9. SPONSORING / MONITORING AGENCY NAME(S) AND ADDRESS(ES)

Environmental Security Technology Certification Program
4800 Mark Center Drive, Suite 16F16
Alexandria, VA 22350-6565

10. SPONSOR/MONITOR'S ACRONYM(S)
ESTCP

11. SPONSOR/MONITOR'S REPORT NUMBER(S) MR-201313

12. DISTRIBUTION / AVAILABILITY STATEMENT

DISTRIBUTION A. Approved for public release: distribution unlimited.

13. SUPPLEMENTARY NOTES

14. ABSTRACT

From 2013 to 2018, CH2M HILL, Inc. (CH2M) performed Environmental Security Technology Certification Program (ESTCP) project MR-201313 to design, build, and demonstrate an underwater advanced time-domain electromagnetic (TEM) system for cued classification of munitions in the underwater environment.

The phased approach consists of initial design and modeling (Phase 1 –completed), engineering design and construction (Phase 2 – completed), underwater evaluation of the system in a freshwater pond (Phase 3 – completed), and demonstration of the system at a saltwater site (Phase 4 – addressed in this document).

15. SUBJECT TERMS

Advanced Geophysical Classification (AGC); Multi-Axis; Munitions Response (MR, MMRP); Time-Domain Electromagnetic Induction (EM, EMI, TDEM); Underwater Munitions

16. SECURITY CLASSIFICATION OF:			17. LIMITATION OF ABSTRACT	18. NUMBER OF PAGES	19a. NAME OF RESPONSIBLE PERSON
					Steve Saville
a. REPORT	b. ABSTRACT	c. THIS PAGE	UNCLASS	159	19b. TELEPHONE NUMBER *(include area code)*
UNCLASS	UNCLASS	UNCLASS			720-261-5367

Standard Form 298 (Rev. 8-98)
Prescribed by ANSI Std. Z39.18

Page Intentionally Left Blank

FINAL REPORT
Project: MR-201313

TABLE OF CONTENTS

Page

TABLE OF CONTENTS (Continued)

Page

TABLE OF CONTENTS (Continued)

Page

LIST OF FIGURES

Page

LIST OF FIGURES

Page

LIST OF TABLES

Page

ACRONYMS AND ABBREVIATIONS

ADCP	acoustic Doppler current profiler
CA	corrective action
CH2M	CH2M HILL, Inc.
CTD	conductivity, temperature, and depth
ESTCP	Environmental Security Technology Certification Program
FRF	Field Research Facility
FUDS	Formerly Used Defense Site
HDF	hierarchical data format
HE	high-explosive
HEAT	high-explosive anti-tank
IDL	Interactive Data Language
ISO	industry standard object
IVS	Instrument Verification Strip
LARC	Lighter, Amphibious Resupply, Cargo
MEC	Munitions and Explosives of Concern
MPPEH	Material Potentially Presenting an Explosive Hazard
NRL	Naval Research Laboratory
NSWCPCD	Naval Surface Warfare Center Panama City Division
RCA	root cause analysis
RMS	root-mean-squared
Rx	receiver
SFT	sensor function test
SNR	signal-to-noise ration
TEM	time-domain electromagnetic
Tx	transmitter
USACE	U.S. Army Corps of Engineers

Page Intentionally Left Blank

ACKNOWLEDGEMENTS

The project team for the Saltwater Demonstration at the U.S. Army Corps of Engineers Field Research Facility at Duck, N.C. included the following Key Personnel who each played an integral role.

Name	Affiliation	Responsibilities
Stuart Bancroft	CH2M	Project Coordination
Tom Bell	Leidos	Data Analyst and Reporting
Kelsey Dubois	Geometrics	Project Engineer
Glenn Harbaugh	Naval Research Laboratory	Project Coordination
Bart Hoekstra	Geometrics	Project Engineer
Jesse McNinch	USACE FRF	Site Lead
John Mogray	CH2M	Dive Lead
John Nichols	Geometrics	Project Engineer
Nick Odlum	Geometrics	Applications Geophysicist
Jason Pipes	USACE FRF	Site Coordinator
Steve Saville	CH2M	Principal Investigator
Ben Sheppard	CH2M	Dive Specialist
Dan Steinhurst	Naval Research Laboratory	Project Scientist

Page Intentionally Left Blank

1.0 INTRODUCTION

1.1 BACKGROUND

This document has been prepared under Environmental Security Technology Certification Program (ESTCP) Project MR-201313, titled "Underwater Advanced Time-Domain Electromagnetic System," to present the results of the saltwater demonstration, the second planned field evaluation of the system developed as part of this project. The Saltwater Demonstration took place May 14-17, 2018 at the U.S. Army Corps of Engineers (USACE) Field Research Facility (FRF) in Duck, N.C.

1.2 OBJECTIVE OF THE DEMONSTRATION

The overall objective of MR-201313 is to design, build, and demonstrate an underwater advanced time-domain electromagnetic (TEM) system for cued classification of munitions in the underwater environment. The phased approach consists of initial design and modeling (Phase 1 – completed), engineering design and construction (Phase 2 – completed), underwater evaluation of the system in a freshwater pond (Phase 3 – completed), and demonstration of the system at a saltwater site (Phase 4 – addressed in this document).

1.3 REGULATORY DRIVERS

Not applicable.

Page Intentionally Left Blank

2.0 TECHNOLOGY

2.1 TECHNOLOGY DESCRIPTION

The Underwater Advanced Time-Domain Electromagnetic System designed, constructed, and demonstrated at a freshwater facility under this project has been described in detail in prior documents, titled *Modeling for Underwater Advanced Time-Domain Electromagnetic System* (June 2014), *Underwater Advanced Time-Domain Electromagnetic System Design* (July 2015), and *System Performance Report* (March 2017). A diagram of the system, as tested in the freshwater pond, is provided as Figure 1. A photograph of the system is provided as Figure 2.

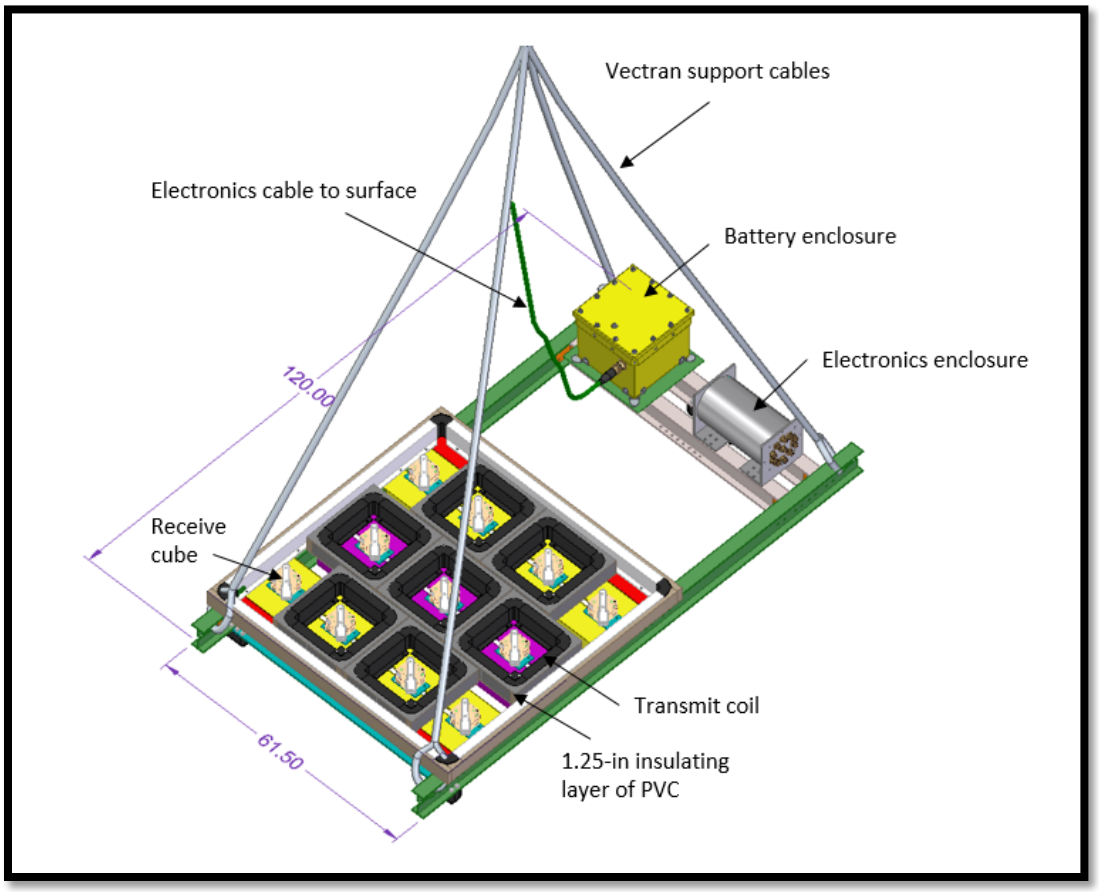

Figure 1. Underwater Advanced Time-Domain Electromagnetic System
Measurements are in inches.

Figure 2. Photograph of the Underwater Advanced Time-Domain Electromagnetic System

Figure 3 presents a diagram identifying transmitter (Tx) and receiver (Rx) locations and nomenclature. The array consists of eleven, 10-centimeter (cm) three-axis receive cubes, denoted by the cube identifier and an "r" indicating "receiver" (i.e., Ar-Kr), seven 40-cm square transmit coils, denoted by the cube identifier and a "t" indicating "transmitter" (i.e., At-Gt), and an outer 1.56-meter (m) square transmit coil (Ht). The resulting total number of data channels is 264. The raw sampling interval is 0.004 milliseconds (ms) and the recorded data are logarithmically averaged over 5 percent windows, resulting in 99 logarithmically spaced decay times ranging from 0.05 ms to 8.124 ms. One hundred measurements are averaged for each recorded measurement.

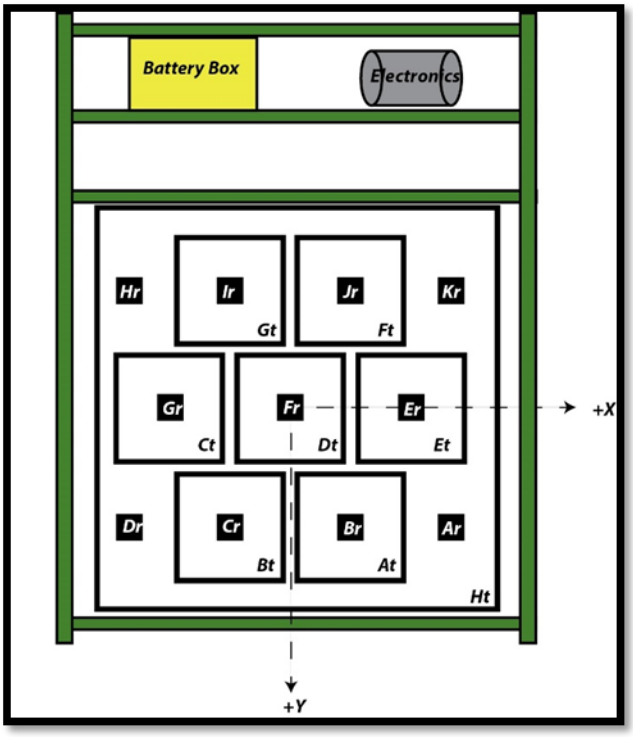

Figure 3. Transmitter and Receiver Locations and Nomenclature

2.2 TECHNOLOGY DEVELOPMENT

As summarized in previous documents under ESTCP Project MR-201313, the EM system was developed across three phases prior to the Saltwater Demonstration (Phase 4). Figure 4 – Figure 7 present products and processes from the previous three phases, and Final Reports for these phases are included as appendices to this report:

- Phase 1: Initial Design and Modeling – Modeling for Underwater Advanced Time-Domain Electromagnetic System White Paper, June 2014 (Appendix B)
- Phase 2: Engineering Design and Construction – Underwater Advanced Time-Domain Electromagnetic System Design, July 2015 (Appendix C)
- Phase 3: Freshwater Evaluation – System Performance Report, March 2017 (Appendix D)

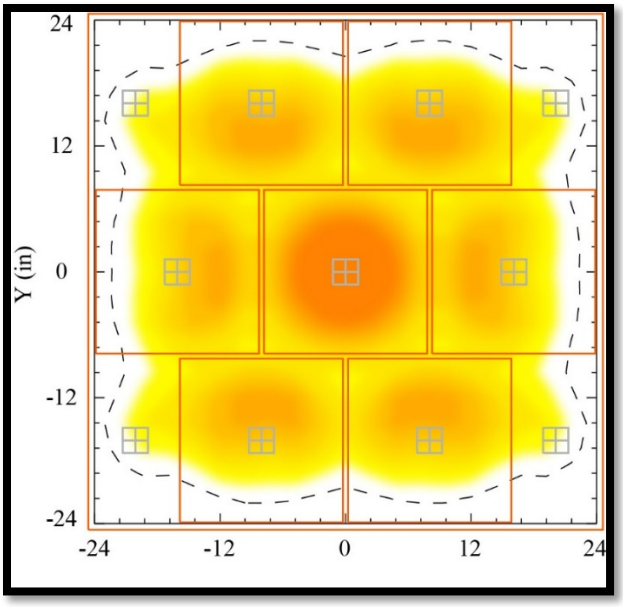

Figure 4. Phase 1 Modeling Results Indicating Sensor Sensitivity Based on EM Array Concept

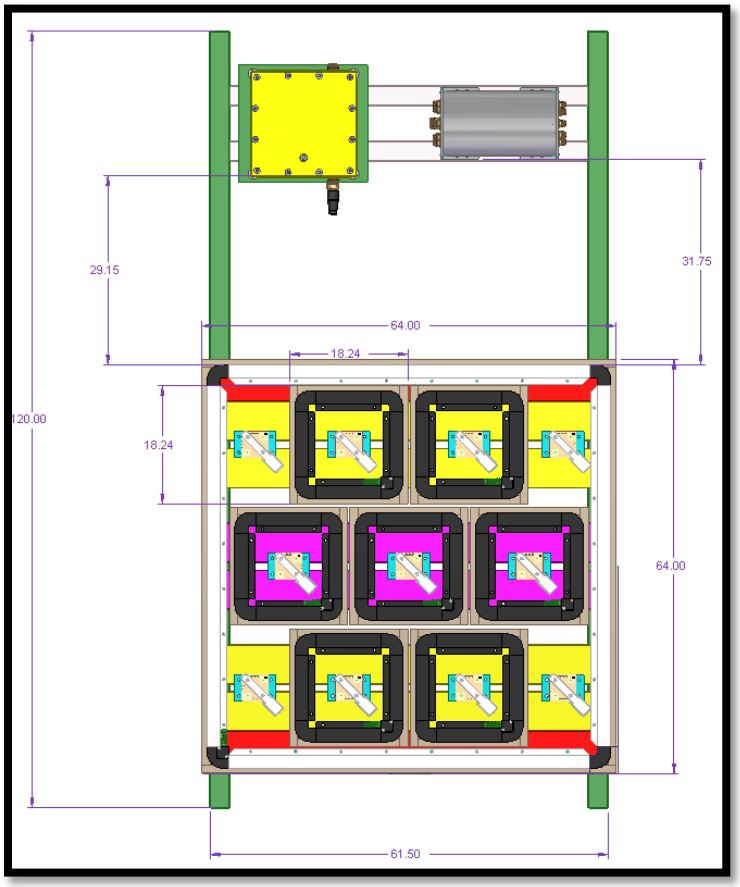

Figure 5. Phase 2 Engineering and Design Drawing of EM System

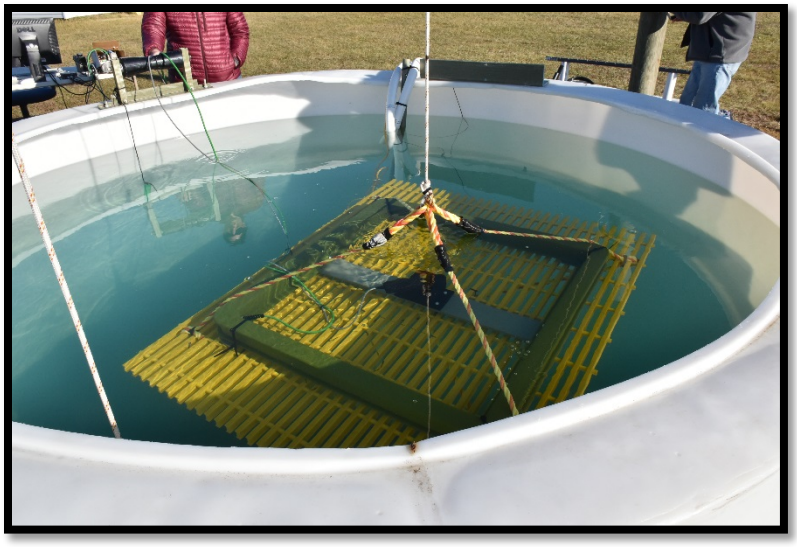

Figure 6. Phase 3 Dunk Test Prior to Freshwater Evaluation

Figure 7. Phase 3 Freshwater Evaluation

2.3 ADVANTAGES AND LIMITATIONS OF THE TECHNOLOGY

The ability to classify EM sources in a dynamic and shallow saltwater environment has the advantages of: 1) reducing costs and safety risks; 2) expanding the range of AGC-suitable environments; and 3) improving data quality process for underwater Munitions Response actions. However, the current EM system configuration is limited by its inability to navigate and collect positional data. The EM system's large form factor, itself a design criterion due to the of lack of positional data, is another limitation that may be improved by integrating positional data. The array's large form factor also limits its maneuverability.

Page Intentionally Left Blank

3.0 PERFORMANCE OBJECTIVES

Table 1 contains a summary of the qualitative and quantitative Performance Objectives identified for the Demonstration, including the performance objective, the associated metric by which to measure success, the data required to evaluate the metric, and the minimum acceptable criteria.

Table 2, at the end of this section, presents all Test Area results for the eleven test items, including:

- Inverted offsets (X, Y, and Z) from center of EM system;
- SNR;
- Fit Coherence;
- Inverted location from center of EM system;
- Library Match (underwater cued measurement data match to free-air cued library data);
- A comparison per metric to the best result during the 2016 Freshwater Demonstration.

Note on Measurement ID: each test item has an identifier (e.g., the Large ISO is O1); the second digit in the Measurement ID denotes each of the six measurement positions per test item, and the third digit in the Measurement ID denotes the 2018 Saltwater Demonstration.

The effects of test item size and test item location may be seen in the results. Larger test items and test items closer to the center of the EM system array generally had higher fit coherence and library match metrics. Test item location #4 (at the outer edge corner of the EM system array) had the lowest average fit coherence and library match metrics for all items (0.863 and 0.581, respectively). Positioning uncertainty of EM system to the emplaced test item applies to all test item locations. More discussion of results is provided in Section 3.4.

Table 1. Performance Objectives

Performance Objective	Metric	Data Requirements	Success Criteria	Results
Quantitative Performance Objectives				
Start-of-project free-air classification	Proper classification for each test item	Dipole inversion parameter values and polarizabilities for each test item from at least one Tx/Rx element	>0.8 fit coherence (using UX-Analyze fit coherence calculation) UX Analyze classification metric >0.9 (library match correlation) <25% difference between calculated and library reference polarizabilities	Met >0.8 fit coherence for all test items Met >0.9 fit metric for all test items Met <25% difference for all test items
Daily sensor response repeatability	Standard response for each tested Tx/Rx element to a known target in a known location.	At start and end of each day the EM system is used, amplitudes from standard item at same distance and orientation for each Tx/Rx element while EM system is at known underwater background location.	≤ 20% Root-Mean-Squared (RMS) variation in amplitude.	Daily Sensor Function Tests show that for functioning data channels the response amplitude variation is <20%.
Daily classification repeatability	Proper classification for each test item	At start and end of each day EM system is used, response curve of test item placed in at least one location within 0.8m of the center of the array	Proper classification with item ≤0.8m of the center of the array >0.8 fit coherence (using UX-Analyze fit coherence calculation). UX Analyze classification metric >0.9 (library match correlation) <25% difference between calculated and site-specific, free-air reference polarizabilities	Properly classified with aluminum sphere <0.8m from center of array. Range of fit coherences: 0.900 – 0.997 Range of library fit metrics: 0.969 – 0.996 Range of percent differences: 10.6 – 19.3

Table 1. Performance Objectives (continued)

Performance Objective	Metric	Data Requirements	Success Criteria	Results
Classification can be achieved if item is within 0.8m f the center of the array in an underwater conductive environment	Classification is possible if item is within 0.8m of the center of the array.	Response curve of metallic object placed at multiple locations within 0.8m of the center of the array.	Proper classification with item ≤0.8m of the center of the array.	Except for the 20mm projectile, all targets were classified properly up to 0.65m from the center of the array. Only the Small ISO and 20mm projectile failed to achieve a fit metric >0.9 at any offset from the center of the array.
Data quality supports inversion to determine target parameters.	Modeled response match observed responses for each test item	Fit coherence from inversion.	>0.8 fit coherence (using UX-Analyze fit coherence calculation).	All but one of the targets with SNR >30 have fit coherence >0.8. No 20mm projectile test item measurement had a reliable fit coherence >0.8.
Target polarizabilities and classification results from data collected in saltwater match corresponding library polarizabilities.	Target polarizabilities for each test item match library responses.	Dipole inversion parameter values and polarizabilities for known test items.	UX Analyze classification metric >0.9 (library match correlation) <25% difference between calculated and library reference polarizabilities	46 of 66 targets (69%) have <25% difference between calculated and library reference polarizabilities. 40 of 66 targets (60%) have UXA library match metric >0.9. 36 of 66 targets (54%) meet both library match criteria. *For targets with SNR >30:* 45 of 53 targets (84%) have <25% difference between calculated and library reference polarizabilities 39 of 53 targets (73%) have UXA library match metric >0.9 35 of 53 targets (66%) meet both library match criteria

Table 1. Performance Objectives (continued)

Performance Objective	Metric	Data Requirements	Success Criteria	Results
Qualitative Performance Objectives				
Sensor can be sufficiently maneuvered in dynamic underwater environment by divers such that the divers' safety is not compromised.	Divers are comfortable that their safety will not be compromised maneuvering the system.	Verbal feedback from divers.	Divers indicate they are comfortable that their safety is not compromised.	The system was lowered 7m to the Test Area using the LARC-mounted davit. Two divers safely moved system laterally (40m across Test Area) during fair weather conditions (wave heights < 1.5m) without aid of weights or lift bags.
Sensor can be sufficiently maneuvered in dynamic underwater environment by divers such that the system can be placed satisfactorily on the desired cue location to collect classification data.	Divers are able to effectively and efficiently maneuver the system to the desired cue location.	Verbal feedback from divers. Time to move system between cue locations.	Divers indicate they are able to effectively and efficiently maneuver the system to the desired cue location and collect data that pass all Quantitative Performance Objectives. Time required to move system between cue locations is less than 10 minutes.	Divers effectively and efficiently maneuvered system through Test Area. A clear data collection plan and two-way communication eliminated any issue of incorrect diver positioning or incomplete data collection. Divers moved system between Test Area cued locations in an average of 1 minute each.
Continued validation that system is sufficiently waterproofed. (Note: This was initially demonstrated in the freshwater pond, but will continue to be closely monitored.)	No indications that water has leaked into system components.	Data collected by system and visual observation.	Data do not indicate water has entered system components.	System is sufficiently waterproofed. After two days of field deployment in saltwater conditions, some corrosion was observed on the electronics cannister, but not at a level which could compromise its integrity over a reasonable operational lifespan of the system.
Calibration method can be used both topside and in an underwater conductive environment.	Baseline response plots are similar to response in water and on land.	Data collected by system and visual observation.	Response plots of system are reasonably similar to baseline plots – qualitative measurement.	With the exception of monostatic Ht-Hr Z-axis response, all sensor function test results for the aluminum ball were consistent and acceptable, whether data were collected in free-air or in saltwater.

3.1 OBJECTIVE: START-OF-PROJECT FREE-AIR CLASSIFICATION

3.1.1 Metric

Proper classification with item ≤0.8m from center of EM system for each test item.

3.1.2 Data Requirements

Dipole inversion parameter values and polarizabilities are required for each test item from at least one test item data collection location. Before testing the EM system underwater, each test item will be measured on land in free-air away from EM sources. Each of the test items will be placed over each of the Tx/Rx pair and data will be collected. Inverted results will be compared to the library and freshwater results, and will be used as baseline for comparison to underwater results.

3.1.3 Success Criteria Evaluation and Results

Free-air measurements were performed for the six test items not measured during the 2016 Freshwater Demonstration (i.e., 20mm projectile, 37mm projectile, 60mm mortar, 81mm mortar, 2.75in rocket warhead, aluminum rod), and for the small ISO, and medium ISO. The data were inverted to determine each test items' polarizabilities. All data were used except malfunctioning data channels (Et, Ft, and Ht transmit data, and Jr receiver Z-axis data). All fit coherences were greater than 0.8. Specific values of the fit coherence for these test items are listed in the table below.

Item	20mm	Small ISO	37mm	60mm	Medium ISO	81mm	2.75in	Aluminum Rod
Fit Coherence	0.954	0.998	0.999	0.997	0.981	0.998	0.923	0.989

Prior data with the EM system were available only for the ISOs. Relative to the polarizabilities calculated using the 2016 Freshwater Demonstration data, the fit metrics were greater than 0.9 (0.914 and 0.961, respectively) and the differences between polarizabilities were <25% (19% and 18%, respectively).

3.2 OBJECTIVE: DAILY SENSOR RESPONSE REPEATABILITY

3.2.1 Metric

Standard response amplitude for each tested monostatic Tx/Rx element to a known target in a known location.

3.2.2 Data Requirements

At start and end of each day the EM system is used, amplitudes are required from a standard test item (e.g., aluminum ball) at same distance and orientation for each Tx/Rx element while EM system is at a known underwater background location.

3.2.3 Success Criteria Evaluation and Results

Response between functioning Tx/Rx elements across time and across array differ <20% RMS (average of 3.0% for monostatic Z-axis response underwater).

3.3 OBJECTIVE: DAILY CLASSIFICATION REPEATABILITY

3.3.1 Metric

Proper classification for standard test item.

3.3.2 Data Requirements

At start and end of each day the EM system is used, dipole inversion parameter values and polarizabilities are required from a standard test item (i.e., aluminum ball) at same distance and orientation for at least one Tx/Rx element while EM system is at known underwater background location. Inverted results will be compared to the freshwater results and free-air results.

3.3.3 Success Criteria Evaluation and Results

Fit coherence, library match metric and polarizability differences for the aluminum ball are listed below.

	May 14th, 2018	May 15th	May 16th (AM)	May 16th (PM)
Fit coherence	0.900	0.988	0.988	0.997
Library metric	0.969	0.978	0.995	0.996
Pol diff (%)	10.6	19.3	15.5	15.1

Target polarizabilities for all four aluminum sphere tests resulted in fit coherence >0.8 (average 0.968), and library match fit metrics >0.9 (average 0.985). Derived target positions match nominal position within 0.02m.

3.4 OBJECTIVE: MEASURE CLASSIFICATION ABILITY IN CONDUCTIVE UNDERWATER ENVIRONMENT

3.4.1 Metric

Classification from data collected in underwater conductive environment is valid. Classification can be achieved if item is <0.8m from the center of the array in an underwater conductive environment. Target polarizabilities for known items match library responses. Classification is possible if item is within 0.8m of the center of the array.

3.4.2 Data Requirements

Dipole inversion parameter values and polarizabilities for known test items. Response curve of metallic object placed at multiple locations within 0.8m of the center of the array.

3.4.3 Success Criteria Evaluation and Results

As discussed in Section 6, there is nothing in the data to indicate that target responses in saltwater are different than the corresponding responses in air. For measurements with SNR >30, the difference between calculated and library reference polarizabilities is <25% for 45 of 53 targets (85% Pass). UX-Analyze classification metric is >0.9 (library match correlation) for 39 of 53 targets (74% Pass). Classification is possible if item is within 0.8m of the center of the EM system. Results for all measurements are below. Those measurements not passing the classification requirement generally are the small items (37mm projectile and smaller) and those placed further from the center of the array (0.65m and greater).

Performance Objective Goal	All SNR	SNR >30
Polarizability Difference <25%	46 of 66 (70%)	45 of 53 (85%)
Fit Metric >0.9	40 of 66 (61%)	39 of 53 (74%)

3.5 OBJECTIVE: DATA QUALITY SUPPORTS INVERSION TO DETERMINE TARGET PARAMETERS

3.5.1 Metric

Modeled response matches the observed response for each test item.

3.5.2 Data Requirements

The dipole fit quality is measured by the fit coherence, equal to the Pearson correlation coefficient of the data and the modeled response. The variance in the measurements which is not accounted for by the modeled response is equal to one minus the fit coherence squared.

3.5.3 Success Criteria Evaluation and Results

The success criterion is that the fit coherence is greater than 0.8. As discussed in Section 6, the fit coherence depends on the signal-to-noise ratio (SNR) of the measurement. Weak targets generally have poor fit coherence because the inversion is trying to fit a significant amount of noise along with the target's signal. Here, SNR is calculated as follows. For each transmit-receive pair the channel SNR is defined as the absolute value of the (background subtracted) signal divided by the standard deviation of the background response, averaged over the time gates. In order to maintain some consistency with performance of the standard 2x2 TEMTADS and MetalMapper arrays (which have 48 data channels) the tabulated SNR is then the average channel SNR over the strongest 48 channels in our array.

All but one target measurement with a SNR greater than 30 had a fit coherence >0.9 (see Table 2). The exception was the Aluminum Rod in position 6. Its SNR was 45, and we suspect that the item was off to the side of the array and poorly illuminated because some of the nearby Tx-Rx combinations were malfunctioning.

None of the in-water measurements of the 20mm projectile test item had a SNR greater than 30, and none had a fit coherence >0.8. It appears that the 20mm projectile test item was simply too far away from the array to provide meaningful signal.

3.6 OBJECTIVE: TARGET POLARIZABILITIES AND CLASSIFICATION RESULTS FROM SALTWATER MATCH CORRESPONDING LIBRARY POLARIZABILITIES

3.6.1 Metric

Target polarizabilities for each test item match corresponding in-air response.

3.6.2 Data Requirements

In-water and in-air polarizabilities the test items.

3.6.3 Success Criteria Evaluation and Results

The UX-Analyze classification metric measures the degree to which two polarizabilities match each other. It is normally used in advanced geophysical classification to compare the polarizabilities of an unknown target with those of targets of interest. Typically, a metric value >0.85 is considered to be an acceptable match. We specified a success criterion of >0.9 for the match between in-air and in-water polarizabilities and a <25% difference between in-water and in-air polarizabilities, which is calculated as the percent deviation of the in-water polarizability from the corresponding in-air polarizability. For targets with SNR >30, 45 of 53 targets (84%) have <25% difference between In-water and in-air polarizabilities and 39 of 53 targets (73%) have a match metric >0.9. The relationship between the two metrics for our data is illustrated in Figure 8.

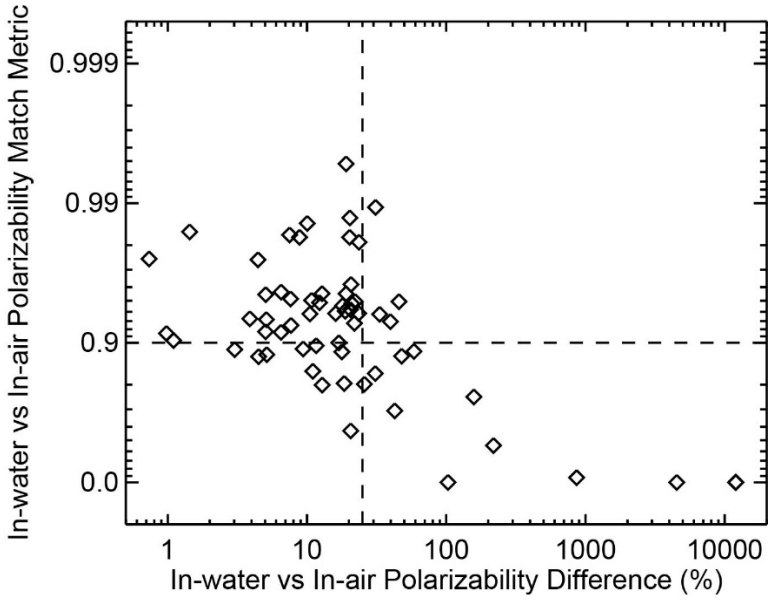

Figure 8. Polarizability Match Quality Versus Polarizability Difference.

3.7 OBJECTIVE: CALIBRATION METHOD CAN BE USED BOTH TOPSIDE AND IN UNDERWATER CONDUCTIVE ENVIRONMENT

3.7.1 Metric

Baseline response plots to the standard aluminum ball are similar in water and on land.

3.7.2 Data Requirements

Data collected by system and visual observation.

3.7.3 Success Criteria Evaluation and Results

System response plots in air and in water are the same. With the exception of the monostatic Ht-Hr Z-axis response, all of the sensor function test results for the aluminum ball were consistent and acceptable, regardless of whether the data were collected in free-air or in saltwater. (See Figures 18 and 21).

3.8 OBJECTIVE: MEASURE PLATFORM MANEUVERABILITY

3.8.1 Metric

Divers are comfortable that their safety will not be compromised maneuvering the EM system. Divers can effectively and efficiently maneuver the system to the desired cued location. EM system can be sufficiently maneuvered in dynamic underwater environment by divers such that the divers' safety is not compromised.

3.8.2 Data Requirements

Verbal feedback from divers. Time to move system between cued locations.

3.8.3 Success Criteria Evaluation and Results

Divers indicated they were comfortable moving the EM system and their safety was not compromised. Divers indicate they can effectively and efficiently maneuver the system to the desired cued location without overexertion. Time required to move system 5m between cued locations was significantly less than 10 minutes, averaging 45 seconds.

Table 2. Cued Target Results

	Measurement ID:	O1-1-3	O1-2-3	O1-3-3	O1-4-3	O1-5-3	O1-6-3	
Large ISO (O1)	X (m)	0.46	0.45	0.29	-0.54	-0.49	-0.46	2016 Freshwater Demonstration Best Result
	Y (m)	0.04	0.31	0.67	0.76	0.41	0.17	
	Z (m)	-0.51	-0.47	-0.48	-0.45	-0.47	-0.50	
	SNR	361.6	694.8	640.7	306.3	766.5	672.2	
	Fit Coherence	0.988	0.994	0.998	0.993	0.996	0.994	0.999
	Distance (m)	0.46	0.55	0.73	***0.93***	0.64	0.49	0.42
	Library Match	0.950	***0.800***	0.980	0.980	0.980	0.990	0.948

	Measurement ID:	O2-1-3	O2-2-3	O2-3-3	O2-4-3	O2-5-3	O2-6-3	
105mm Projectile (O2)	X (m)	0.51	0.40	0.35	-0.31	-0.39	-0.47	2016 Freshwater Demonstration Best Result
	Y (m)	0.05	0.36	0.74	0.66	0.31	-0.03	
	Z (m)	-0.45	-0.41	-0.41	-0.44	-0.45	-0.46	
	SNR	616.3	1870.6	677.8	919.3	1059.4	735.5	
	Fit Coherence	0.985	0.997	0.999	0.997	0.994	0.995	0.999
	Distance (m)	0.51	0.54	***0.82***	0.73	0.49	0.47	0.21
	Library Match	0.940	0.990	0.960	0.950	0.970	0.920	0.997

	Measurement ID:	O3-1-3	O3-2-3	O3-3-3	O3-4-3	O3-5-3	O3-6-3	
105mm HEAT (O3)	X (m)	-0.05	-0.04	-0.12	-0.93	-0.91	-0.87	2016 Freshwater Demonstration Best Result
	Y (m)	-0.34	0.19	0.63	0.52	0.29	0.21	
	Z (m)	-0.45	-0.44	-0.45	-0.43	-0.45	-0.48	
	SNR	404.8	1308.1	924.0	117.6	138.3	156.4	
	Fit Coherence	0.989	0.993	0.997	0.993	0.997	0.984	0.999
	Distance (m)	0.34	0.20	0.64	***1.07***	***0.96***	***0.90***	0.06
	Library Match	0.940	0.990	***0.570***	***0.890***	0.980	0.950	0.992

Table 2. Cued Target Results (continued)

	Measurement ID:	O4-1-3	O4-2-3	O4-3-3	O4-4-3	O4-5-3	O4-6-3	
Aluminum Rod (O4)	X (m)	0.10	0.09	0.01	-1.90	-0.84	-0.77	2016 Freshwater Demonstration Best Result
	Y (m)	-0.04	0.40	0.82	1.09	0.41	0.11	
	Z (m)	-0.48	-0.48	-0.47	-0.85	-0.51	-0.52	
	SNR	175.6	193.0	74.7	26.2	55.7	45.1	
	Fit Coherence	0.766	0.940	0.843	0.939	0.989	0.991	0.997
	Distance (m)	0.10	0.41	***0.82***	***2.19***	0.94	0.78	0.14
	Library Match	0.86	0.95	***0.06***	0.95	0.99	0.98	n/a

	Measurement ID:	O5-1-3	O5-2-3	O5-3-3	O5-4-3	O5-5-3	O5-6-3	
Medium ISO (O5)	X (m)	0.18	0.13	0.10	-0.73	-0.74	-0.74	2016 Freshwater Demonstration Best Result
	Y (m)	-0.36	0.16	0.63	0.62	0.15	-0.10	
	Z (m)	-0.34	-0.36	-0.37	-0.37	-0.38	-0.39	
	SNR	290.5	482.6	479.9	137.2	230.7	169.0	
	Fit Coherence	0.964	0.995	0.999	0.998	0.999	0.999	0.999
	Distance (m)	0.40	0.21	0.64	***0.96***	0.75	0.75	0.04
	Library Match	***0.690***	0.960	0.980	0.900	0.920	0.950	0.968

	Measurement ID:	O6-1-3	O6-2-3	O6-3-3	O6-4-3	O6-5-3	O6-6-3	
81mm Mortar (O6)	X (m)	0.27	0.07	0.07	-0.85	-0.75	-0.75	Object not tested in 2016 Freshwater Demonstration
	Y (m)	-0.16	0.30	0.74	0.78	0.32	0.11	
	Z (m)	-0.47	-0.48	-0.48	-0.48	-0.50	-0.50	
	SNR	230.6	408.3	226.9	25.1	57.6	79.5	
	Fit Coherence	0.988	0.996	0.996	0.987	0.945	0.983	
	Distance (m)	0.31	0.31	0.74	***1.15***	***0.82***	0.76	
	Library Match	0.960	0.940	0.940	***0.880***	***0.880***	0.910	

Table 2. Cued Target Results (continued)

2.75in Rocket (O7)	**Measurement ID:**	**O7-1-3**	**O7-2-3**	**O7-3-3**	**O7-4-3**	**O7-5-3**	**O7-6-3**	Object not tested in 2016 Freshwater Demonstration
	X (m)	0.01	0.06	0.13	-0.69	-0.71	-0.68	
	Y (m)	-0.12	0.39	0.84	0.78	0.49	0.12	
	Z (m)	-0.46	-0.43	-0.44	-0.40	-0.45	-0.44	
	SNR	746.2	1447.9	518.0	79.4	274.9	297.6	
	Fit Coherence	0.989	0.995	0.995	0.937	0.994	0.974	
	Distance (m)	0.12	0.40	***0.85***	***1.04***	***0.87***	0.69	
	Library Match	0.930	0.940	***0.880***	***0.840***	0.950	0.900	

60mm Mortar (O8)	**Measurement ID:**	**O8-1-3**	**O8-2-3**	**O8-3-3**	**O8-4-3**	**O8-5-3**	**O8-6-3**	Object not tested in 2016 Freshwater Demonstration
	X (m)	0.29	0.13	0.10	-0.76	-0.75	-0.71	
	Y (m)	-0.04	0.36	0.73	0.58	0.33	0.08	
	Z (m)	-0.37	-0.38	-0.39	-0.37	-0.39	-0.39	
	SNR	259.7	281.9	165.1	70.2	111.5	162.2	
	Fit Coherence	0.980	0.997	0.999	0.993	0.996	0.999	
	Distance (m)	0.29	0.38	0.73	***0.96***	***0.82***	0.72	
	Library Match	0.950	0.930	0.940	***0.870***	0.930	0.950	

37mm Projectile (O9)	**Measurement ID:**	**O9-1-3**	**O9-2-3**	**O9-3-3**	**O9-4-3**	**O9-5-3**	**O9-6-3**	Object not tested in 2016 Freshwater Demonstration
	X (m)	0.20	0.09	0.17	-0.90	-0.67	-0.66	
	Y (m)	0.01	0.33	0.77	0.87	0.46	0.14	
	Z (m)	-0.37	-0.38	-0.39	-0.45	-0.40	-0.40	
	SNR	55.6	94.5	42.7	17.8	19.9	38.1	
	Fit Coherence	0.991	0.988	0.975	0.916	0.987	0.990	
	Distance (m)	0.20	0.34	0.79	***1.25***	***0.81***	0.67	
	Library Match	0.930	0.970	***0.800***	***0.080***	0.900	0.920	

Table 2. Cued Target Results (continued)

	Measurement ID:	O10-1-3	O10-2-3	O10-3-3	O10-4-3	O10-5-3	O10-6-3	
Small ISO (O10)	X (m)	0.13	0.03	0.24	-1.05	-0.50	-0.52	Object not tested in 2016 Freshwater Demonstration
	Y (m)	0.25	0.53	1.01	0.92	0.31	0.12	
	Z (m)	-0.46	-0.50	-0.41	-0.74	-0.45	-0.44	
	SNR	53.0	39.9	25.2	9.4	32.4	26.0	
	Fit Coherence	0.955	0.950	0.924	0.862	0.976	0.956	
	Distance (m)	0.28	0.53	***1.04***	***1.40***	0.59	0.53	
	Library Match	***0.890***	***0.880***	***0.460***	***0.000***	***0.800***	***0.830***	

	Measurement ID:	O11-1-3	O11-2-3	O11-3-3	O11-4-3	O11-5-3	O11-6-3	
20mm Projectile (O11)	X (m)	0.14	-2.76	-0.46	0.04	-2.90	-0.54	Object not tested in 2016 Freshwater Demonstration
	Y (m)	0.29	7.57	1.00	-0.02	3.31	-0.86	
	Z (m)	-3.63	-2.37	-3.96	-0.11	6.75	-5.63	
	SNR	12.2	17.8	15.6	19.9	17.0	24.1	
	Fit Coherence	0.623	0.885	0.743	0.164	0.803	0.684	
	Distance (m)	0.32	***8.05***	***1.10***	0.04	***4.40***	***1.01***	
	Library Match	***0.000***	***0.000***	***0.000***	***0.000***	***0.000***	***0.000***	

Notes:
X, Y and distance values (relative to the center of the array) greater than 0.8m are ***bold underlined italicized red***
Library match values below 0.9 are ***bold underlined italicized red***

Page Intentionally Left Blank

4.0 SITE DESCRIPTION

4.1 SITE SELECTION

The FRF is an internationally recognized coastal observatory facility located within the northern Outer Banks of North Carolina. The facility is located on Bodie Island, bounded by the Atlantic Ocean to the east and Currituck Sound to the west. Central to the facility is an 1,840-foot-long pier and specialized vehicles. An overview map of the facility is shown as Figure 9 and an aerial photograph of the pier is shown as Figure 10. The FRF supported this demonstration by providing two Lighter Amphibious Resupply Cargo (LARC) vessels (Figure 11) and access to the FRF pier, as well as storage areas and power supplies. Staff from FRF supported the daily launch and recovery of the EM system and the CH2M HILL, Inc. (CH2M) dive team with their two LARCs. Additionally, staff from FRF provided acoustic Doppler current profiler (ADCP) data from their nearby network of ADCP sensors. A castaway Conductivity, Temperature, and Depth (CTD) instrument was used to measure profiles hourly from the Duck FRF pier and/or the LARCs.

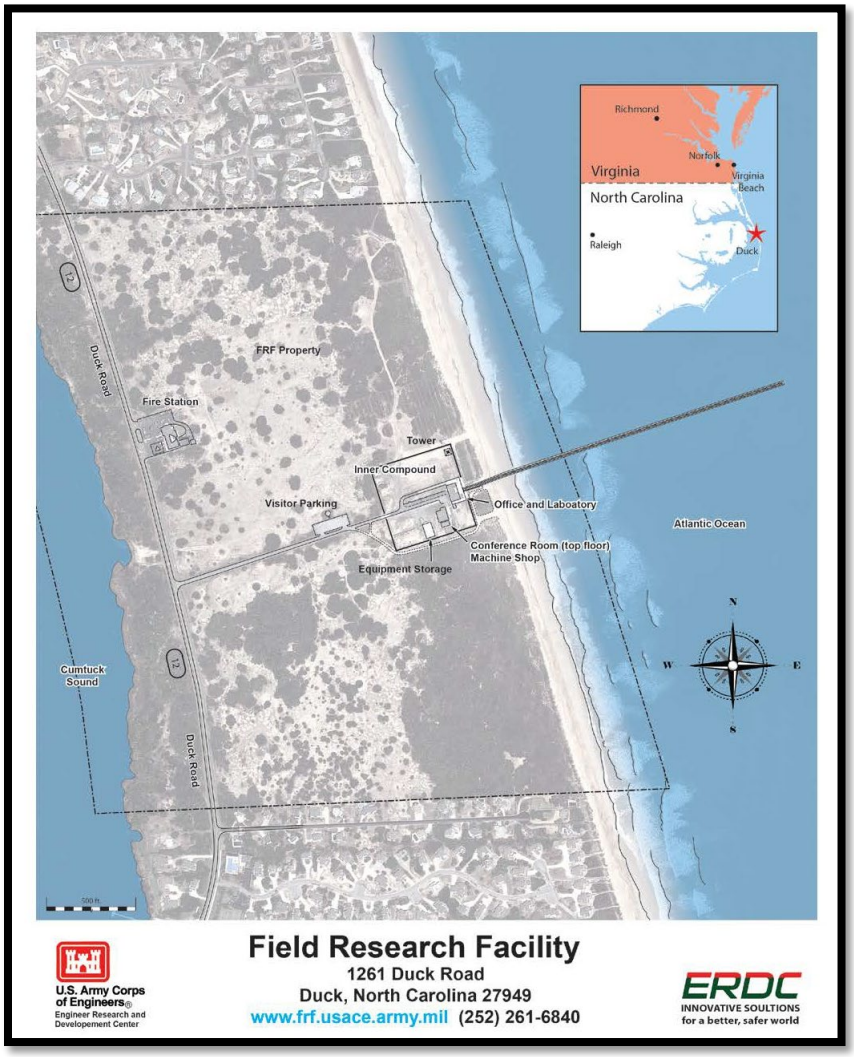

Figure 9. Field Research Facility Overview Map

Figure 10. Photographs of the 1,840-foot-long FRF Pier

Figure 11. Photographs of the Lighter Amphibious Resupply Cargo (LARC)

4.2 SITE HISTORY

The Duck Naval Target Range was established as a 200-acre air-to-ground practice range in 1941. A target location was presumed to be located on the island north of the pier. The Norfolk Navy yard conducted bombing and rocket launch practice runs from 1941-1965. The range was transferred to the Department of the Army in 1973. The FRF was established in 1977 by USACE and is part of the Coastal and Hydraulics Laboratory (headquarters in Vicksburg, Mississippi).

4.3 SITE GEOLOGY

The Outer Banks refer to a group of barrier islands along the coast of North Carolina, extending into Virginia. Barrier islands are uniquely geologically young features (<12000 years old) and uniquely morphologically dynamic. The barrier islands of the Outer Banks run generally parallel to the mainland in narrow bands periodically interrupted by inlets. Test cores and seismic data indicate that the stratigraphy near Bodie Island is composed of a Quarternary sequence up to 90 m thick filling a regional basin with a veneer of up to 10 m of Holocene sand. The lack of consolidated rock allows the forces of ocean waves, tides, flowing rivers, and episodic storms to continuously change the island geomorphology. Like many other barrier island environments, the islands of the Outer Banks have experienced heavy human development and modification of sediment deposition due to coastal structures and artificial beach renourishment. The sediment along the coastline and nearshore environments is typically composed of quartz sand with minor amounts of feldspar-based sand.

4.4 MUNITIONS CONTAMINATION

The former Duck Target Facility, a USACE-managed Formerly Used Defense Site (FUDS), received a Site Inspection and Remedial Investigation for potential munitions contamination. To date, no munitions or explosives of concern (MEC), or material potentially presenting an explosive hazard (MPPEH) have been found. USACE FRF does not require MEC-specific safety measures for its operations, therefore, this Demonstration proceeded with anomaly avoidance and the 3R's (Recognize, Retreat, and Report) safety protocol in the event of encountering suspected MEC or MPPEH during any phase (e.g., Test Area construction, data collection).

5.0 TEST DESIGN

5.1 CONCEPTUAL EXPERIMENT DESIGN

The overall objective of the project was to design, build, and demonstrate an underwater advanced EM system for cued classification of munitions in the underwater environment. The phased approach consists of initial design and modeling (Phase 1 – completed), engineering design and construction (Phase 2 – completed), underwater evaluation of the system in a freshwater pond (Phase 3 – completed), and demonstration of the system at a saltwater field site (Phase 4 – addressed in this document).

As the fourth and final phase of the project, the Saltwater Demonstration was designed to test all elements of the EM system in a conductive and dynamic environment. The Test Area and the data collection plan were designed to include all test items used during the 2016 Freshwater Demonstration, as well as smaller test items to challenge the EM system. To ensure proper EM system function prior to the May 2018 mobilization to Duck, N.C., this Demonstration included pre-deployment EM system testing in March 2018 at Blossom Point, Md. After EM system testing and recovery, the Demonstration proceeded as described in this Section, with initial data analyses performed onsite during the field, and thorough data review performed offsite for this Demonstration Report.

5.1.1 Overview of Field Operations

A brief overview of field operations is provided here as an outline for additional detail provided in this Section:

Monday May 14th: personnel from CH2M, Geometrics, Leidos, NRL, and USACE FRF assembled for safety briefing. Staff lined up ADCP and CTD data sources and performed free-air testing of EM system. Dive team and FRF staff set moorings in Test Area. Dive Team assembled gear and installed Test Area travel lines.

Tuesday May 15th: Geometrics and Leidos resolved low transmit amp record-writing issue and collected free-air data of new test items for Library. Data Team directed Dive Team in the collection of underwater cued data at to-be-seeded locations in Test Area prior to seeding. Dive Team collected sensor function test data.

Wednesday May 16th: Dive Team seeded the Test Area with eleven test items, then collected start-of-day sensor function test data. Data Team directed Dive Team in the collection of underwater cued data at eleven test items plus background locations in Test Area. Due to foul weather forecast, Dive Team collected end-of-day sensor function test data. Field operations were called off at approximately 2:30p EDT due to forecasted thunderstorms.

Thursday May 17th: Staff packed equipment and demobilized.

5.1.2 Dive Operations

Specific to this phase of the project and Demonstration, CH2M's engineer dive team performed dive operations in cooperation with FRF staff. Divers used surface-supplied air and had communication with topside for real-time coordination of data collection and EM system maneuvers (Figure 12). A project-specific Dive Operations and Accident Prevention Plan was prepared by CH2M for its internal safety and operations reviews. Dive Operations included:

- Setting travel lines for establishing the Test Area;
- Assisting with raising and lowering the EM system by crane between LARC and bottom;
- Maneuvering EM system across Test Area between measurement locations;
- Collecting cued background data measurements at pre-seeded locations within the Test Area;
- Seeding the Test Area with eleven test items;
- Collecting cued test data at eleven test items.

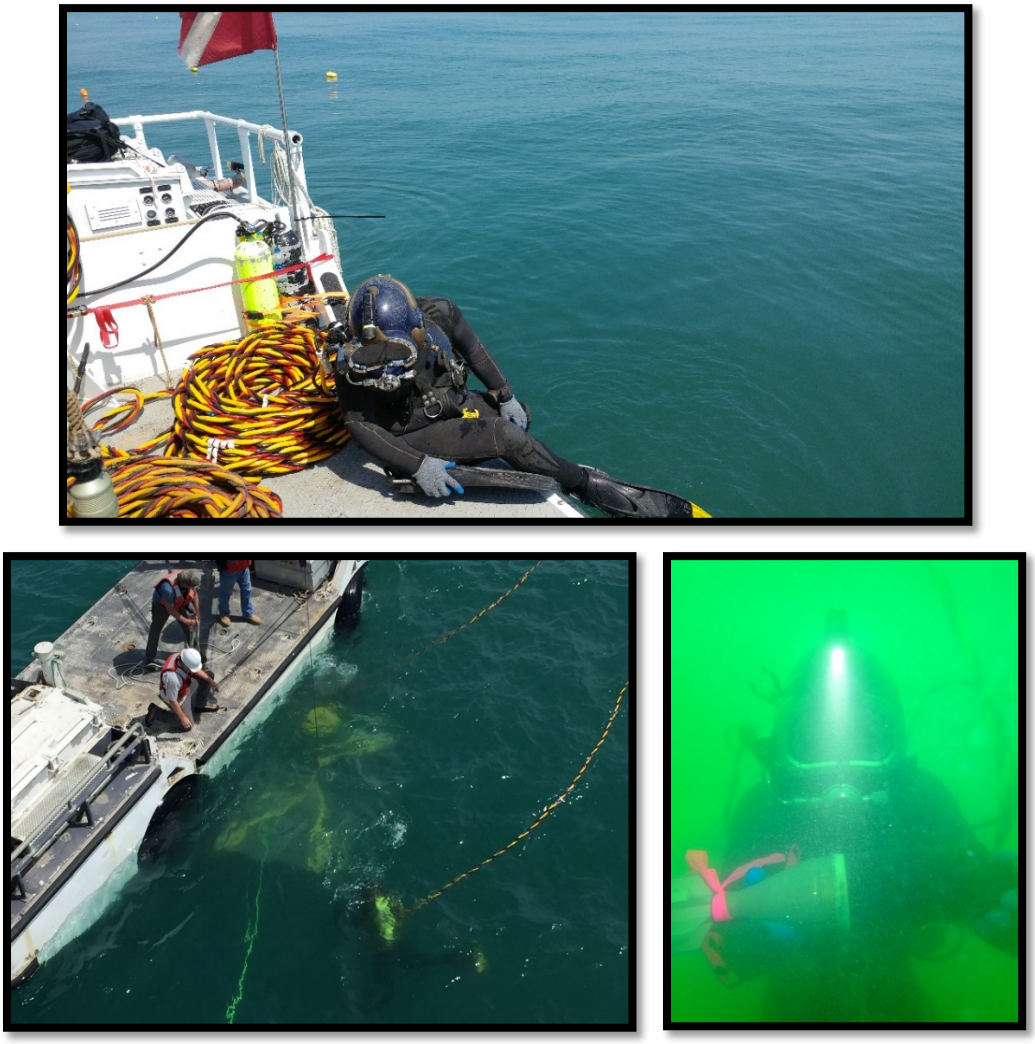

Figure 12. Surface Supplied Diver Operations from LARC, Including EM System Maneuvers and Test Item

5.2 SITE PREPARATION

Test items used for the underwater EM system demonstration were buried in the sediment along the test lines by CH2M's divers. Travel lines of synthetic rope, secured by sand screws at each end, were used to establish three parallel straight-line transects along which items were placed at a spacing of approximately 10m, leaving sufficient space for background measurements between each item. The travel line was visually and physically marked (e.g., knots, flagging) so the divers could identify the intended and then actual locations of the buried items, as well as the locations for background measurements halfway between each item (i.e., the travel line was marked every 5m). Eleven test items were planned for the Test Area (Figure 13). The items were buried in the sediment bed at shallow depths, with the intent of providing sufficient signal for classification purposes. In retrospect, the 20mm projectile should have been buried at a shallower depth than the nominal 0.5ft planned depth. Table 3 presents the items to be tested and their depths and orientations, Figure 14 shows the layout of the Test Area, and Figure 15 shows a test item prior to emplacement in the Test Area.

Table 3. Test Area Items, Depths, and Orientations

Item	Target Depth	Orientation / Inclination	Note
Large ISO (4"x12" steel pipe nipple)	1ft	30° off travel line / parallel to seabed	tested during 2016 freshwater effort
Medium ISO (2"x8" steel pipe nipple)	0.5ft	30° off travel line / parallel to seabed	tested during 2016 freshwater effort
Small ISO (1"x4" steel pipe nipple)	0.5ft	30° off travel line / parallel to seabed	new test item
Aluminum rod (3"x12")	0.5ft	30° off travel line / parallel to seabed	tested during 2016 freshwater effort
105mm projectile	1ft	30° off travel line / parallel to seabed	tested during 2016 freshwater effort
105mm HEAT projectile	1ft	parallel to travel line / parallel to seabed	tested during 2016 freshwater effort
20mm projectile	0.5ft	parallel to travel line / parallel to seabed	new test item
37mm projectile	0.5ft	parallel to travel line / parallel to seabed	new test item
60mm projectile	0.5ft	30° off travel line / parallel to seabed	new test item
2.75" rocket	0.5ft	30° off travel line / parallel to seabed	new test item
81mm projectile	0.5ft	30° off travel line / parallel to seabed	new test item

Figure 13. Specific Test Items Used in the Saltwater Demonstration Test Area

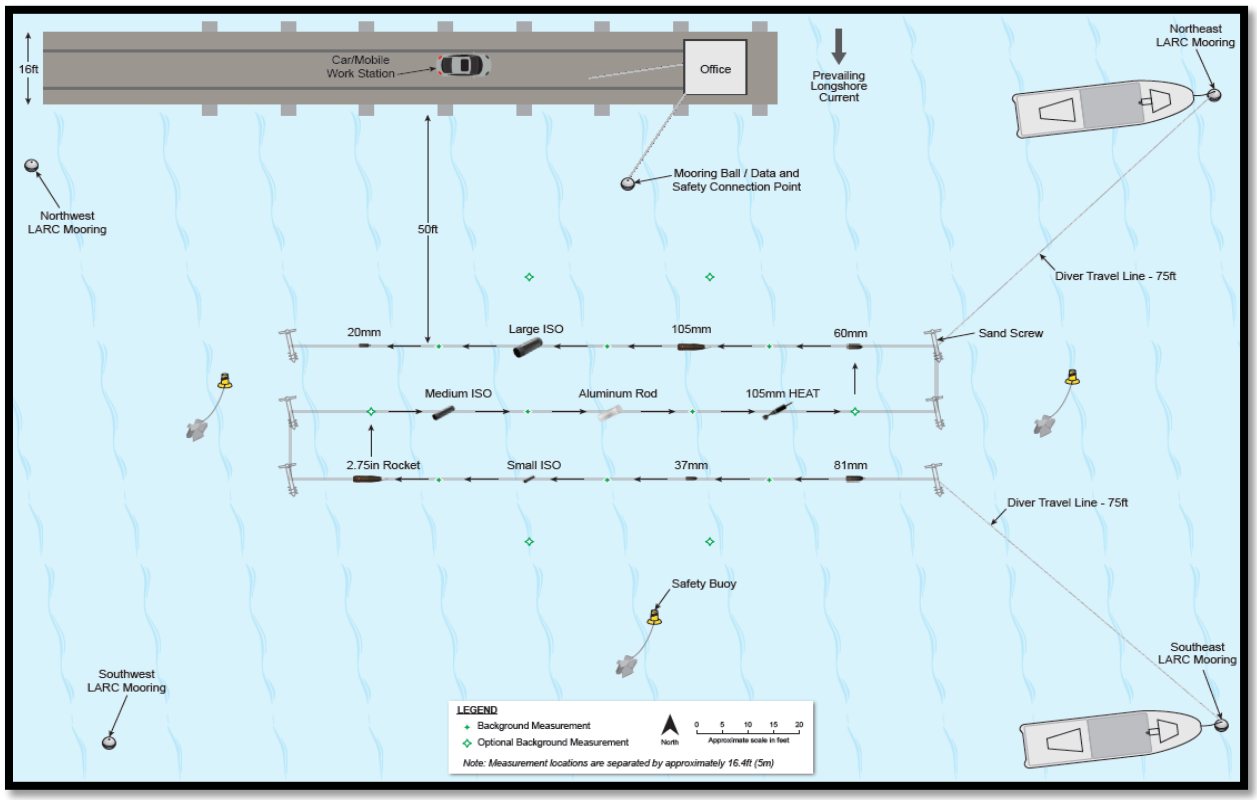

Figure 14. Plan View of Test Area Demonstration

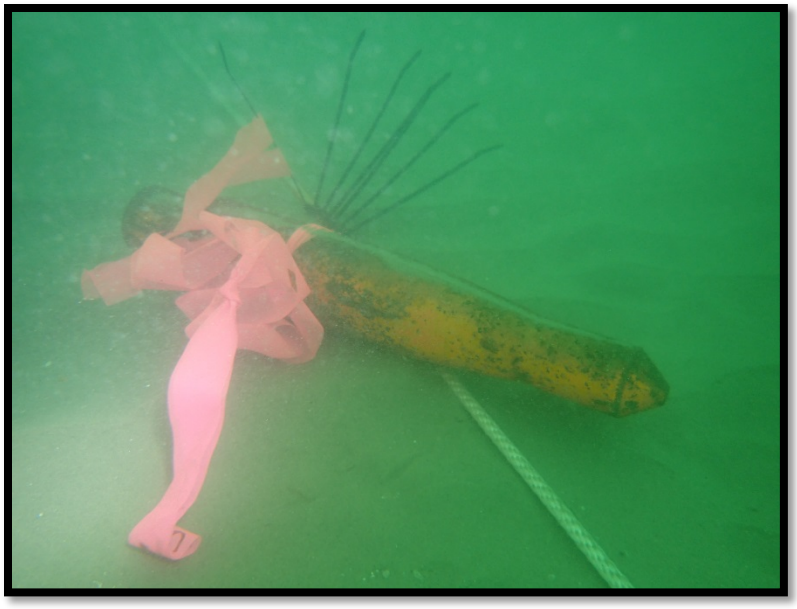

Figure 15. 2.75" Rocket Test Item Prior to Burial in Test Area

5.3 SYSTEM SPECIFICATION

As described in Section 2.1, the array consists of eleven, 10-centimeter (cm) three-axis receive cubes. No positional or attitudinal data are acquired or used. The receivers are denoted by the cube identifier and an "r" indicating "receiver" (i.e., Ar-Kr), seven 40-cm square transmit coils, denoted by the cube identifier and a "t" indicating "transmitter" (i.e., At-Gt), and an outer 1.56-meter (m) square transmit coil (Ht). The resulting total number of data channels is 264. The raw sampling interval is 0.004 milliseconds (ms) and the recorded data are logarithmically averaged over 5 percent windows, resulting in 99 logarithmically spaced decay times ranging from 0.05 ms to 8.124 ms. One hundred measurements are averaged for each recorded measurement. Table 4 presents a summary of the transmitter (Tx) and receiver (Rx) sequencing for each cued data collection.

Table 4. Summary of Transmitter and Received Data Channel Recording

Tx	Rx	Axis	On (ms)	Off (ms)	+/- Cycle	Stacks	Seconds/TX	Channels
At	Ar-Kr	Z-Y-X	8.33	8.33	1	100	3.33	33
Bt	Ar-Kr	Z-Y-X	8.33	8.33	1	100	3.33	33
Ct	Ar-Kr	Z-Y-X	8.33	8.33	1	100	3.33	33
Dt	Ar-Kr	Z-Y-X	8.33	8.33	1	100	3.33	33
Et	Ar-Kr	Z-Y-X	8.33	8.33	1	100	3.33	33
Ft	Ar-Kr	Z-Y-X	8.33	8.33	1	100	3.33	33
Gt	Ar-Kr	Z-Y-X	8.33	8.33	1	100	3.33	33
Ht	Ar-Kr	Z-Y-X	8.33	8.33	1	100	3.33	33
						Totals:	**27 sec**	**264 channels**

The data cable runs topside from the EM system, and carries Ethernet (transmitting user commands to the system and data from the system to the computer) and an on/off signal to the batteries (Figure 16). The data cable is 70m in length, which was long enough for the system to be operated by laptop from the pier. The On/Off switch allowed the system to be turned on and off to preserve battery power when the system is not in use. In this way, the system could remain underwater for longer periods of time and eliminate the need to raise and lower the system multiple times per day. This function was not necessary across the course of the Saltwater Demonstration.

Figure 16. Connecting Pier-based Laptop to EM System by Lowering Cable from Pier

5.4 CALIBRATION ACTIVITIES

In March 2018, Geometrics performed pre-mobilization testing of the EM System at NRL's Blossom Point, Md. facility to identify and correct any hardware or software performance issues prior to the May 2018 mobilization to the Duck FRF. Once mobilized to the Duck FRF, system function tests were performed on the system before launch and after recovery each day of testing.

Free-air measurements were taken at the start of the Demonstration by placing each of the eleven test items to be seeded, plus a 4" diameter aluminum ball, over each of the monostatic Tx/Rx elements. Free-air measurements were also taken using the aluminum ball at the start and end of each day the EM system was used during the Demonstration.

The goal of the free-air testing was to verify the system was working properly prior to underwater deployment. Proper functioning is defined as roughly identical response (microTesla/Ampere-second [μT/As] and classification result [modeled location and fit coherence]) for each of the Tx/Rx elements tested. Significant differences (e.g., >20%) between Tx/Rx pairs, or within one Tx/Rx pair over time, would have required inspection of the EM system, software, and collection variables to identify cause. The verification test consisted of placing an aluminum ball above each of the receiver cubes and taking a measurement. When components are working properly, the response in the Z-axis will be largest in the receiver cube above which the aluminum ball is located.

5.4.1 Free-air EM System Tests

Free-air data were collected May 14th and the morning of May 15th inside a large garage workshop at FRF to evaluate EM system performance and collect library signature data for the new test items not used during the 2016 Freshwater Demonstration at Panama City, Florida. The test items from Panama City were a 105mm projectile, 105mm HEAT, large ISO, medium ISO and a 3" x 12" aluminum rod. The new test items were a 2.75" rocket, 81mm mortar, 60mm mortar, small ISO, 37mm projectile and 20mm projectile. Each of the actual test items used are shown in Figure 12. Library signature data were also acquired for the aluminum rod. (This had not been measured at Panama City.) The larger test items (i.e., 2.75" rocket, 81mm mortar, 60mm mortar, aluminum rod) were placed on a notched rack positioned over the array as shown in Figure 17 and Figure 18. The top of the rack was 35cm above the top of the EM system's coils. Measurements were taken at rack locations 4, 5, and 6 corresponding to (X, Y) positions (-0.16m, 0.35m), (-0.36m, 0.35m), and (0.56m, 0.35m) from the center of the array. The smaller test items (i.e., small ISO, 37mm, 20mm) were placed on a plastic box set under each of the rack locations in turn. Other data collected on May 14th and 15th were for diagnosing system problems (i.e., inaccurate transmit current amperage), and are not included in the data deliverable. Several receiver cubes were switched around after the medium ISO measurements. First, receivers Er and Kr were switched, then Dr and (the new) Er were switched. Free-air data for the large ISO, 105mm projectile and 105mm HEAT were not collected. (Signature data and polarizabilities for these items are in the DoD TOI library.)

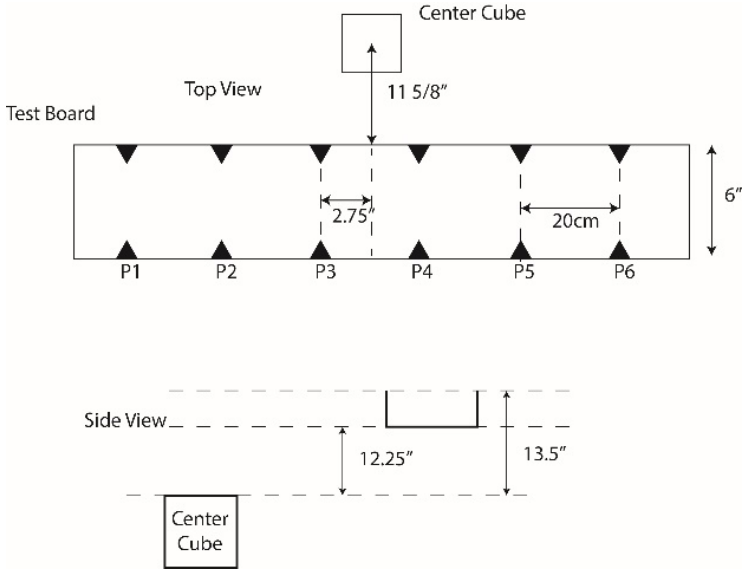

Figure 17. Free-air Test Rack Schematic

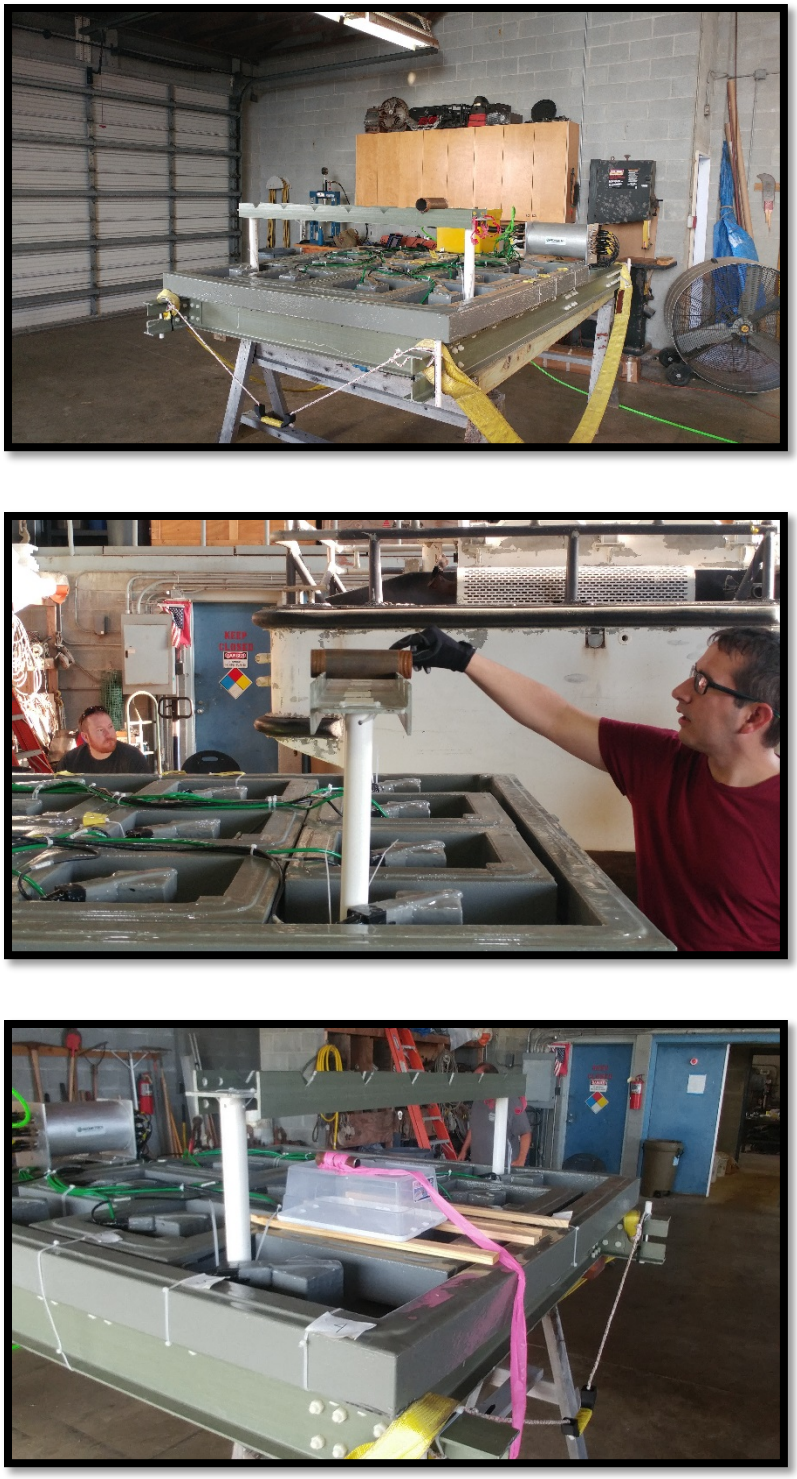

Figure 18. Free-air Testing at FRF

5.4.2 Free-air EM System Function Tests

Free-air system function test (SFT) data were collected prior to underwater deployment to evaluate EM system performance and identify malfunctioning data channels. These tests each comprised a set of 11 measurements with a 4" diameter aluminum ball placed on a PVC stand 24cm above the top of each of the 11 receivers in turn. Figure 19 is a plot of the free-air SFTs done on May 14th in the garage with the EM system ~1m above the floor (Figure 20). There was an intermittent problem with the recording of the transmit currents, so nominal values of 10A and 6A were used to normalize the signals for the inner and outer transmitters, respectively. There was no indication in the data that the actual transmit currents were off from these nominal values by more than a few percent. Four plots show decays measured by the different receivers with background responses subtracted. Positive signals are plotted as solid lines, and negative signals are dashed. The upper left plot shows the monostatic Z-axis decays when the aluminum ball was over receivers Br, Cr, Er, Fr, Gr, Ir and Jr. All of the curves should overlay. The upper right plot shows Z-axis decays with the aluminum ball over each receiver, excited by the outer (Ht) transmitter. These should all overlay within ±5% and be within a few percent of the monostatic decays shown in the upper left plots. The lower left plot shows X-axis decays for various bistatic combinations (At-Ar, At-Cr, Bt-Br, Bt-Dr, Et-Fr, Dt-Er, Dt-Gr, Ct-Fr, Ft-Kr, Ft-Ir, Gt-Jr, Gt-Hr) with the ball over the transmit coil. Decays for all of the inner receivers (Br, Cr, Er, Fr, Gr, Ir and Jr) are plotted in black and should overlay. Decays for the corner receivers (Ar, Dr, Hr and Kr) are plotted in blue and should be about 1.7 times stronger than the others. The bottom right plot shows Y-axis decays for various bistatic combinations (At-Er, At-Fr, Bt-Fr, Bt-Gr, Et-Ar, Et-Br, Et-Kr, Et-Fr,Dt-Jr, Dt-Br, Dt-Cr, Dt-Ir, Ct-Cr, Ct-Gr, Ct-Jr, Gt-Hr, Ft-Er, Ft-Fr, Gt-Fr, Gt-Gr) with the ball over the transmit coil. Decays for all of the inner receivers (Br, Cr, Er, Fr, Gr, Ir and Jr) are plotted in black and should overlay. Decays for the corner receivers (Ar, Dr, Hr, and Kr) are plotted in blue and should be about 1.3 times stronger than the others.

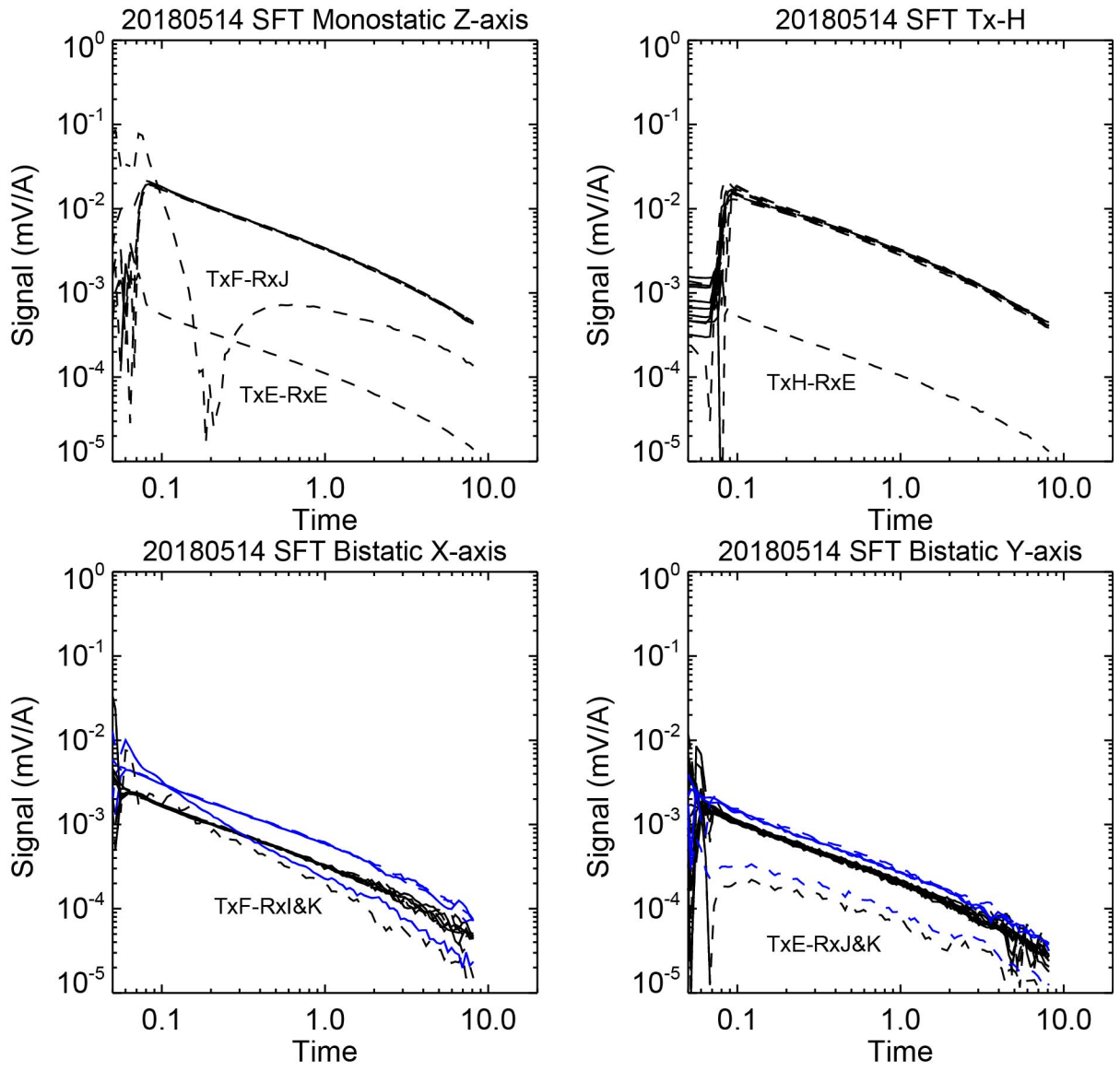

Figure 19. System Function Test with Aluminum Ball in Air on May 14th

Upper left: Monostatic Z-axis responses. All should overlay. Upper right: Z-axis responses to transmitter H. All should overlay and have same amplitude as monostatic Z to within 5%. Lower left: Bistatic X-axis responses. Corner receivers in blue, inner receivers in black. Each set should overlay, with corner receiver responses 1.7 times stronger than inner receiver responses. Lower right: Bistatic Y-axis responses. Corner receivers in blue, inner receivers in black. Each set should overlay, with corner receiver responses 1.3 times stronger than inner receiver responses.

Figure 20. Free-air Sensor Function Test

All but two of the monostatic Z-axis responses are the same. The exceptions are the decays measured by receivers Er and Jr paired with transmitters Et and Ft respectively. The Er receiver was switched with the Kr receiver during testing in the garage on the morning May 15th. The Er receiver Z-axis response to transmitter Ht is also different. The bistatic X-axis responses in free-air are all as expected except that the decays at receivers Ir and Kr trail off more rapidly than expected. They are both excited by the Ft transmitter in this case. All the bistatic Y-axis responses are as expected except for Et-Jr and Et-Kr. There does not appear to be a problem with Y-axis responses when transmitter Ft is fired, nor is there a problem with X-axis responses when transmitter Et is fired.

5.5 DATA COLLECTION

5.5.1 EM System Launch and Recovery

The EM system was transported each day from shore to the Test Area by one of the two LARCs (i.e., the Data LARC), where it received the data cable from the pier for connection to the pier-based data acquisition laptop. A lifting bridle was attached to the EM system frame. Once the EM system was connected and powered up, the EM system was lowered into the water, received by the two surface-supplied air divers operating off the second LARC (i.e., the Dive LARC), and the EM system was lowered to the Test Area by winch, assisted by the divers. Figure 21 presents images from the FRF Pier of the EM system being launched and recovered. The system weighs approximately 716 pounds (lb) in air and has an estimated buoyancy of 689lb in saltwater. The weight of the submerged system in saltwater is an estimated 27lb, which was easily managed by two divers. To recover the system, this process was performed in reverse.

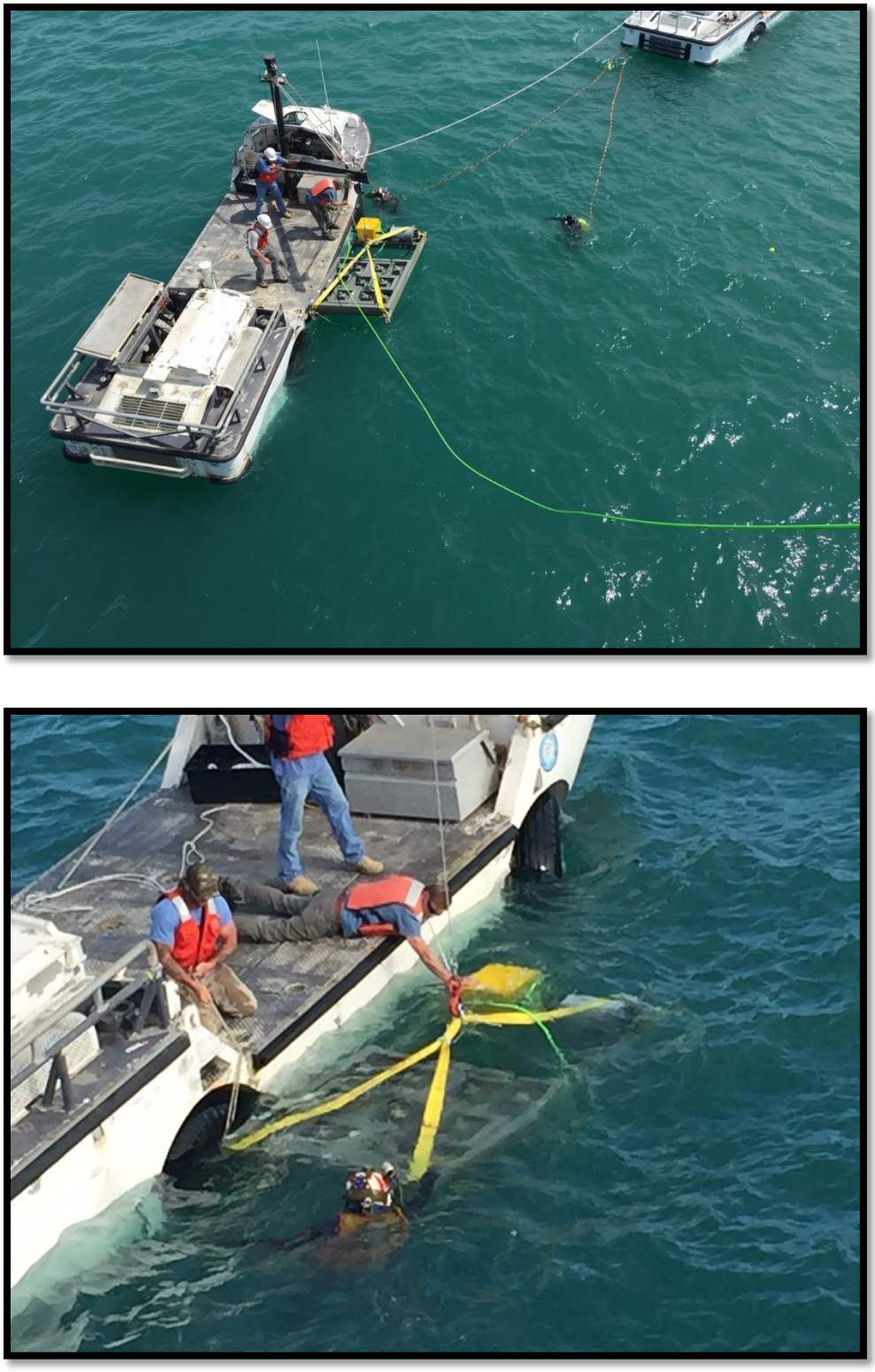

Figure 21. Launch and Recovery of the EM System from the LARC

5.5.2 Underwater System Function Tests

Underwater sensor function tests were performed at the start of underwater cued background survey of May 15th and at the start and finish of underwater cued test item survey of May 16th. Figure 22 - Figure 24 are plots of the SFTs done in saltwater. These SFTs each comprised a set of 11 measurements with a 4" diameter aluminum ball placed on a PVC stand 24cm above the top of each of the 11 receivers in turn (Figure 25). Each SFT figure has four plots showing decays measured by the different receivers with background responses subtracted. Signals > 0 are plotted as solid lines, < 0 as dashed. The upper left plot shows the monostatic Z-axis decays when the ball was over receivers Br, Cr, Er, Fr, Gr, Ir, and Jr. All the curves should overlay. The upper right plot shows Z-axis decays with the aluminum ball over each receiver, excited by the outer (Ht) transmitter. These should all overlay within ±5% and be within a few percent of the monostatic decays shown in the upper left plots. The lower left plot shows X-axis decays for various bistatic combinations (At-Ar, At-Cr, Bt-Br, Bt-Dr, Et-Fr, Dt-Er, Dt-Gr, Ct-Fr, Ft-Kr, Ft-Ir, Gt-Jr, Gt-Hr) with the aluminum ball over the transmit coil. Decays for all of the inner receivers (Br, Cr, Er, Fr, Gr, Ir, and Jr) are plotted in black and should overlay. Decays for the corner receivers (Ar, Dr, Hr, and Kr) are plotted in blue and should be about 1.7 times stronger than the others. The bottom right plot shows Y-axis decays for various bistatic combinations (At-Er, At-Fr, Bt-Fr, Bt-Gr, Et-Ar, Et-Br, Et-Kr, Et-Fr, Dt-Jr, Dt-Br, Dt-Cr, Dt-Ir, Ct-Cr, Ct-Gr, Ct-Jr, Gt-Hr, Ft-Er, Ft-Fr, Gt-Fr, Gt-Gr) with the aluminum ball over the transmit coil. Decays for all inner receivers (Br, Cr, Er, Fr, Gr, Ir, and Jr) are plotted in black and should overlay. Decays for the corner receivers (Ar, Dr, Hr, and Kr) are plotted in blue and should be about 1.3 times stronger than the others.

Transmitter Et was malfunctioning in all of the sensor function tests. Except for receivers Hr, Ir, and Jr, the Z-axis signals from transmitter Ht were significantly different from the expected responses. The monostatic Z-axis response to transmitter-receiver Ht-Hr also differed somewhat in the first test on May 16th, and appeared reasonable during the other two in-water tests; however, monostatic Z-axis response Ht-Hr differed significantly during free-air testing (Figure 22). The cause of this difference is unknown. Additionally, in the Y-axis bistatic tests the Ft-Er and Ft-Fr responses were much too weak.

Based on both free-air and underwater sensor function tests, transmitters Et and Ht and receiver Jr Z-axis were determined unreliable, and an intermittent problem was found with transmitter Ft.

Table 5 presents a summary percent variation in response for the Free-air (May 14th) and Underwater (May 15th-16th) Sensor Function Tests. The percentage variation is against the mean Sensor Function Test response for each of the channels used in processing the Sensor Function Test data.

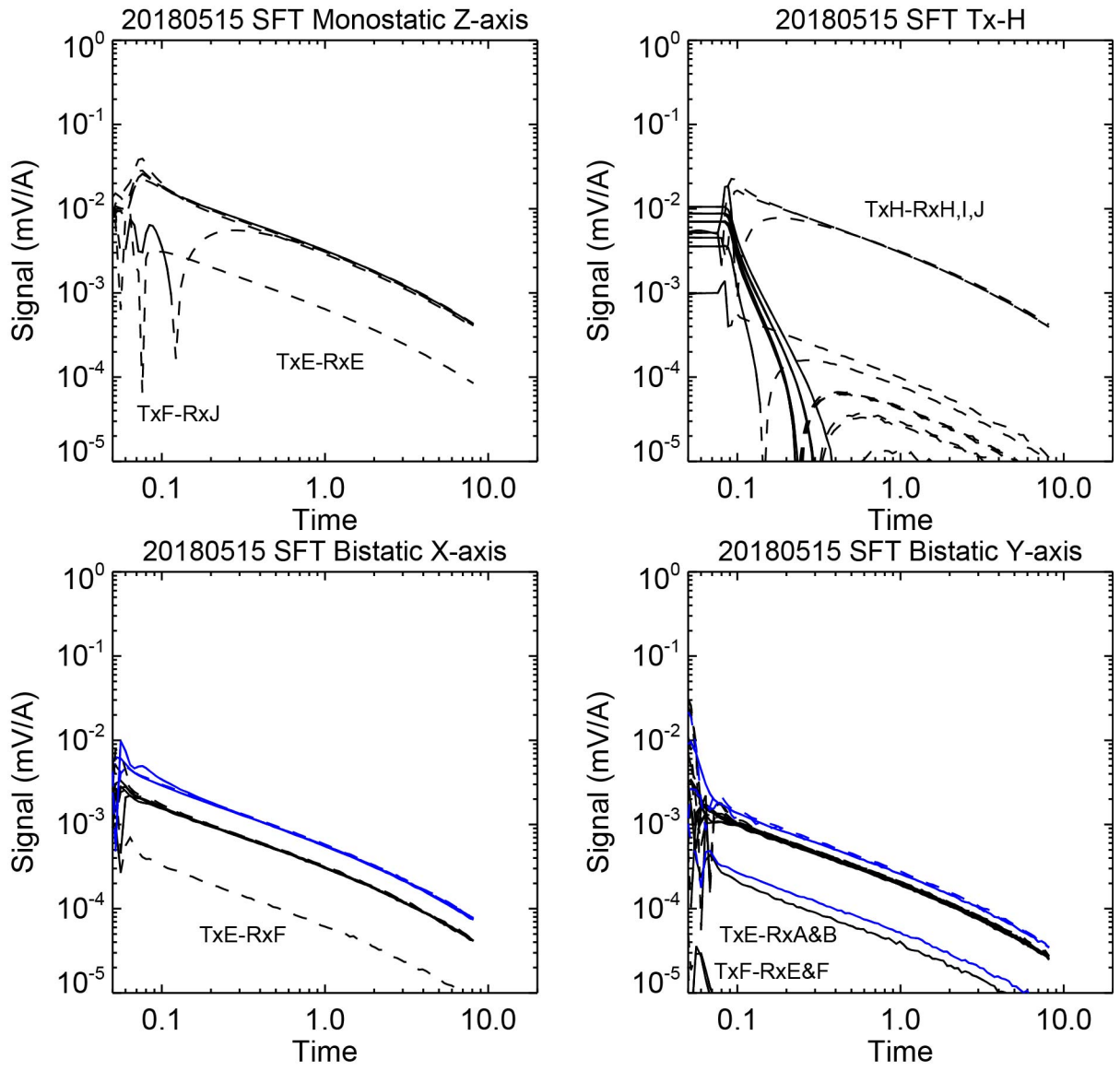

Figure 22. System Function Test with Aluminum Ball in Water on May 15th

Upper left: Monostatic Z-axis responses. All should overlay. Upper right: Z-axis responses to transmitter Ht. All should overlay and have same amplitude as monostatic Z to within 5%. Lower left: Bistatic X-axis responses. Corner receivers in blue, inner receivers in black. Each set should overlay, with corner receiver responses 1.7 times stronger than inner receiver responses. Lower right: Bistatic Y-axis responses. Corner receivers in blue, inner receivers in black. Each set should overlay, with corner receiver responses 1.3 times stronger than inner receiver responses.

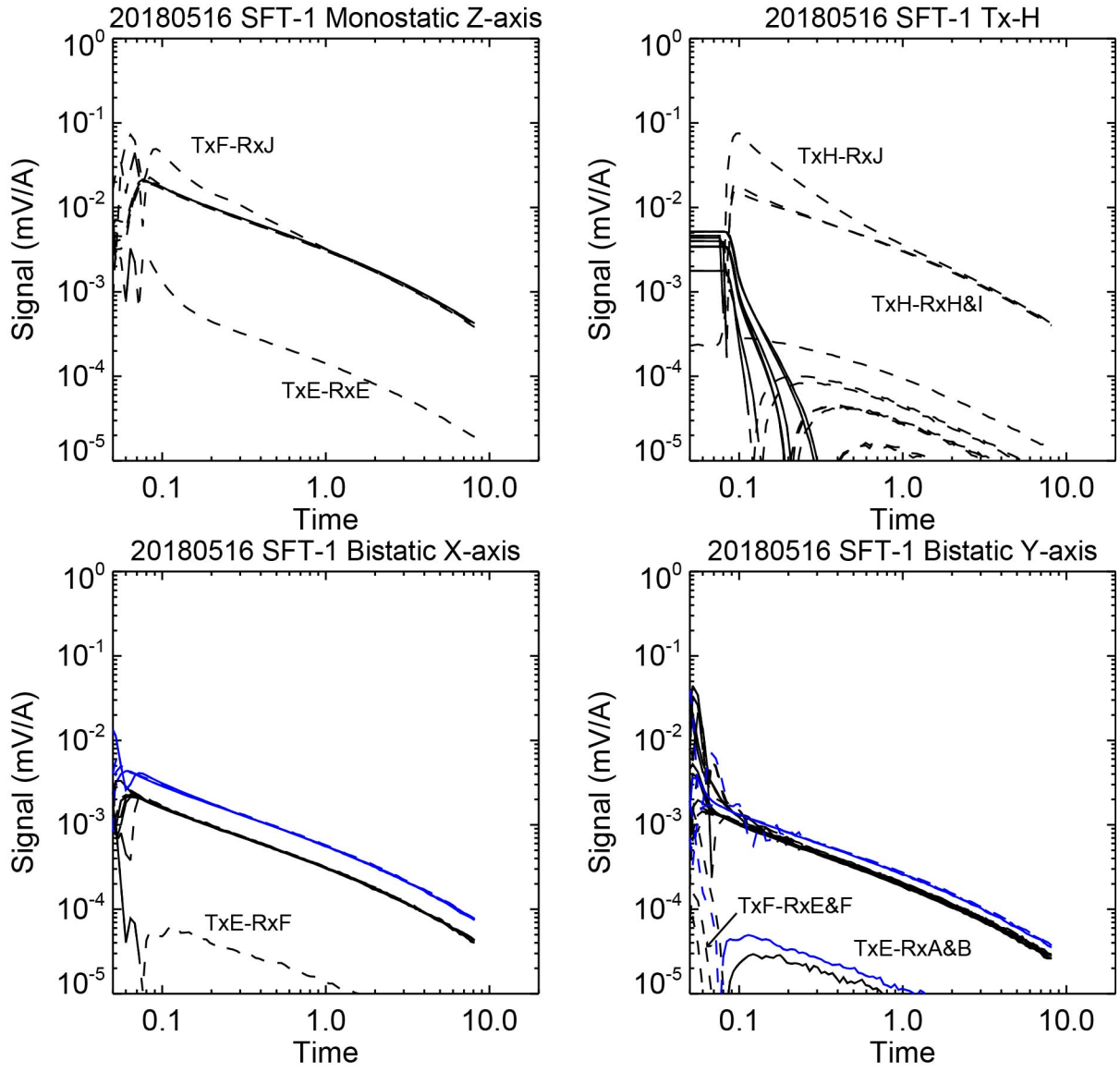

Figure 23. First System Function Test with Aluminum Ball in Water on May 16th

Upper left: Monostatic Z-axis responses. All should overlay. Upper right: Z-axis responses to transmitter Ht. All should overlay and have same amplitude as monostatic Z to within 5%. Lower left: Bistatic X-axis responses. Corner receivers in blue, inner receivers in black. Each set should overlay, with corner receiver responses 1.7 times stronger than inner receiver responses. Lower right: Bistatic Y-axis responses. Corner receivers in blue, inner receivers in black. Each set should overlay, with corner receiver responses 1.3 times stronger than inner receiver responses.

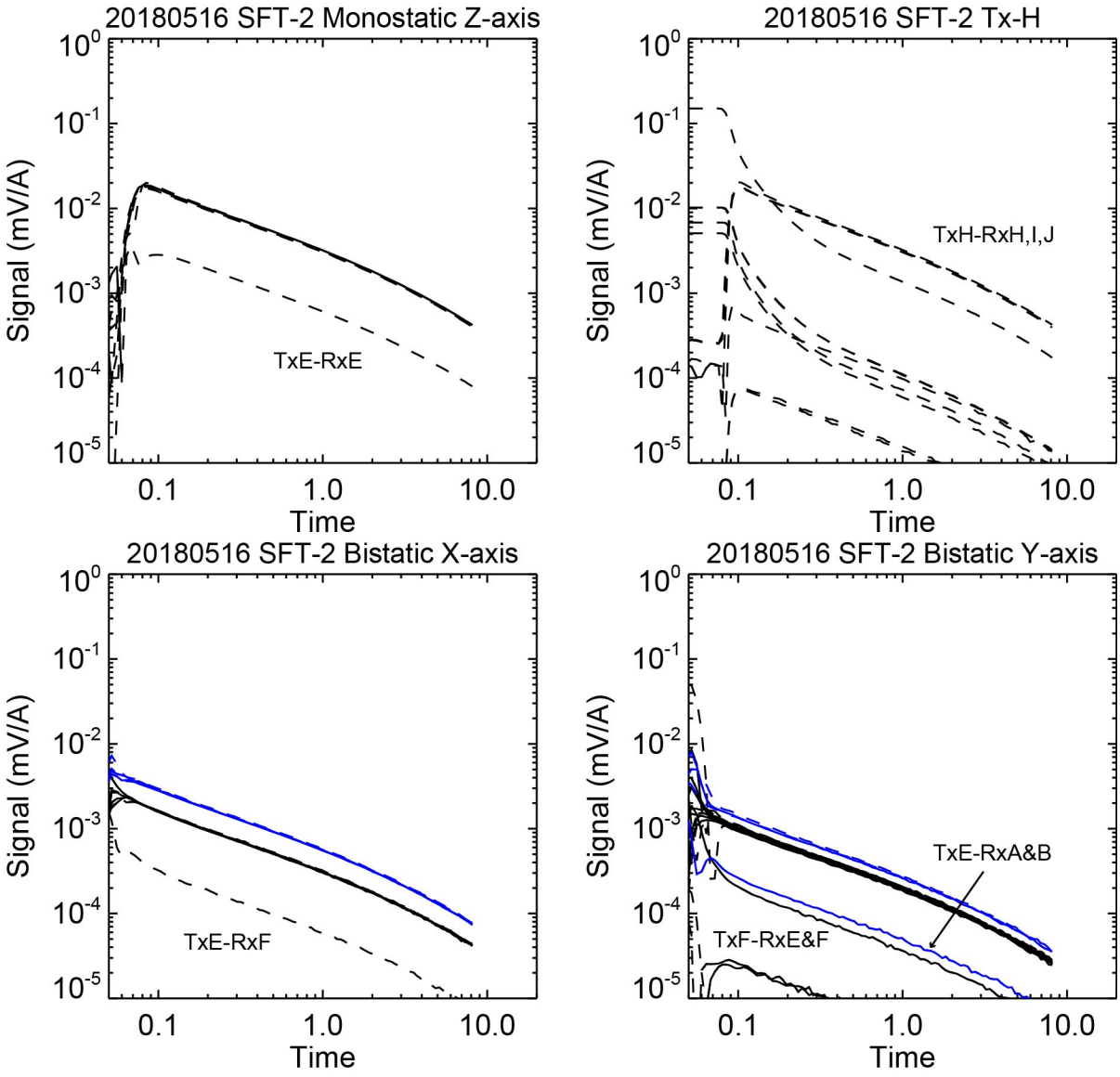

Figure 24. Second System Function Test with Aluminum Ball in Water on May 16th

Upper left: Monostatic Z-axis responses. All should overlay. Upper right: Z-axis responses to transmitter Ht. All should overlay and have same amplitude as monostatic Z to within 5%. Lower left: Bistatic X-axis responses. Corner receivers in blue, inner receivers in black. Each set should overlay, with corner receiver responses 1.7 times stronger than inner receiver responses. Lower right: Bistatic Y-axis responses. Corner receivers in blue, inner receivers in black. Each set should overlay, with corner receiver responses 1.3 times stronger than inner receiver responses.

Table 5. Percent Variation in Response for Sensor Function Test Data

	14 May 2018	15 May 2018	16 May 2018 (AM)	16 May 2018 (PM)
monostatic Z	2.9	4.4	2.2	2.5
bistatic X	4.6	5.9	5.4	5.7
bistatic Y	6.9	5.7	5.5	6.8

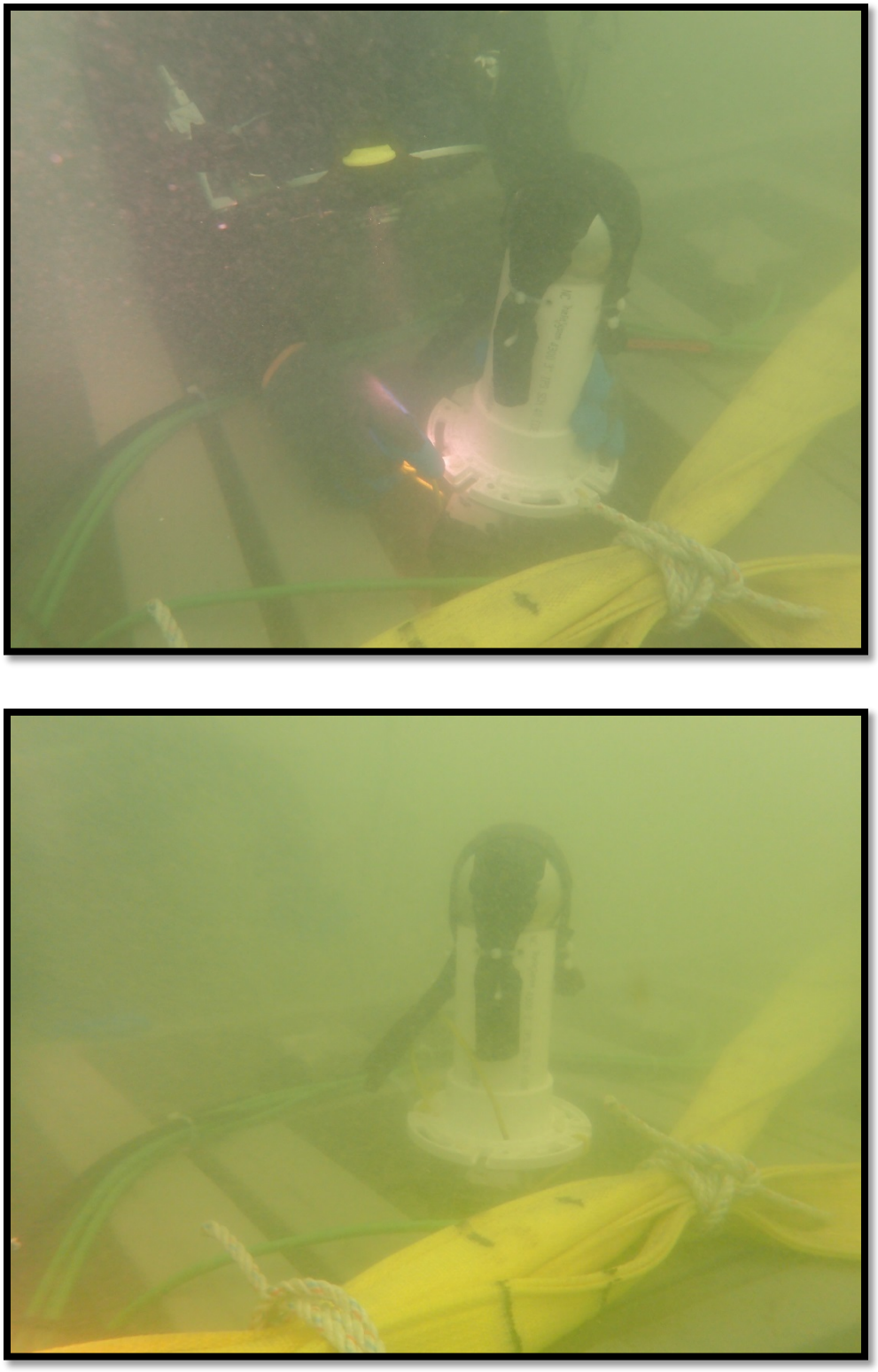

Figure 25. Underwater Sensor Function Testing with Aluminum Ball

5.5.3 Test Area Background Survey

Background measurements were taken at each of the Nodes on May 15th. The background response at Line 2 Node 4 showed evidence of metallic contamination. That was the planned location for the aluminum rod. The aluminum rod was emplaced at Line 2 Node 5 instead, and Node 4 was not used.

The observed background response is compared with model predictions in Figure 26. The data are from Line 2 Nodes 1-3 with an average depth of 7.1m. The plotted data are signals measured at Duck minus the corresponding signals measured in freshwater during the Panama City tests (ESTCP, 2017). Blue symbols are used for positive signals and red for negative. The dashed lines show the RMS variability observed during the background survey, not including Line 2 Node 4. Included is response from the outer transmitter (Ht) measured at receiver Hr because that channel seems to give consistent responses in the System Function Tests (Figure 22 and Figure 23), although other receivers do not. The model calculation is based on the four-layer model (air, water and two sediment layers) from SERDP Project MR-2409. The basic model parameters were water depth 7.1m and water conductivity 4.0 S/m. The two-layer sediment model is consistent with published data on local sediment properties (Miselis, et al, 2006) reporting a homogeneous surface sand layer about 0.77m thick on average, with back-barrier/lagoonal sediments underneath. The conductivity of the upper layer was estimated using Archie's Law (Archie, 1942):

$$\sigma_S = \varphi^m \sigma_w,$$

where σ_S and σ_w are the conductivities of the sand layer and the water, and φ is the porosity of the sand. Using a porosity of 0.45 (Roman-Sierra, et al, 2014) with an exponent value of 1.5 (Jackson, et al 2007), the conductivity of the sand layer works out to be 1.2 S/m. The best fit to the measured background response required a conductivity of 0.6 S/m for the underlying sediments. The model matches the data to about 1ms. Beyond this time, noise effects and possible mismatch between the fundamental background responses at Panama City and Duck adversely affect the measured background response.

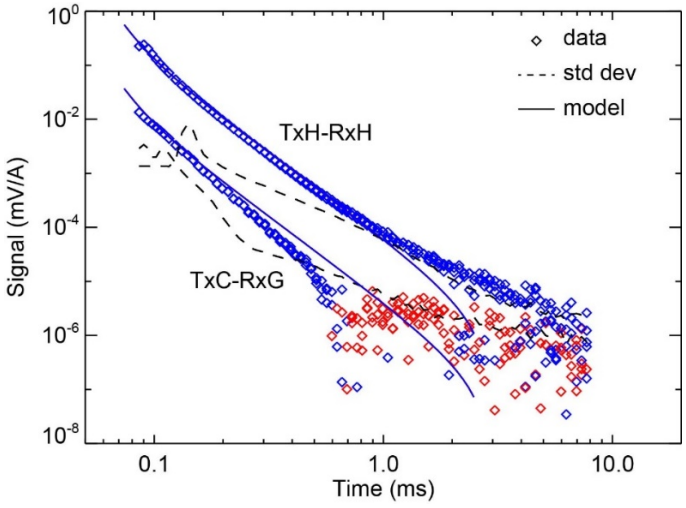

Figure 26. Measured Background Response Compared with Calculated Response Using Models from SERDP Project MR 2409

5.5.4 Test Area Cued Data Survey

The eleven test items were buried in the Test Area on May 15th. The cued survey was performed on May 16th. Figure 27 and Figure 28 present images from the Saltwater Demonstration field effort. The EM system was moved by two divers along each of the Lines, taking background and test item measurements per Node. At each test item location, six measurements were taken with the EM system positioned at different locations relative to the buried test item. The nominal locations of the test item for each of the six measurements are shown in Figure 29. They correspond roughly to (X,Y) = (0,0), (0,-0.25), (0,-0.5), (-0.6,-0.5), (-0.6,-0.25), (-0.6,0). During data collection, the divers retreated away from the EM system. Figure 30 presents a photograph taken by a diver at the approximate offset during data collection.

Figure 27. Surface Weather Conditions May 16th, 2018 at Duck, FRF

The two divers were in constant communication with topside personnel through an in-water communications system, which allowed real-time direction on data collection (e.g., when to move the system to the next location). Marks were made along the outer edges of the EM system at identical distances from the corners on opposite sides, to assist the divers in orienting the EM system over the test items as accurately as possible; however, absolute placement of the system in exact locations was not a demonstration requirement. Non-metallic weights and diver lift-bags were available, but not needed, to help adjust buoyancy and maneuverability of the array.

Figure 28. Test Area Cued Survey

Note Layback from Water Current of Two Diver Umbilicals Between Dive LARC (upper right) and Divers' Bubbles (center left)

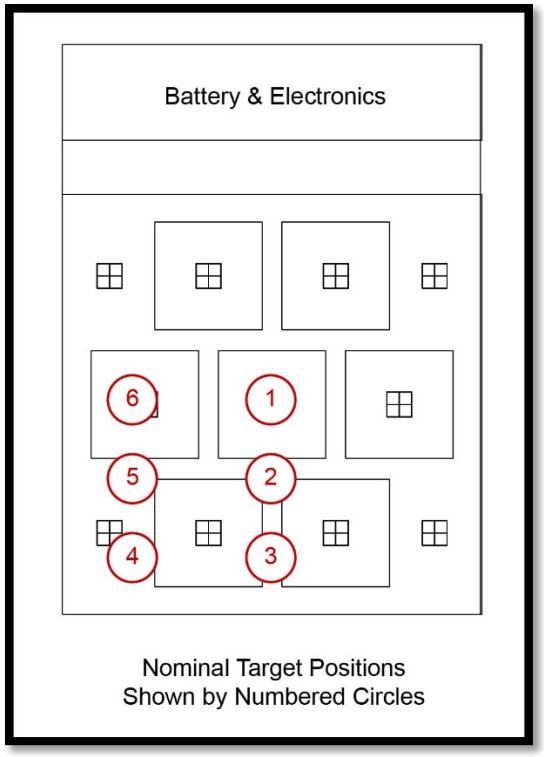

Figure 29. Nominal Measurement Locations

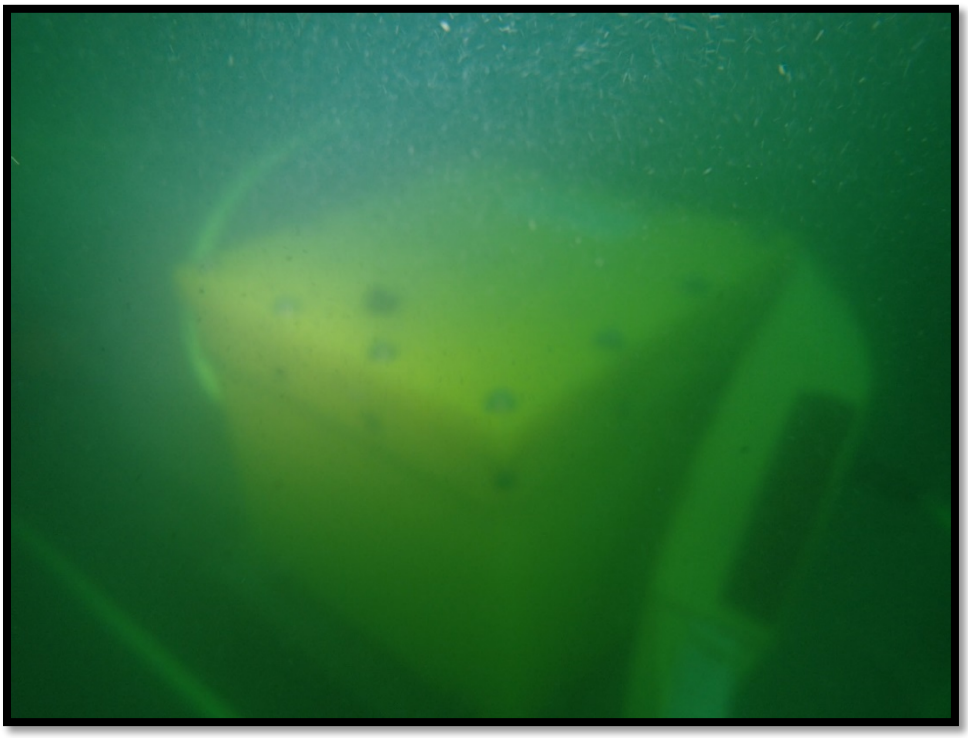

Figure 30. Photograph Taken from Approximate Offset Position of Diver During Data Collection.

5.5.5 Other Data Measurements

5.5.5.1 System Depth Sensor

A small water level sensor (HOBO 30-foot Depth Titanium Water Level Data Logger) was attached to the array superstructure to monitor system depth continuously during deployment. Data were downloaded from the device when the system was recovered at the end of each day. Depth was measured with an Onset HOBO Water Level pressure sensor attached to the array near the electronics housing at a height of 24cm above the bottom when the system was deployed. At some point one of the cable ties holding the sensor broke and it slipped down 10-15cm. A second water level sensor was placed on a workbench in the FRF garage, recording for the same periods of time to provide an atmospheric pressure reference for the depth calculations. Figure 30 shows water depth for each of the data files during the in-water measurements as a function of local time of day. The depth variations are primarily due to tidal variations (see Table 6). The tide range averaged 1.3m.

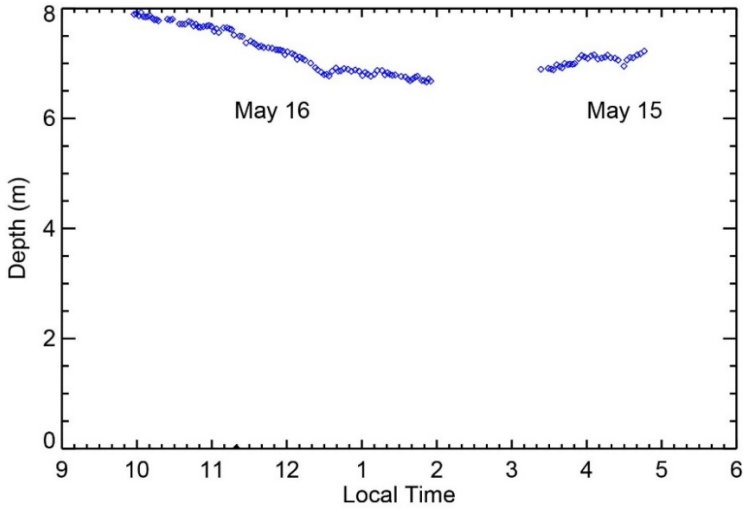

Figure 31. Water Depth During the Saltwater Demonstration as a Function of Local Time

Table 6. Tide Table During Saltwater Demonstration

Date	Time (EDT)	Height (m)	Phase
5/15/2018	1:59 AM	-0.06	low tide
5/15/2018	7:59 AM	1.10	high tide
5/15/2018	1:58 PM	-0.06	low tide
5/15/2018	8:20 PM	1.34	high tide
5/16/2018	2:47 AM	-0.09	low tide
5/16/2018	8:48 AM	1.10	high tide
5/16/2018	2:45 PM	-0.09	low tide
5/16/2018	9:08 PM	1.34	high tide

5.5.5.2 Seawater Conductivity Measurements

Water conductivity was determined from Conductivity Temperature Depth (CTD) profiles taken from the pier three times a day using FRF's CTD sensor. Figure 32 shows conductivity profiles for the two days of in-water testing (May 15th and 16th, 2018). Surface waters had a conductivity of 4 S/m. Conductivity did not vary with depth on May 15th. A slight thermocline was present at 4-6m on May 16th, with bottom water conductivity reduced to 3.7 S/m.

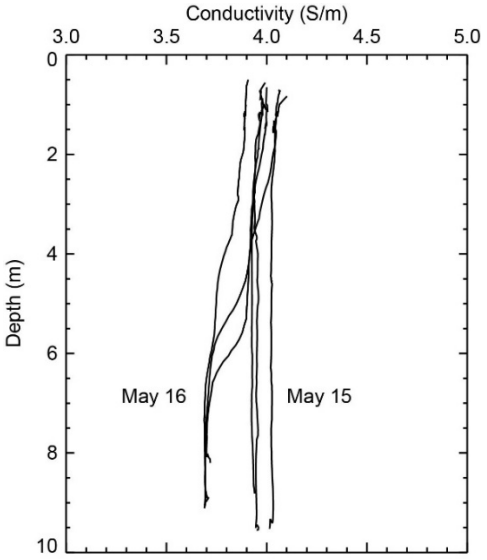

Figure 32. Conductivity Profiles During the Saltwater Demonstration

5.6 VALIDATION

Not applicable.

Page Intentionally Left Blank

6.0 DATA ANALYSIS AND PRODUCTS

Dr. Thomas Bell (Leidos) performed data analyses offsite during the Pre-Deployment Testing, onsite during the Saltwater Demonstration, and on-going offsite after the Saltwater Demonstration.

6.1 PREPROCESSING

Data from the EM system were downloaded in HDF5 format and imported to the Interactive Data Language (IDL) processing environment. Data were leveled using background measurements collected within the Test Area in close proximity to the test items (see Section 5.5.3).

6.2 TARGET SELECTION FOR DETECTION

This Demonstration did not include a detection-then-classification progression. The goal of this Demonstration was to collect EM response data of known seeded test items and known backgrounds. The seeded test items (Table 2) were selected to include all test items measured during the 2016 Freshwater Demonstration, and to add smaller munitions types to test classification (i.e., 20mm and 37mm projectiles) and other common items (60mm and 81mm projectiles, and 2.75" rockets).

6.3 PARAMETER ESTIMATION

As in the 2016 Freshwater Demonstration at Panama City, background-subtracted target data were inverted to estimate target polarizabilities using the UX-Analyze dipole fit algorithm with SNR weighting. Malfunctioning data channels identified during EM system testing were not included in parameter estimation. Calculated polarizabilities were compared with free-air polarizabilities using the UX-Analyze classification algorithm. For this, "signal" is the absolute value of the measured response (at each time gate for each transmit-receive pair) after background subtraction and "noise" is the standard deviation of the measured background responses. Figure 33 (solid lines) shows the noise levels for monostatic and bistatic Z and X,Y channels during the seed target measurements. The dashed lines show the corresponding noise levels during seed target measurements in the Panama City fresh water pond test. The noise levels for the two tests are comparable.

The dipole fit quality is measured by the fit coherence, equal to the Pearson correlation coefficient of the data and the modeled response. The variance in the measurements which is not accounted for by the modeled response is equal to one minus the fit coherence squared. Fit quality generally improves with the target's signal-to-noise ratio. Figure 34 is a plot of dipole fit quality versus SNR. The dashed line shows the expected inverse proportionality between one minus fit coherence and the SNR. On this diagonal a fit coherence of 0.85 is reached at a SNR of about 25, and all but one of the targets with SNR > 30 has a fit coherence > 0.9. The exception was the aluminum rod in position 6, and it appears that the rod was off to the side of the array and poorly illuminated because some of the nearby transmit receive combinations were malfunctioning.

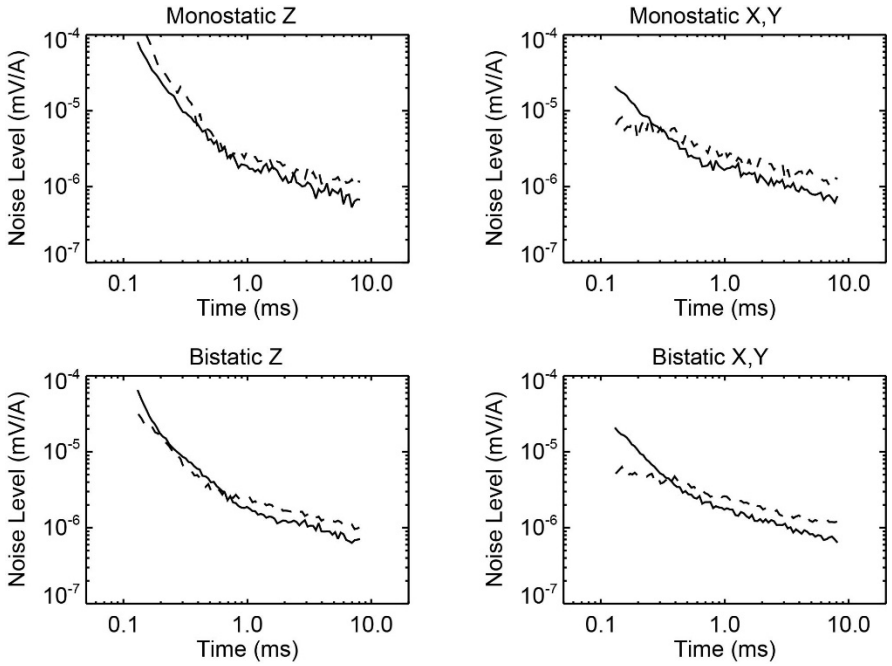

Figure 33. In-water Monostatic and Bistatic Z and X,Y Noise Levels for the Duck Saltwater Target Measurements (solid lines). Dashed Lines Show the Corresponding Noise Levels for the Panama City Freshwater Target Measurements.

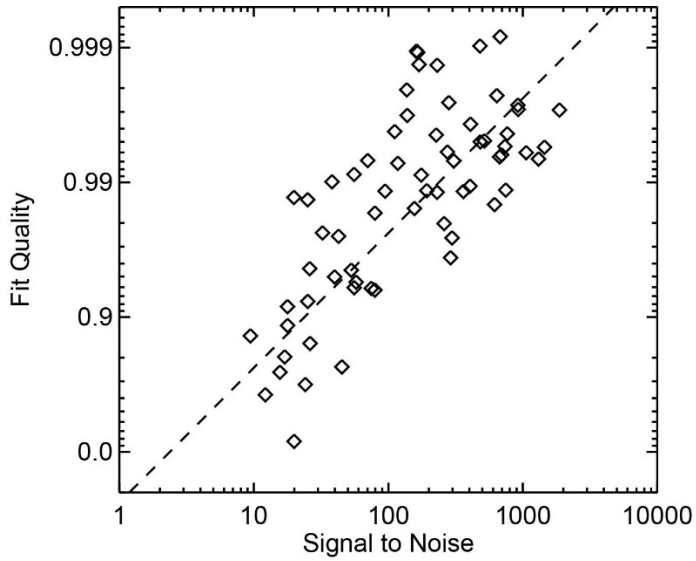

Figure 34. Dipole Fit Quality versus SNR.

Dashed line corresponds to 1 – fit coherence inversely proportional to SNR

6.4 CLASSIFIER AND TRAINING

The UX-Analyze algorithm was used to compare modeled results to the library, but true classification and training was not performed (or applicable) for this Demonstration. A discussion of library match results per test item is included in Section 7.0.

The UX-Analyze polarizability match metric is a combination of three comparisons between target and reference polarizabilities. The first comparers the strengths of the primary polarizabilities and the other two compare ratios of secondary to primary polarizabilities for the target and reference

The in-water versus in-air polarizability match improves with the quality of the in-water dipole fit. This is illustrated in Figure 35. There is one outlier in that plot, corresponding to the 105 HEAT in position 3. This has a good dipole fit (0.997) but a poor match to the in-air polarizability (0.57). Visually, there is not much difference between the in-air and in-water polarizabilities. Based on the strength of the polarizabilities the target appears to be the correct size, although the in-water polarizabilities suggest a more spherical or plate-like target than a munitions-shaped one. In the past, we have observed that HEAT rounds can be somewhat problematic depending on how they are illuminated.

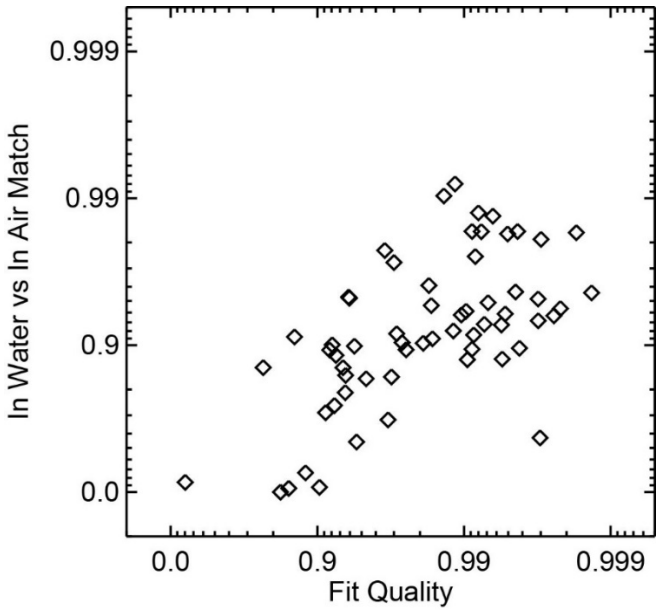

Figure 35. In-water vs In-air Polarizability Match Metric vs In-water Dipole Fit Quality.

The following eleven pages of figures compare the in-water polarizabilities with the corresponding in-air polarizabilities for all target measurements (Figures 36a – k). Except for the 20mm projectile, measurement data result in good fits to the saltwater data with polarizabilities that match the corresponding free air polarizabilities. The exceptions seem to correspond to situations where the target is off to the side of the array and/or not sufficiently illuminated because of malfunctioning Tx-Rx channels (see Figure 37). The 20mm projectile appears to have been too far from the array to give sufficiently strong response.

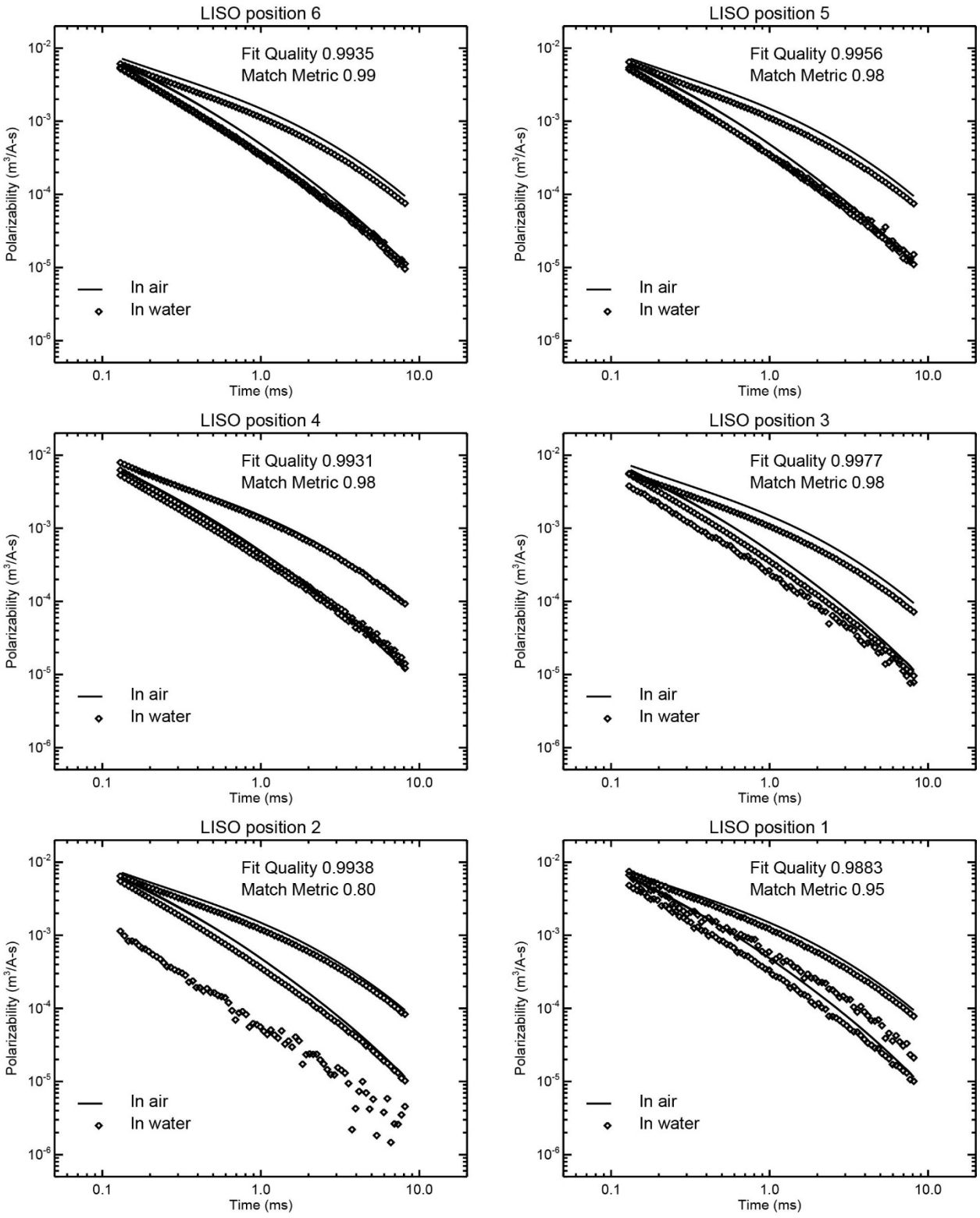

Figure 36a. Large ISO Polarizability Curve Comparisons

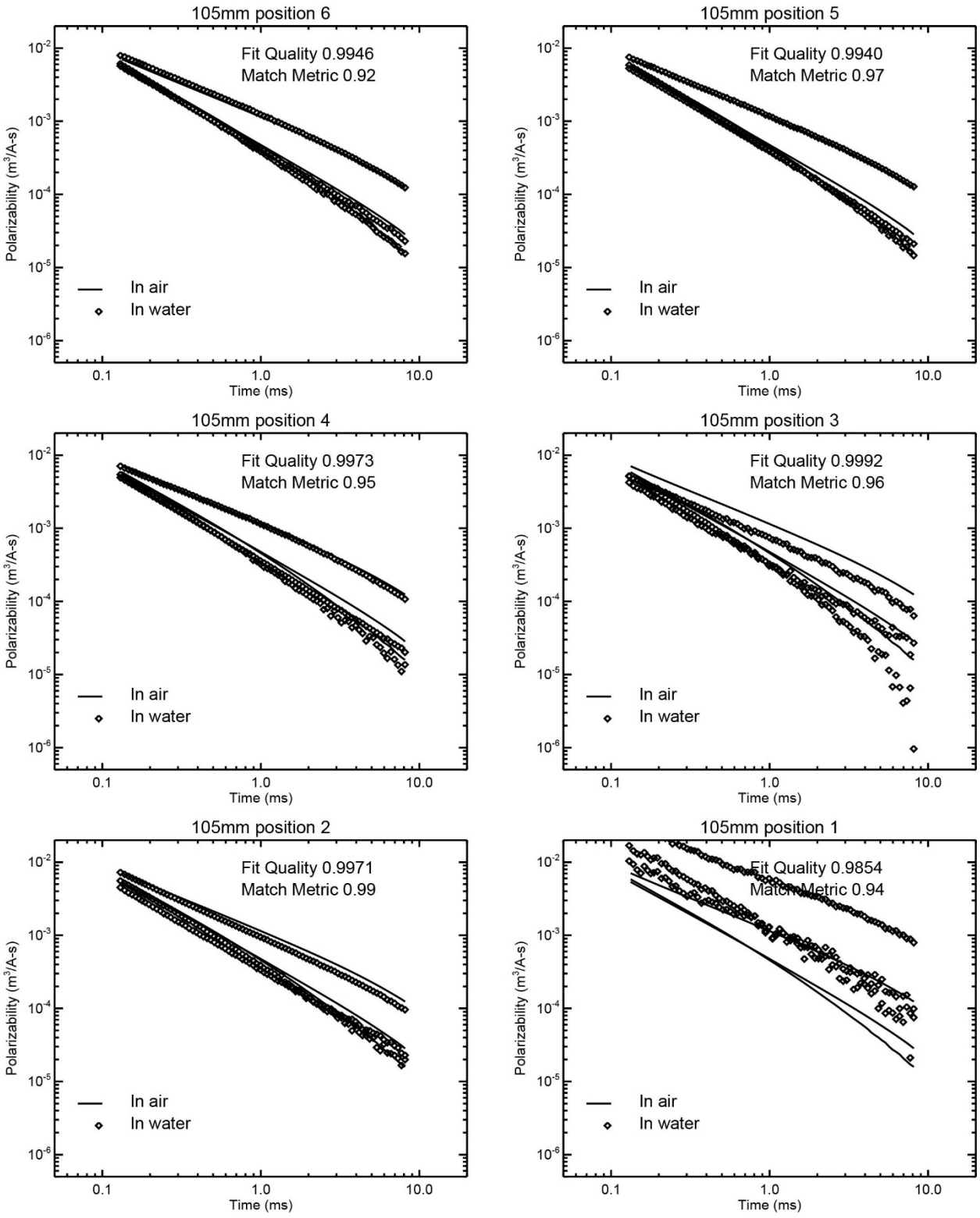

Figure 36b. 105mm Polarizability Curve Comparisons

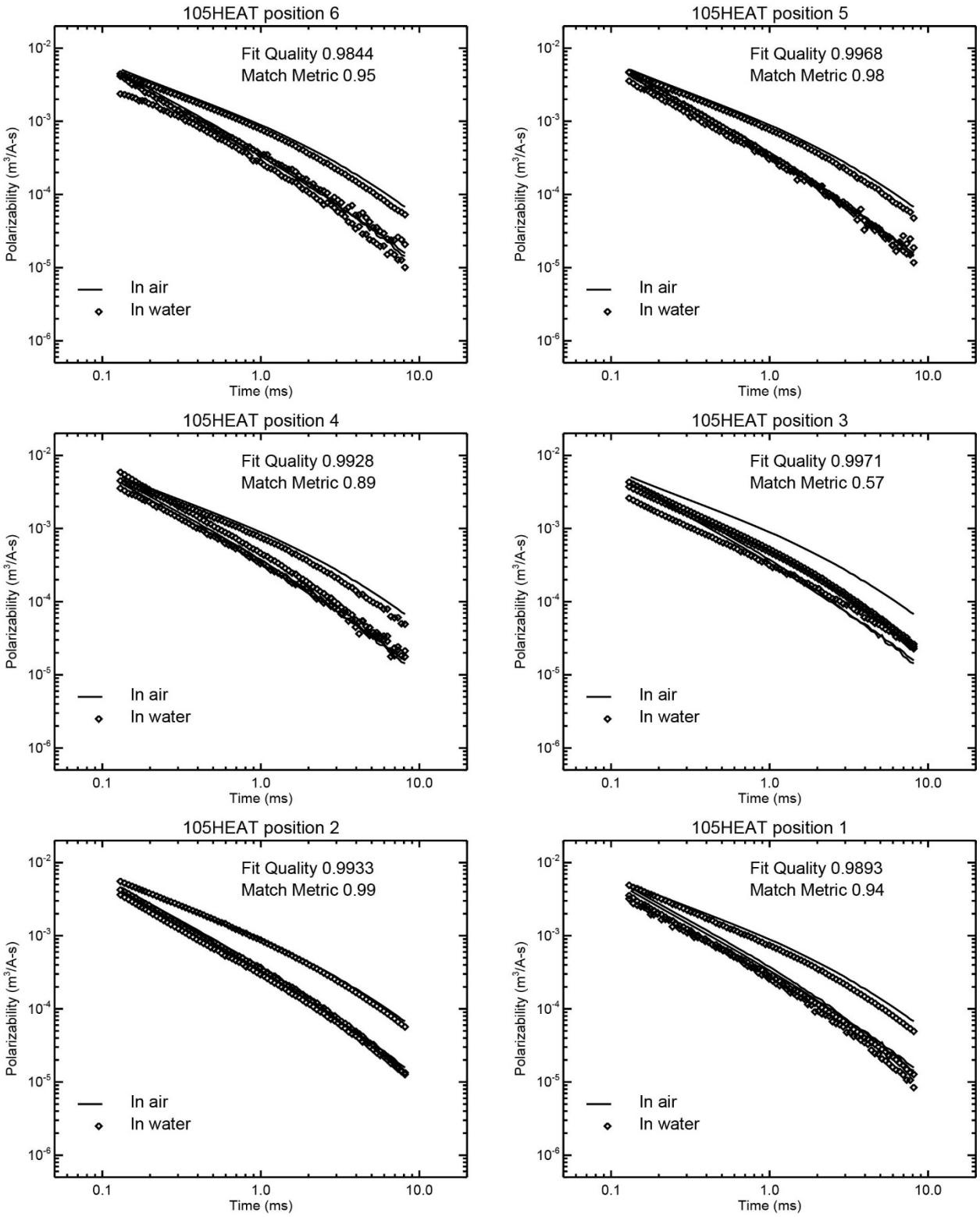

Figure 36c. 105HEAT Polarizability Curve Comparisons

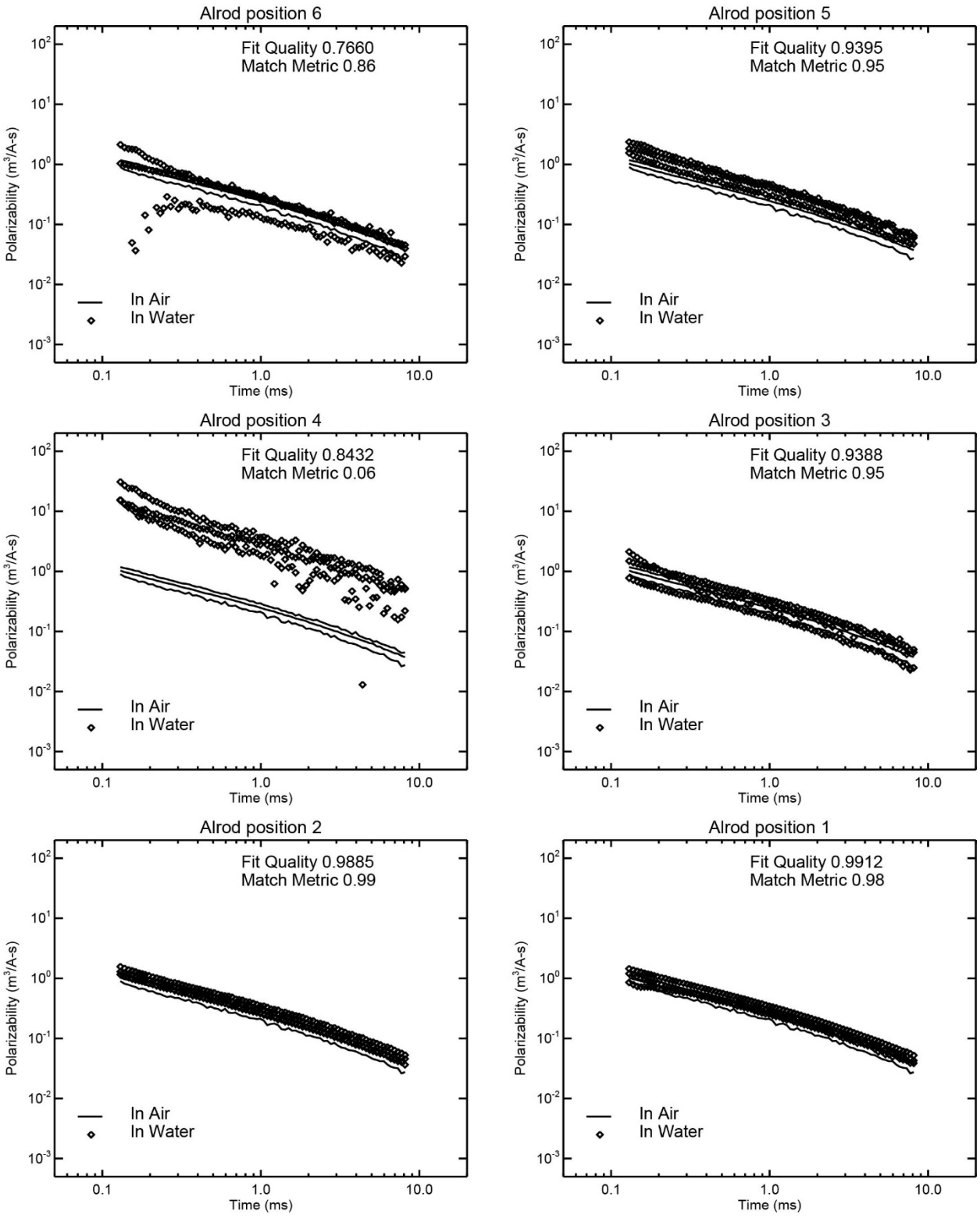

Figure 36d. Aluminum Rod Polarizability Curve Comparisons

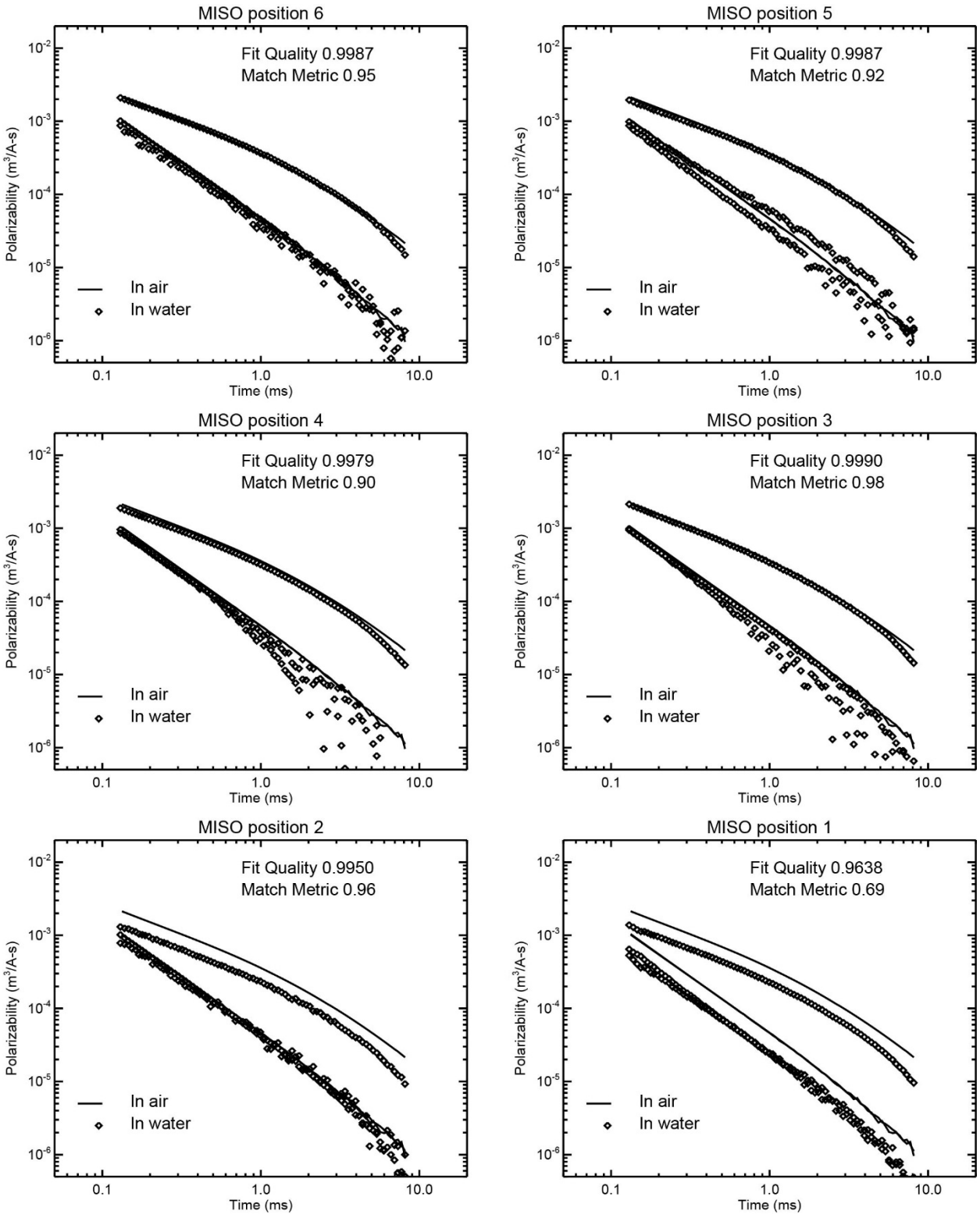

Figure 36e. Medium ISO Polarizability Curve Comparisons

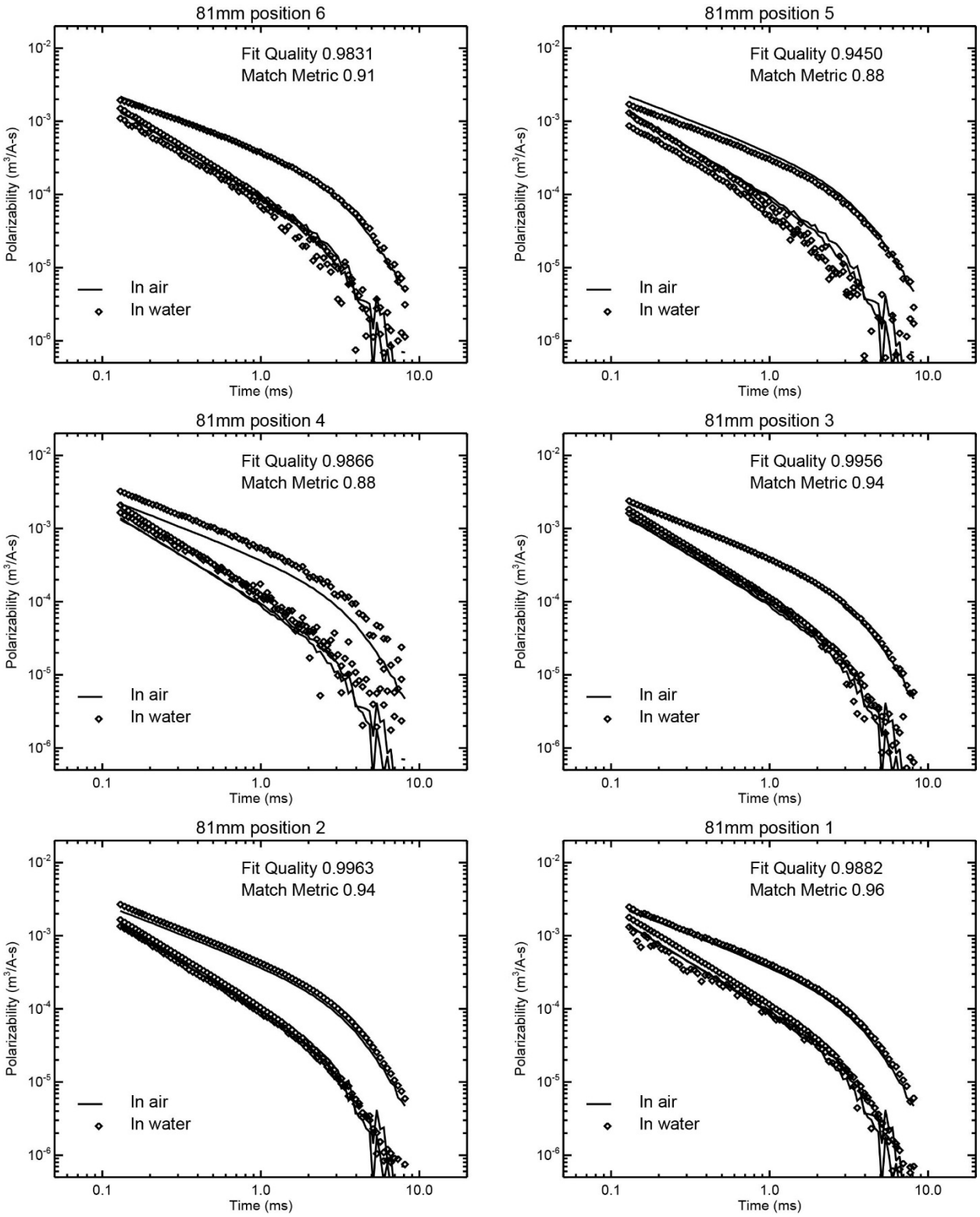

Figure 36f. 81mm Polarizability Curve Comparisons

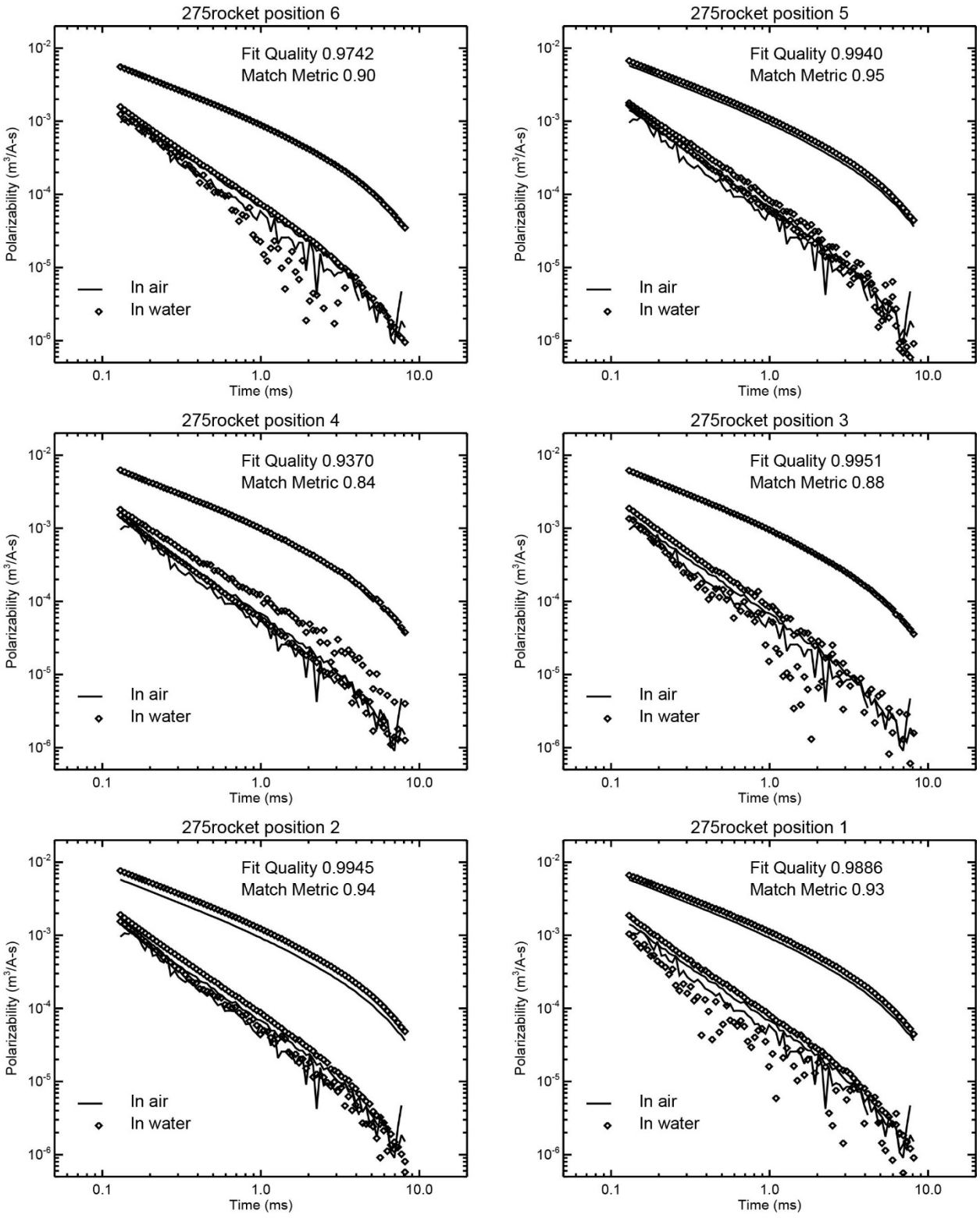

Figure 36g. 2.75in rocket Polarizability Curve Comparisons

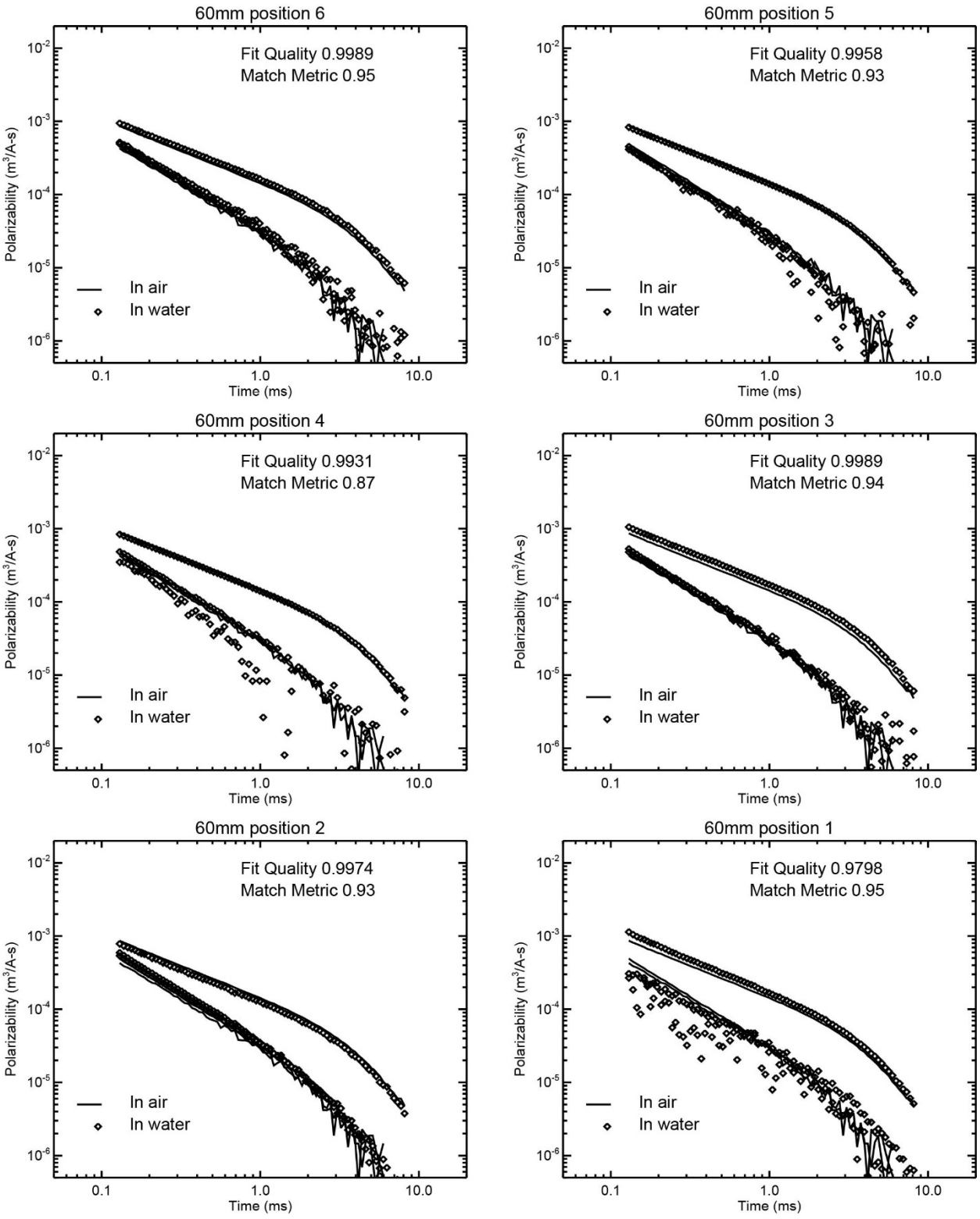

Figure 36h. 60mm Polarizability Curve Comparisons

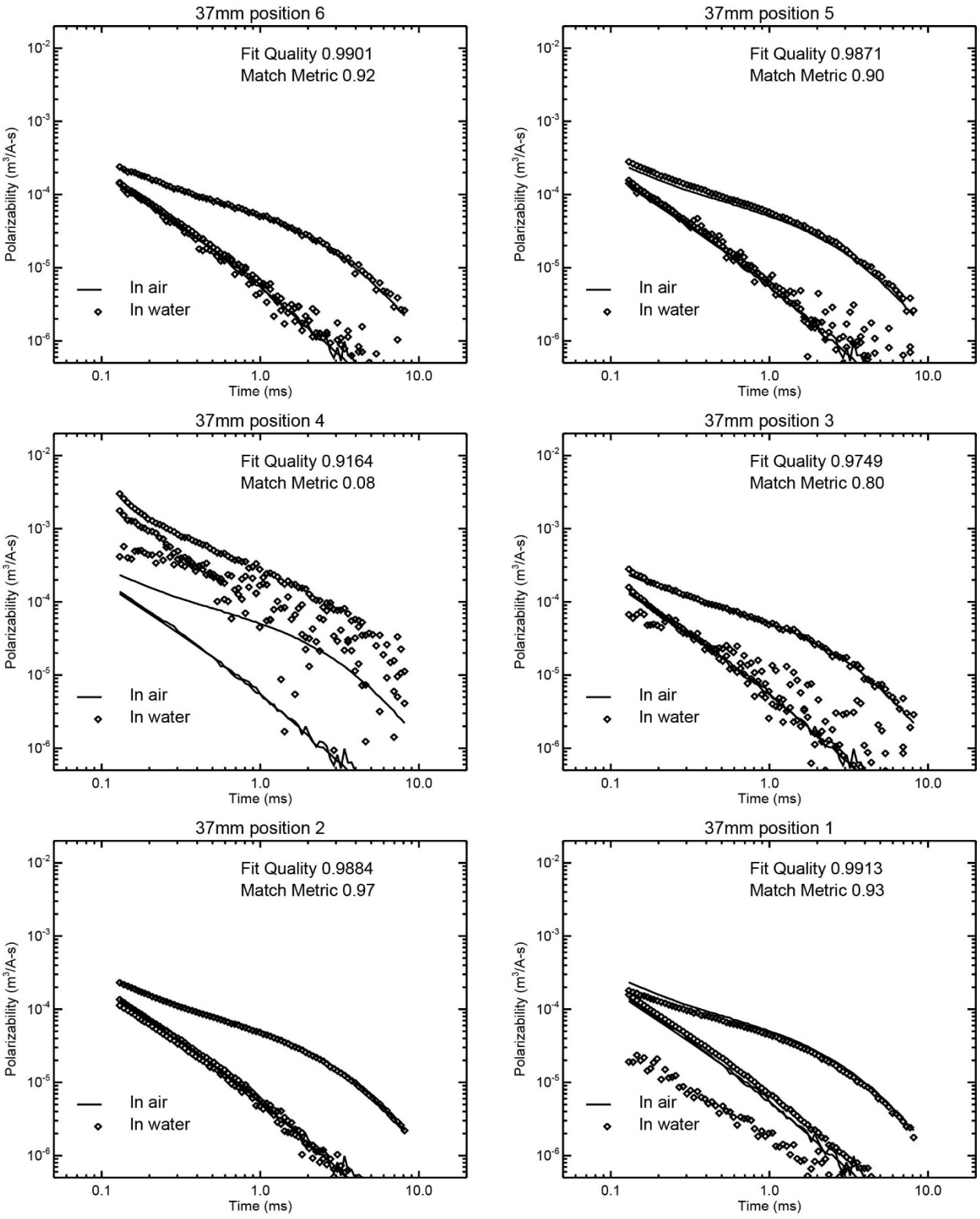

Figure 36i. 37mm Polarizability Curve Comparisons

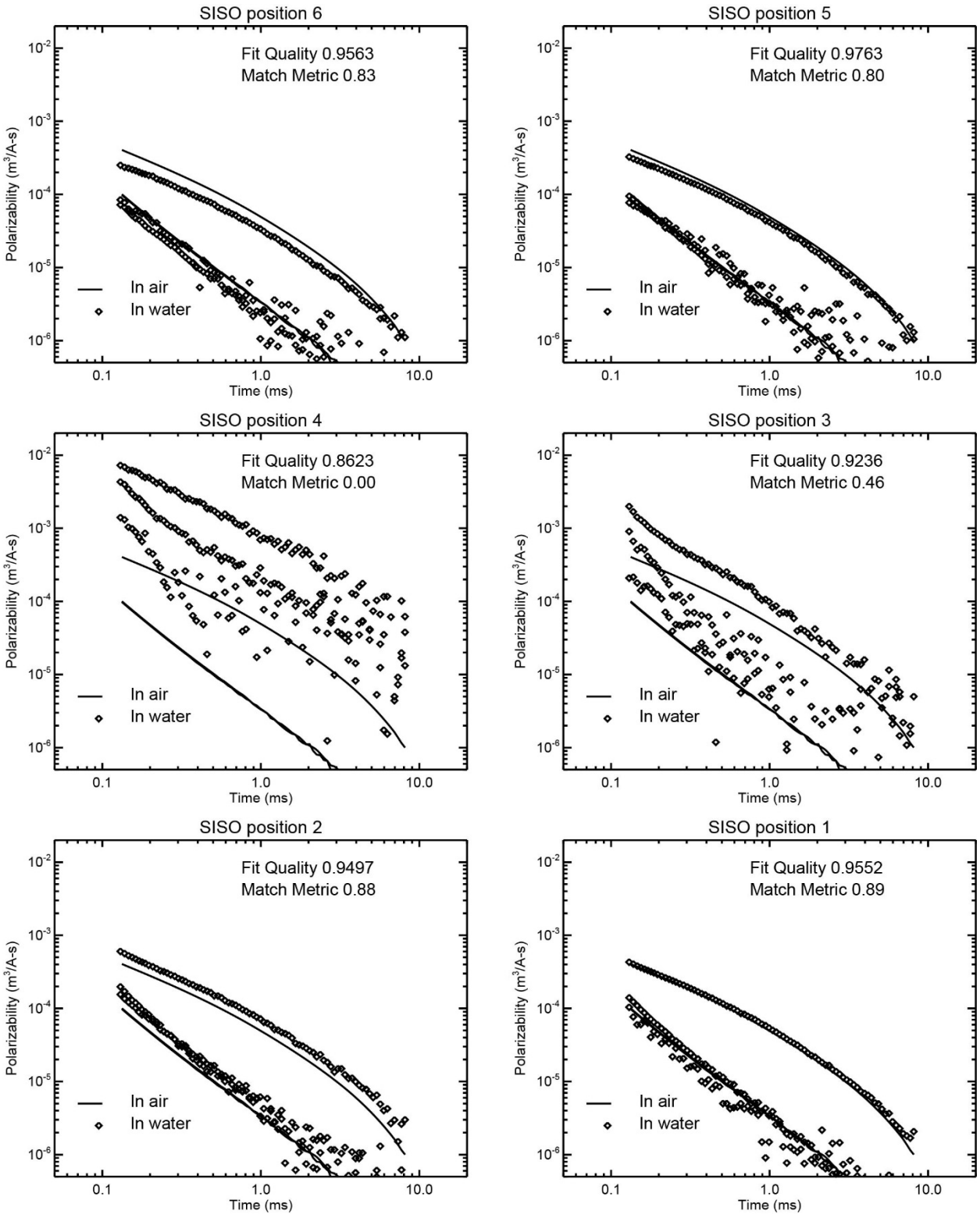

Figure 36j. Small ISO Polarizability Curve Comparisons

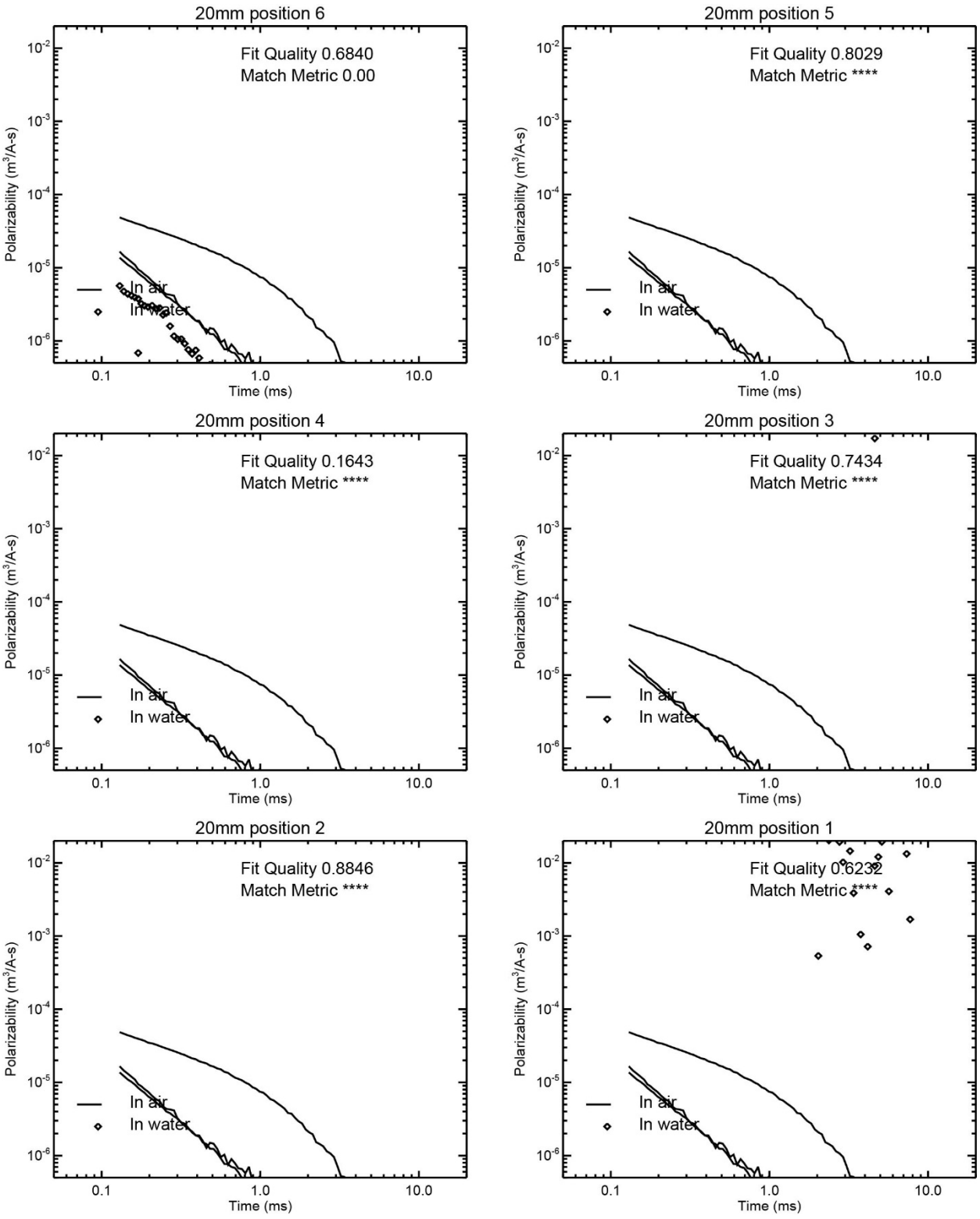

Figure 36k. 20mm Polarizability Curve Comparisons

6.5 DATA PRODUCTS

Data produced during the Saltwater Demonstration include EM system raw files (i.e., HDF5), field notes, processed data sets, archived data sets (e.g., CSVs) and other data files created during advanced geophysical classification. Project data were archived at the close of the Demonstration with instructions for future data users.

Page Intentionally Left Blank

7.0 PERFORMANCE ASSESSMENT

As in the 2016 Freshwater Demonstration at Panama City, background-subtracted target data were inverted to estimate target polarizabilities using the UX-Analyze dipole fit algorithm. Malfunctioning data channels (Et, Ft, and Ht transmitter data and Jr receiver Z-axis) were not included, and the first 18 timegates ($t < 0.132$ ms) were not used. The calculated polarizabilities were compared with free-air polarizabilities using the UX-Analyze classification algorithm. The results are summarized in Table 2 and Table 3. To maintain some consistency with performance of the standard 2x2 TEMTADS and MetalMapper (which have 48 data channels), the tabulated signal to noise ratio (SNR) is the average over the strongest 48 channels in the EM system. The "pol dev" is the average fractional difference between measured and library polarizabilities. Fifty-eight of the 66 target measurements (88%) have fit coherence >0.8. This is suspected to be a signal to noise issue. Fifty-three of 53 (100%) measurements with SNR > 30 have fit coherence >0.8. Only 40 of the targets (61%) have a library match metric >0.9. Restricted to targets with SNR >30, the percentage of targets with library match metric increases to 74% (39 of 53).

Figure 37 compares the target fit locations (diamonds) with the nominal target locations (red circles). The deviations are due to combined effects of inversion failures and uncertainty in the actual EM system's location. Less than half (31 of 66) of the target fit locations are within 0.4m of the nominal location. A similar fraction (23 of 53) of targets with SNR > 30 have fit locations within 0.4m of the nominal location.

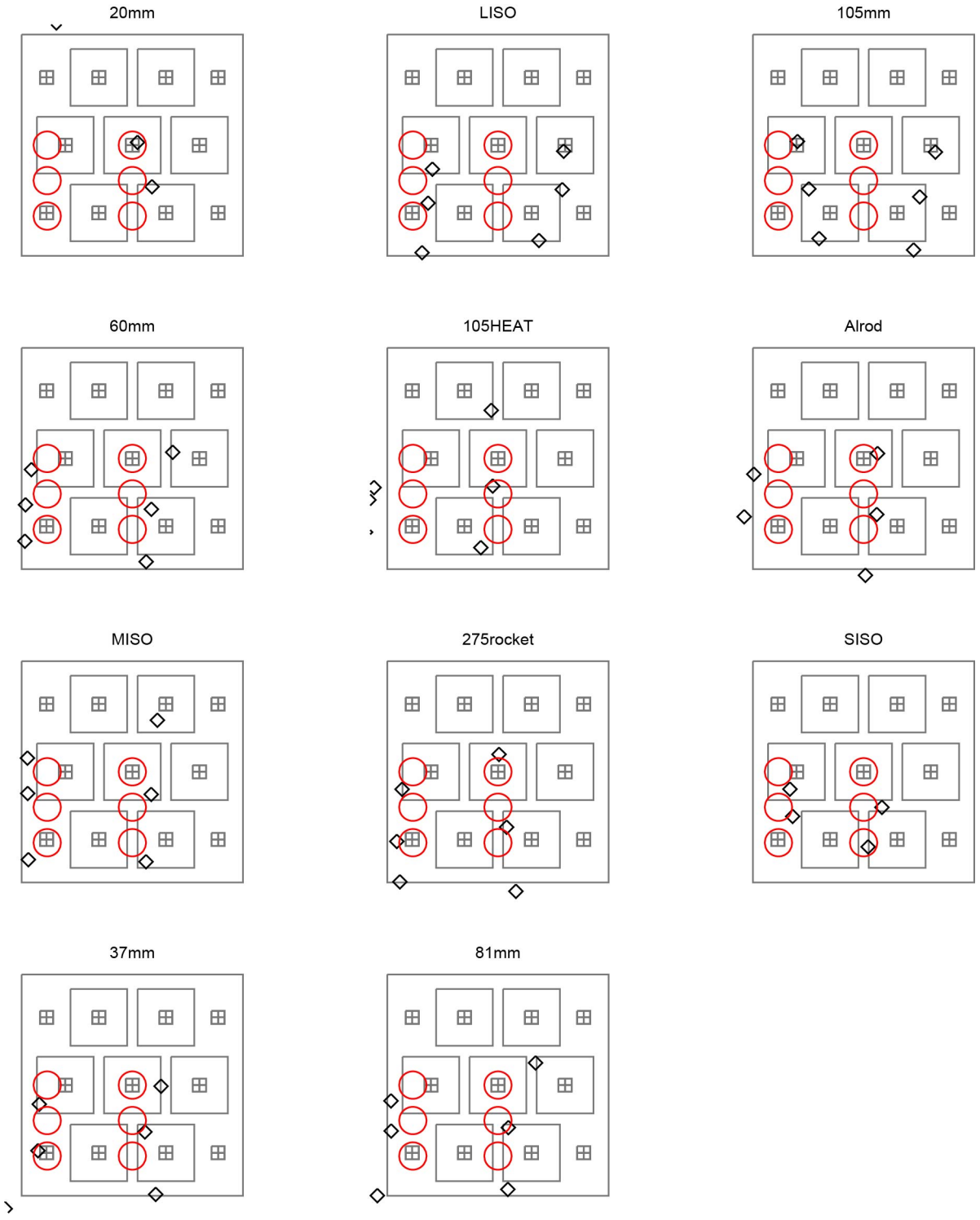

Figure 37. Target Fit Locations (Diamonds) Compared to Nominal Target Locations (Red Circles).

There is no indication that having the array in seawater affects its classification performance. By way of example, Figure 38 shows 60mm polarizabilities measured in seawater (symbols) and the corresponding free-air library polarizabilities. For this target the SNR is 162, the fit coherence is 0.9989, and the library match metric is 0.95.

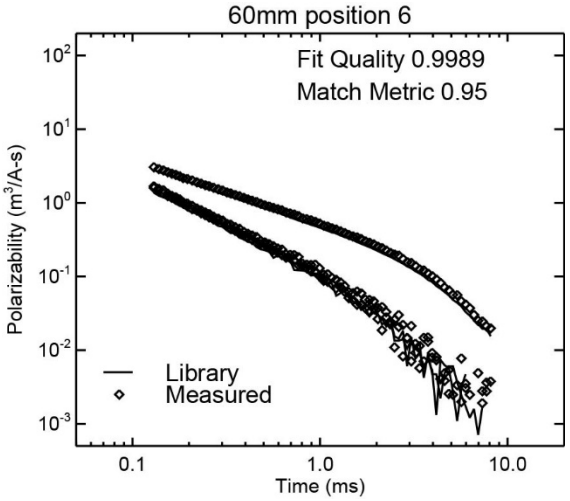

Figure 38. 60mm Polarizabilities Measured in Seawater Compared to In-air (Library) Polarizabilities.

Page Intentionally Left Blank

8.0 COST ASSESSMENT

No Cost Assessment was performed for the Saltwater Demonstration. Any cost assessment for production use of the EM system would have limited accuracy and usefulness due to the short duration of the Saltwater Demonstration and the overall goal of MR-201313. Additionally, certain costs did not apply to the demonstration (e.g., deployment vessels), or were not included in the demonstration (e.g., EOD-qualified divers and intrusive operations).

Page Intentionally Left Blank

9.0 IMPLEMENTATION ISSUES

The underwater EM system demonstrated is custom-built by Geometrics. The hardware and software are based on the commercially-available Metal Mapper. Though the demonstration was successful, no subsequent demonstrations are planned to progress the EM system from a prototype to commercially available equipment.

Data collection times and transit times between cued data collection locations are minimal compared to the time required to launch and recover the EM system. Improvements to deployment methods will improve overall efficiency, production rates, and cost effectiveness.

Vessel navigation and dive operations for underwater cued AGC data collection are significantly different from traditional underwater geophysical operations (e.g., DGM), and require specialized skills and equipment. For example, real time data review is best implemented with continuous communication between a topside Data Team and the Dive Team.

Divers must be able to safely transport the EM system between cued data collection locations, typically in low visibility settings. The size and weight of the EM system in its current configuration requires two divers to transport with both hands. Reducing the number of transmitters and receivers in the EM system array is possible, and would reduce its dimensions and drag, but would also reduce the effective footprint of the cued data collection and the 'positioning error budget' for effectively illuminating the subsurface item. This may be a permissible reduction in EM system performance if positional data are incorporated into cued AGC data collection.

The LARCs used in the Saltwater Demonstration are larger than necessary and are the property of USACE FRF. Smaller vessels can deploy the current EM system and vessel requirements must be considered for future underwater EM systems. Commercially-available vessels (e.g., pontoon boat) could be used or modified to launch and recover the EM system.

The finite lengths of the divers' surface supplied air umbilical cords and the EM system's data cables limit the workable configurations between the two LARCs, the divers, and the topside data acquisition computer. The distance between the LARCs must be far enough to prevent collision, but less than the length of the umbilical cord so that the divers can assist with launch and recovery. The data acquisition computer, whether on a vessel or fixed (e.g., on the FRF pier during this demonstration), must be close enough to the divers and EM system to not stretch or break the data cable (currently 70m). This may be improved by placing the data acquisition computer on a vessel.

Page Intentionally Left Blank

10.0 REFERENCES

Archie GE. 1942. *The electrical resistivity log as an aid in determining some reservoir characteristics.* Transactions of the AIME. 146(01):54-62.

ESTCP. 2017. *System Performance Report, Underwater Advanced Time-Domain Electromagnetic System, MR-201313.*

Jackson, Darrell, and Michael Richardson. 2007. *High-frequency seafloor acoustics.* Springer Science & Business Media, p. 106.

Miselis, Jennifer L., and Jesse E. McNinch. 2006. *Calculating shoreline erosion potential using nearshore stratigraphy and sediment volume: Outer Banks, North Carolina.* Journal of Geophysical Research: Earth Surface 111.F2.

Popenoe, P., and Ward, L.W. 1983. *Description of high-resolution seismic reflection data collected in the Albemarle and Croatan Sounds, North Carolina.* U.S. Geological Survey Open-File Report 83-513.

Román-Sierra, Jorge, Juan J. Muñoz-Perez, and Marina Navarro-Pons. 2014. *Beach nourishment effects on sand porosity variability.* Coastal Engineering 83: 221-232.

USACE. 2015. *Final Site Inspection Report, Former Naval Duck Target Facility, Duck, N.C.*

USACE. 2017. *Draft Remedial Investigation Report, Former Naval Duck Target Facility, Duck, N.C.*

United States Department of Interior. 1977. *Soil Survey of the Outer Banks, North Carolina.*

Page Intentionally Left Blank

APPENDIX A POINTS OF CONTACT

Point of Contact Name	Organization	Phone Email	Role in Project
Steve Saville	CH2M 2095 Lakeside Centre Way Suite 200 Knoxville, TN 37922	720-261-5367 Steve.Saville@ch2m.com	Principal Investigator
John Mogray	CH2M	828-446-7676 John.Mogray@ch2m.com	Engineering Dive Lead
Nick Odlum	Geometrics	408-428-4297 Nick@geometrics.com	Systems Designer
Bart Hoekstra	Geometrics	831-272-2278 Bart@geometrics.com	Systems Designer
Dr. Tom Bell	Leidos	301-712-7021 Thomas.H.Bell@leidos.com	Data Modeler and Analyst
Dr. Dan Steinhurst	Naval Research Laboratory	202-767-3556 Daniel.Steinhurst.ctr@nrl.navy.mil	Systems Analyst
Dr. Jesse McNinch	USACE Field Research Facility	804-684-7191 Jesse.McNinch@usace.army.mil	Facility Lead
Jason Pipes	USACE Field Research Facility	252-305-3568 Jason.O.Pipes@usace.army.mil	Facility Support

Page Intentionally Left Blank

APPENDIX B MODELING FOR UNDERWATER ADVANCED TIME-DOMAIN ELECTROMAGNETIC SYSTEM

1. Introduction and Recommendation

This white paper has been prepared under Environmental Security Technology Certification Program (ESTCP) Project MR-201313, titled Underwater Advanced Time-Domain Electromagnetic System, to summarize results of Phase I of the project. Phase I, *Initial Design and Modeling,* consisted of a modeling study of the performance of the proposed system in salt water. The results indicate that the advanced transient electromagnetic (TEM) technology which we propose can be used to reliably classify targets in the marine environment, and our recommendation is to proceed to the *Phase II Engineering Design and Construction*.

The models used in this study are briefly described in Section 2 below. Section 3 documents the results of our array design study. The key finding is that a 2x2 meter (m) square modified TEMTADS array comprising a staggered 2-3-2 array of 67 centimeter (cm) transmit loops with an outer transmit loop around the perimeter and eleven three-axis receive cubes is compatible with the engineering constraints of Geometrics' MetalMapper data acquisition system and will support good classification performance. Seawater effects are addressed in Section 4. These include signal distortion due to propagation effects in salt water, signal contributions from current channeling effects, and effects arising from electromagnetic induction (EMI) signals produced by the seawater and bottom sediments. Our findings here are:

1) Signal distortion due to propagation through seawater is restricted to very early times and the effects are negligible beyond a few 10^{th}s of a millisecond
2) The current channeling response will not have a noticeable effect on the target signal in situations of interest to this project
3) The seawater response is comparable to the inherent background response of current TEM sensors and background variations arising from operations in the marine environment are no worse than those encountered on land

These results indicate that our advanced TEM technology can be used to reliably classify targets in the marine environment, and support a Go decision to proceed to Phase II of the project.

2. Models

For most of the array-specific calculations we coded up relevant expressions derived in original source material (included in the cited references in Section 6) using the Exelis IDL development environment. This included array performance calculations, signal distortion in seawater and current channeling effects.

Standard geophysical software packages (Leroi and Lemma) were used for the background response calculations and as a crosscheck on our IDL calculations. These calculations included seawater/sediment variations, conductivity and magnetic susceptibility.

Leroi models the response of, and can invert for, one or more 3D thin plate targets in a horizontally layered host. It is part of the P223F-EM Modeling Software Suite developed by CSIRO/AMIRA International and open sourced in 2008. Dr. Art Raiche is the Project Leader.

Lemma is an open source C++ Electromagnetics Modelling API. Its authors are Trevor Irons, Andy Kass, and others. Lemma currently supports forward modeling in the frequency and time-domain in layered media for a range of source types (E-dipole, H-dipole, polygon loop) and receivers (E-Dipole, grounded wire, H-dipole).

3. Array Design

Our criteria for evaluating the sensor designs are based on engineering constraints and on considerations of how well the array supports classification. We consider in-air performance in evaluating array designs here, and address limitations imposed by operation in the marine environment in subsequent sections. As a practical matter we want a planar array with a reasonably large footprint. Two possible sensor array configurations were described in the proposal. Both were square planar arrays measuring two meters on a side. One was based on the TEMTADS concept, consisting of nine 67 cm square transmit loops paired with nine 3-axis receiver cubes. The other was based on the MetalMapper concept, but using only single-axis transmitters. This design consisted of four 100 cm square transmit loops, each paired with a constellation of five 3-axis receiver cubes.

The new Geometrics electronics board, which will form the basis for the system electronics, has the following components:

1) Main digital board – this handles timing, communication, data handling and control of the transmitter board,
2) A/D boards – There are two 12-channel A/D boards that can communicate with each digital board for a total of 24 channels, and
3) Transmitter board – one transmitter board per digital board. Each transmitter board can handle 4 transmitter coils

Additional transmitters and/or receivers require an additional digital board, one or two A/D boards and another transmitter board. There is functionality built in to synchronize two of these board sets, but synchronizing three board sets would be difficult. The MetalMapper-based concept could be implemented with two board sets, but the TEMTADS-based concept would require three. This led us to consider the modified TEMTADS-based design shown in **Figure 1**, which has a staggered 2-3-2 array of 67 cm transmit loops with an outer transmit loop around the perimeter and eleven three-axis receive cubes. In the diagram, transmit loops are colored red and the small gray crossed squares represent the receive cubes.

A target sensitivity map is overlaid on the array schematic. An EMI array's inversion sensitivity is based on the steepness or curvature of the chi-squared surface with respect to the model parameters. The standard inversion algorithm finds the set of model parameters that minimizes the chi-squared quantity:

$$\chi^2 = \sum_i \frac{(y_i - f_i(X_0, Y_0, Z_0; \mathrm{B}))^2}{{\sigma_i}^2}$$

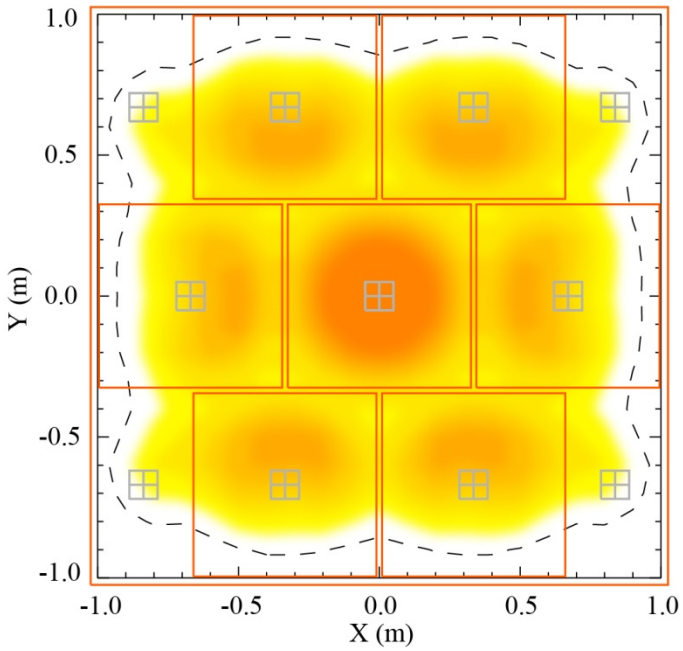

Figure 1. Modified TEMTADS array design with overlaid target sensitivity map. Warmer colors correspond to higher target sensitivity.

where y_i is the measured data, f_i the model output for a given set of parameters, and σ_i is the measured noise. The sum is over all of the transmit/receive coil combinations. The model parameters are object location, (X_0, Y_0, Z_0), and the object's polarizability tensor B. The curvature of the χ^2 surface determines the accuracy of parameter estimation in accordance with the Cramer-Rao bound [1, §2.7]. Higher curvature produces better parameter estimates. The most sensitive dimension of the χ^2 surface corresponds to the depth variable, Z_0. The EMI signal changes rapidly with depth and a small error in fit depth produces larger errors in the polarizability amplitudes. The overlay shows the variation of the χ^2 curvature in the Z-direction over the array with a target 45 cm below the array. The χ^2 curvature values are normalized by the central peak value. The dashed line shows the 0.1 contour level and the level increases from 0.2 to 1 in the colored region. Warmer colors correspond to higher target sensitivity. Similar calculations were done for the other array concepts as well. Across all of the arrays, the 0.2 level seems to indicate where the χ^2 curvature drops off to the point where inversion uncertainties in depth will start increasing dramatically. Simply put, the colored area corresponds to the "sweet spot" of the array. Depending on target depth below the array, this sweet spot measures between 1.4 and 1.6 m square for the modified TEMTADS array. Inversion results would usually not be reliable beyond the central 1.8 m square area of the array. By way of comparison, the original 5X5 TEMTADS system has good coverage over a central square region of roughly 1.6 by 1.6 meters.

Suitability of the array for classification also depends on how well it measures the target's response in all three principal axis directions. This depends on the number and orientation of the transmitter and receiver loops. We evaluate how well the array interrogates the three principal axes of the target by considering the performance of the various possible sets of three transmit and three receive coils. The eigenvectors of such 3x3 transmit/receive matrices correspond to the coefficients of the linear combinations of transmitters and receivers which interrogate the target in three orthogonal directions, while the eigenvalues correspond to relative weights in the three directions. If all eigenvalues are equal, then the three axes are interrogated equally well. The condition number of the transmit/receive matrix is the ratio of the largest to the smallest eigenvalue. As the condition number gets large, the array becomes less effective in interrogating the target in one or two of the directions. By this measure the modified TEMTADS array performs almost as well as the original 3x3 concept, and significantly better than the 2x2 MetalMapper which has fewer transmitters. For a target 45 cm below the array, the average condition number is 4.0 over the central 1.8 m square for the modified TEMTADS array *vs.* 3.5 for the 3x3 TEMTADS and 6.5 for 2x2 MetalMapper array.

Key Finding: A 2x2 m square modified TEMTADS array comprising a staggered 2-3-2 array of 67 cm transmit loops with an outer transmit loop around the perimeter and eleven three-axis receive cubes is compatible with the engineering constraints and will support good classification performance.

4. Seawater Effects

The basic dipole response model used for EMI classification on land is expressed by the equation

$$V(t) = \mu_0 I_0 C_R \cdot C_T \mathrm{B}.$$

V is the voltage induced in a receiver coil by the interaction of the primary magnetic field from a transmitter coil with some target which is characterized by a polarizability tensor B. C_T and C_R are the coil response functions based on Biot-Savart integrals of the transmit and receive coils. The magnetic polarizability tensor B contains the target information used for classification. μ_0 is the permeability of free space and I_0 is the transmitter current prior to cutoff. If the cutoff time is not short compared to the time scales of interest in B (typically some 10's of microseconds [μs] and longer) then B is convolved with the transmit waveform. For underwater applications the basic model is modified in two ways. First, while in air the coil response functions do not depend on time, in water they include a time delay and broadening of the transmit pulse, and the products become convolutions in time. Second, the seawater supports electrical currents arising from the changing magnetic field from the transmitter, and there is an additional signal from the distortion of these currents by the target. This is the so-called "current channeling" signal. Finally, we can have a significant background signal from the seawater and bottom sediments which must be cancelled out.

Propagation

The first effect of a conducting medium that has to be considered is the spreading and delay of the transient magnetic fields excited by the transmitter. In air, the magnetic field $\boldsymbol{H}$ at a range $\boldsymbol{r}$ from a magnetic dipole source with moment $\boldsymbol{m}$ is given by

$$\boldsymbol{H} = \frac{1}{4\pi r^3}\left\{\frac{3\boldsymbol{r}(\boldsymbol{m}\cdot\boldsymbol{r})}{r^2} - \boldsymbol{m}\right\}.$$

In a medium with conductivity σ, this becomes

$$\boldsymbol{H} = \frac{1}{4\pi r^3}\left\{f_1(t/t_D)\frac{3\boldsymbol{r}(\boldsymbol{m}\cdot\boldsymbol{r})}{r^2} - f_2(t/t_D)\boldsymbol{m}\right\},$$

where the diffusion time scale $t_D = \sigma\mu_0 r^2/4$ [2, eq. 2.59]. For the step down excitation used in TEM systems, the functions f_1 and f_2 both start out at 1 at t = 0 and asymptotically approach 0 as t → ∞. The primary field step is distorted, but its overall strength is unchanged. The distortion can be dramatic when the differences between the time dependences of f_1 and f_2 alter the balance between the first and second terms within the curly brackets, but everything occurs rather quickly. For seawater with σ ≈ 3-4 S/m, at a range of 50 cm the diffusion time scale is about ¼ μs. Although this is short in comparison to typical transmit current cutoff times of order 10 μs, the functions f_1 and f_2 decay algebraically. Depending on the geometry their effects can persist for longer times. **Figure 2** shows what happens in an extreme case. It compares the strength of the induced dipole moment for a shotput-sized hollow steel ball in air (dashed curves) and in seawater with conductivity 4 S/m (solid curves). The transmit loop is 67 cm square.

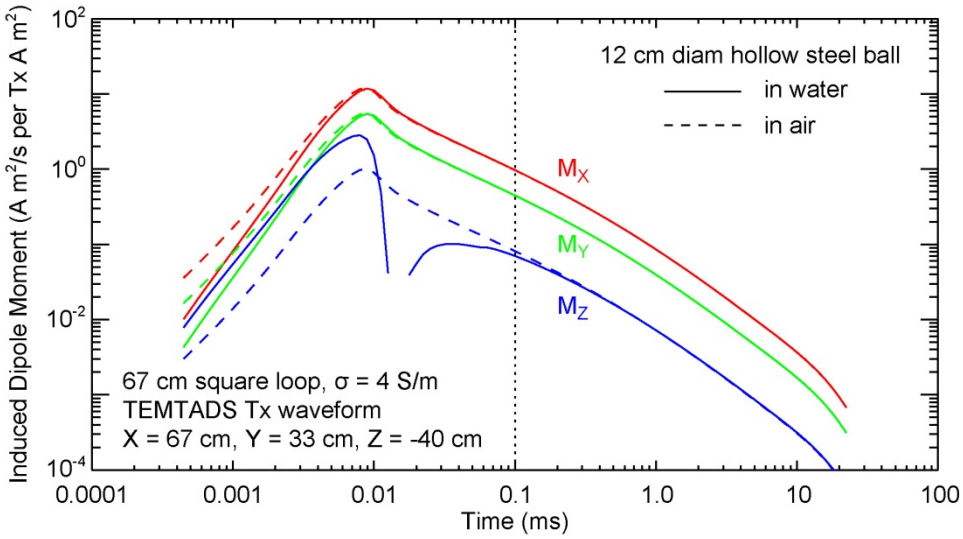

Figure 2. Strength of induced dipole moment for shotput-sized steel shell in air and in seawater.

The target is a 12 cm diameter, 1 cm thick steel shell with conductivity 6.5x10^6 siemens per meter (S/m) and relative permeability 75, located 40 cm below the loop and offset 67 cm in the X-direction and 33 cm in the Y-direction from the center of the loop. The target's polarizability was calculated using expressions derived by Hjelt [3] for the transient response of a layered sphere. This was convolved with the standard TEMTADS transmit waveform and the seawater transfer function to produce the induced dipole moment components. The seawater transfer function was approximated by summing up contributions from 10^4 dipole current sources, each with a dipole moment of 10^{-4} amp-meter squared (A m^2), spread evenly over the area enclosed by the 67 cm square transmit loop. This approximation was

checked by comparing corresponding electric fields with transient fields from a square current loop in seawater calculated using the Lemma electromagnetics modelling API.

The geometry in **Figure 2** is extreme, with the target directly under an adjacent sensor in the modified TEMTADS array, yet distortions in the seawater case are restricted to very early times. Differences between the X- and Y-component dipole moments in air and in seawater are negligible beyond 10 μs. The Z-component is affected the most. It has a sign reversal between 10 and 20 μs where the time dependences of f_1 and f_2 alter the balance between terms in the expression for the Z-component primary field, but the residual effect is less than 10% beyond 0.14 millisecond (ms) decay time. It looks more like the X- and Y-component dipole moments when the target is actually under the transmit loop.

Key Finding: Signal distortion due to propagation through seawater is restricted to very early times and the effects are negligible beyond a few 10ths of a millisecond.

Current Channeling

The transmit current step also produces transient electric fields and currents in the seawater. **Figure 3** shows the magnetic field (top) and electric field (bottom) components at the target location used in **Figure 2**. In this case the time axis is linear rather than logarithmic. Note the field reversal in the Z-component magnetic field. This only arises at offsets where the static field has reversed sign, and is not present for locations directly under the transmit loop. The electric field is impulsive rather than step-like, and is restricted to very early times and off-axis locations.

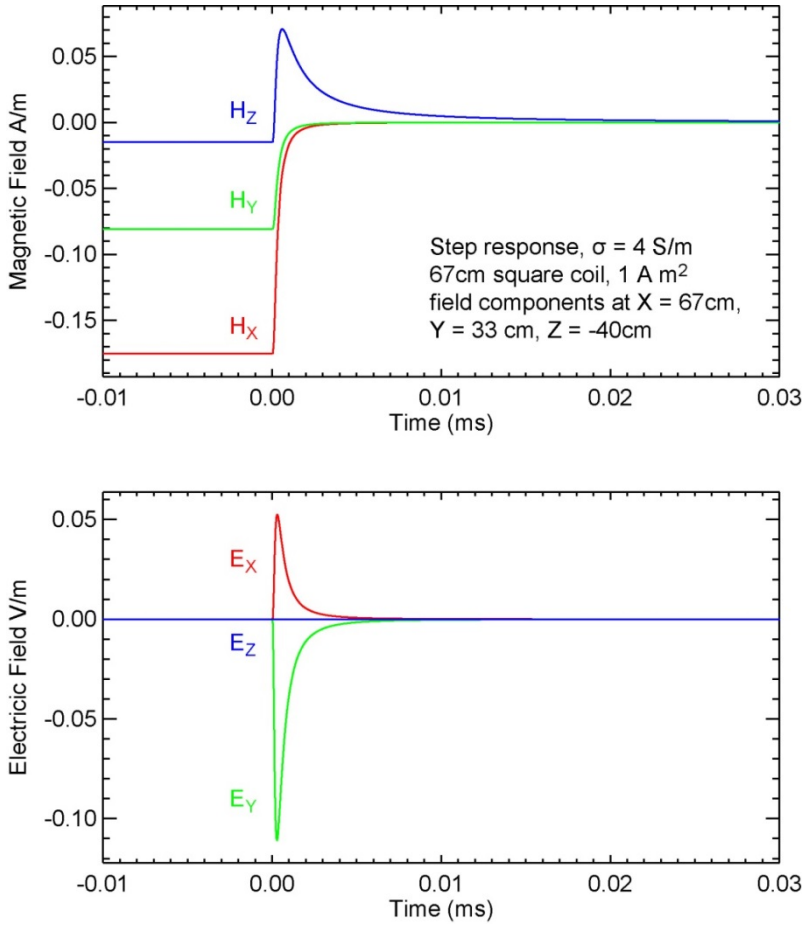

Figure 3. Magnetic (top) and electric (bottom) field components in seawater from a 67 cm square transmit loop.

The target's response to the electric field adds a new signal component. A target which is a good conductor gathers currents much like a magnetic target gathers magnetic flux. This current gathering or channeling effect produces a transient electric dipole response from the target, while the familiar eddy current effect produces a transient magnetic dipole in the target in response to the primary field cutoff. In the quasi-static EMI limit, the frequency-domain Maxwell's equations relating the magnetic and electric fields $\boldsymbol{H}$ and $\boldsymbol{E}$ are

$$\nabla \times \boldsymbol{E} = -i\omega \boldsymbol{B}$$

$$\nabla \times \boldsymbol{H} = \boldsymbol{J}$$

with $\boldsymbol{B} = \mu \boldsymbol{H}$ and $\boldsymbol{J} = \sigma \boldsymbol{E}$, μ and σ being the magnetic permeability and the electrical conductivity, respectively. Excluding the boundaries between different materials, $\nabla \cdot \boldsymbol{B} = 0$ and $\nabla \cdot \boldsymbol{J} = 0$. Boundary conditions are that the normal component of $\boldsymbol{B}$ and the tangential component of $\boldsymbol{H}$ are continuous, while the normal component of $\boldsymbol{J}$ and the tangential component of $\boldsymbol{E}$ are continuous. There is a symmetry here which allows us to easily calculate current channeling effects from the solution for the corresponding magnetic problem. We simply interchange $\boldsymbol{E}$ with $\boldsymbol{H}$ and σ with $-i\omega\mu$. The major difference is that the magnetic flux density $\boldsymbol{B}$ is not zero in free space because the permeability of free

space μ_0 is finite, whereas in free space there is no current density $\boldsymbol{J}$ accompanying an electric field because the free space conductivity is zero. Using this approach to calculate a target's electric polarizability in a conducting medium is strictly appropriate only in the limit that the skin depth $\sqrt{2}/\omega\sigma\mu$ in the host medium is large compared to the size of the target, which is in the spirit of McNeill *et al.* [4] and fundamentally compatible with the concept of a dipole response model.

As discussed in [5], the EMI response of a sphere displays all of the essential properties of the eddy current decay signature, and the responses of other more realistic targets can be approximated using the responses of equivalent spherical targets. Following Wait and Spies [6], the magnetic polarizability of a conducting, permeable sphere having a radius a, conductivity σ and relative permeability $k = \mu/\mu_0$ is given by

$$\mathrm{B}(t) = \frac{12\pi a}{\sigma\mu_0}\sum \frac{\xi_n^2}{(k+2)(k-1)+\xi_n^2} exp\left(-\frac{\xi_n^2 t}{\sigma\mu a^2}\right)$$

for $t > 0$, where the ξ_n are roots of

$$tan(\xi) = \frac{(k-1)\xi}{k-1+\xi^2}.$$

The induced magnetic dipole moment is given by the convolution of this polarizability with the magnetic field from the transmit coil. Following the standard convention we have used the impulse response in the definition of polarizability rather than the step response since the signal measured by the receive coil is proportional to the rate of change of the flux through the coil.

The polarizability decays exponentially at late times when the eddy currents have diffused throughout the object. The rate is determined by the body mode time scale $\tau_0 = \sigma\mu a^2/\xi_0^2$. For $k >> 1$, $\xi_0 \equiv 4.493$ for the sphere. At very early times, $B \propto t^{-1/2}$, transitioning to $t^{-3/2}$ at the surface mode time scale $\tau_S = \sigma\mu a^2/k^2$. For more general objects, these time scales and the strength of the response are shifted about depending on the shape and orientation of the object relative to the primary field, but the fundamental character of the response is not changed [7].

For the current channeling response, we have an induced electric dipole moment which is given by the convolution of the corresponding electric polarizability P with the electric field from the transmit coil. In this case

$$\mathrm{P}(t) = \frac{12\pi}{\sigma\mu^2 a}\sum \frac{\xi_n^4}{(k+2)(k-1)+\xi_n^2} exp\left(-\frac{\xi_n^2 t}{\sigma\mu a^2}\right),$$

provided that we replace k with the relative conductivity σ/σ_0 in the equation for the roots ξ_n. The response has the same form as the magnetic response, except for a time derivative arising from the $i\omega$ factor and the fact that the surface mode time scale gets shifted much earlier in time by a factor of $(\sigma_0\mu/\sigma\mu_0)^2$, which is of order 10^{-9} for parameter values of interest here. **Figure 4** compares the magnetic and electric polarizabilities for the hollow steel ball from **Figure 2**.

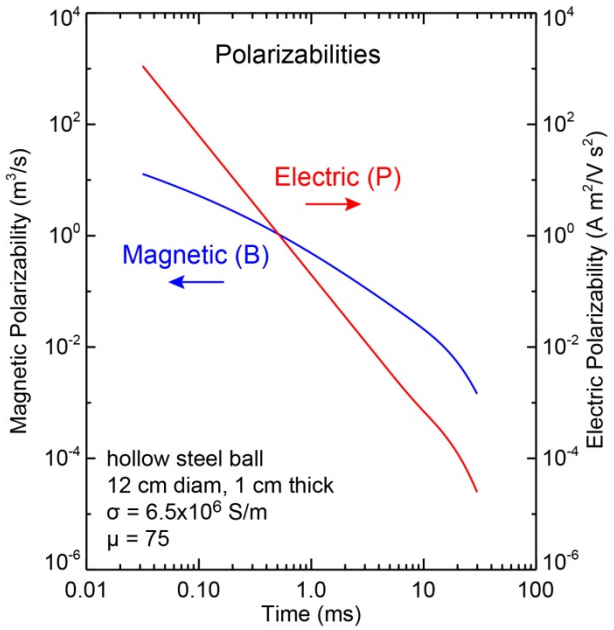

Figure 4. Magnetic and electric polarizabilities for a 12 cm diameter hollow steel ball in seawater.

Ignoring the geometric factors which arise because of the orthogonality between magnetic and electric fields, the ratio of the signals due to the current channeling and the eddy current responses scales as

$$\frac{V_{CC}}{V_{EC}} \sim \mu_0 r^2 \frac{\mathrm{P}}{\mathrm{B}}$$

which is very small for any sensible range r. Referring to **Figure 4** we see that although the electric polarizability decays much more rapidly than the magnetic polarizability, they are comparable in magnitude at about 0.5 ms. We can safely conclude that the current channeling response is not likely to have a noticeable effect on the signal for our problem. This is entirely consistent with the observation in MR-1321 that the current channeling effect is basically a very high frequency phenomenon [8].

Key Finding: The current channeling response will not have a noticeable effect on the target signal in situations of interest to this project.

Background Response

Returns from the seawater itself and bottom sediments also contribute to the measured response, and this background response can be modulated by variations in the proximity of the sensor to the sea surface due to waves or motion of the sensor. **Figure 5** (left) compares the seawater background response at several sensor heights above the bottom with the signal from our hollow steel ball. The water depth is 10 m, with conductivity 3.2 S/m. The conductivity of the bottom sediments is taken to be 0.32 S/m (more on this later). The transmitter is the 67 cm square loop carrying a 1 A current. There are four background response curves corresponding to sensor heights above the bottom of 10 cm (blue), 20 cm (green), 30 cm (red) and 5 m (black). The target is the 12 cm diameter hollow steel ball described earlier, suspended 40 cm directly below the sensor. The target calculations are actually the in-air

response, but from the seawater propagation results discussed above it is clear that differences between the in-air and in-water responses would not be distinguishable on this plot. Differences in the background response between 10 cm and 30 cm above the bottom are about 7% of the response at 20 cm at 0.1 ms and drop to zero in a few ms. The difference between the background responses at mid depth and near the bottom is about 16% at 0.1 ms. The plot on the right shows the effect of water depth. In this case the sensor is 20 cm above the bottom.

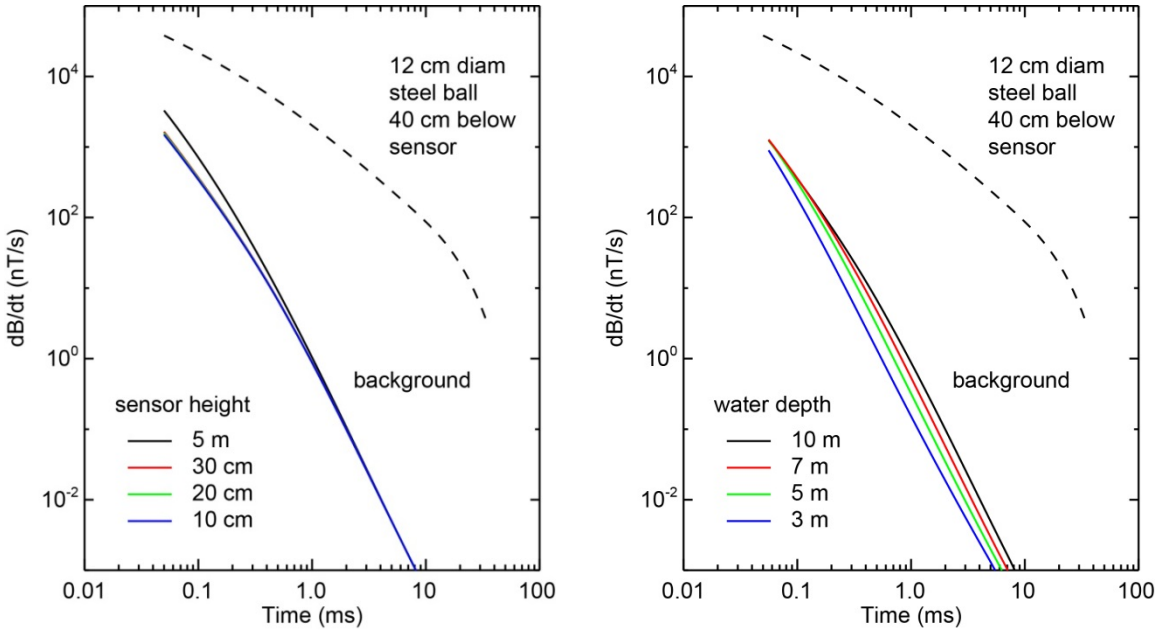

Figure 5. Left: Seawater background signal *vs.* sensor height above bottom; Right: Effect of water depth.

Local water depth variations due to surface waves will produce background noise. The noise level will depend on the water depth and the wave height and spectral content, but is bounded by background variations due to wholesale depth changes. In this example the effect is strongest around 1 ms. **Figure 6** plots the effect of water depth variation on the background signal at 0.1 ms and 1 ms and 10 ms. The ordinate is the fractional change in background signal for depth change of 30.5 cm (1 ft). The sensor is 20 cm above the bottom. At 1 ms this varies from 3.8% in water 10 m deep to 10.6% in 5 m water and is generally smaller at earlier and later times. Because the response involves spatial averaging over the surface, the measured background variation due to surface waves will be less than this. Exactly how much less depends on the water depth and the wavelength content of the surface wave field.

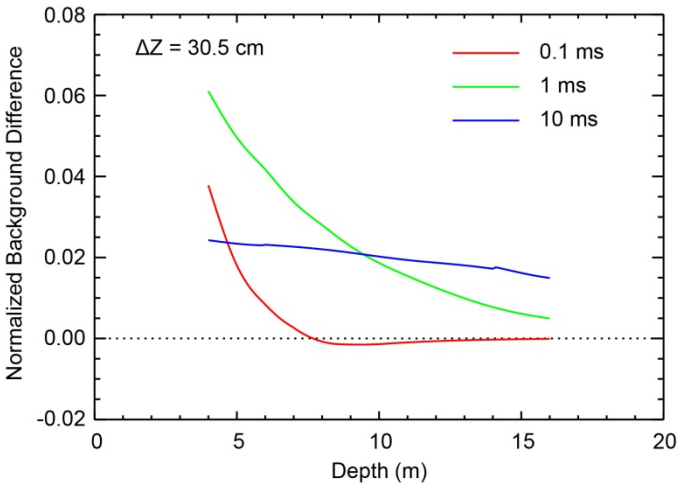

Figure 6. Background signal variation due to depth variation of 30.5 cm.

Sediment conductivity is primarily determined by the sediment porosity, pore water conductivity and the sediment type and corresponding pore structure [9, §4.4.2]. **Figure 7** (left) shows the effect of variation in the conductivity contrast between seawater and the underlying sediments on background signal levels. The sensor is 20 cm above the bottom. We include the signal from our hollow steel ball 40 cm below the sensor for comparison. The background variation for a seawater/sediment conductivity contrast range of 1-10 is <1% of the target signal. Effects arising from magnetic susceptibility of sediments are generally small. **Figure 7** (right) shows the effect on the background response for frequency-dependent susceptibility with low frequency susceptibilities of 350 (red), 3500 (green) and 35000 (blue) μSI units. The conductivity contrast is 10, and the black curve corresponds to nonmagnetic sediments. 35000 μSI is at the high end of the low frequency susceptibility values reported for soil profiles at Kaho'olawe, HI [10]. These highly magnetic soils significantly degraded munitions detection and classification performance with EMI sensors in demonstrations at the site. Watkins and Maher [11] measured 321 rock, sediment and soil samples from potential sediment source areas around the North Atlantic. Low frequency susceptibility values ranged from about 20 to 50000 μSI units, with the median value around 500 μSI units. Values measured at the Blossom Point, MD test site for an ESTCP project on the quantification of EMI noise sources [12] were typically less than 100 μSI units. In such environments susceptibility effects will only appear at late times and are generally overpowered by the conductivity effects.

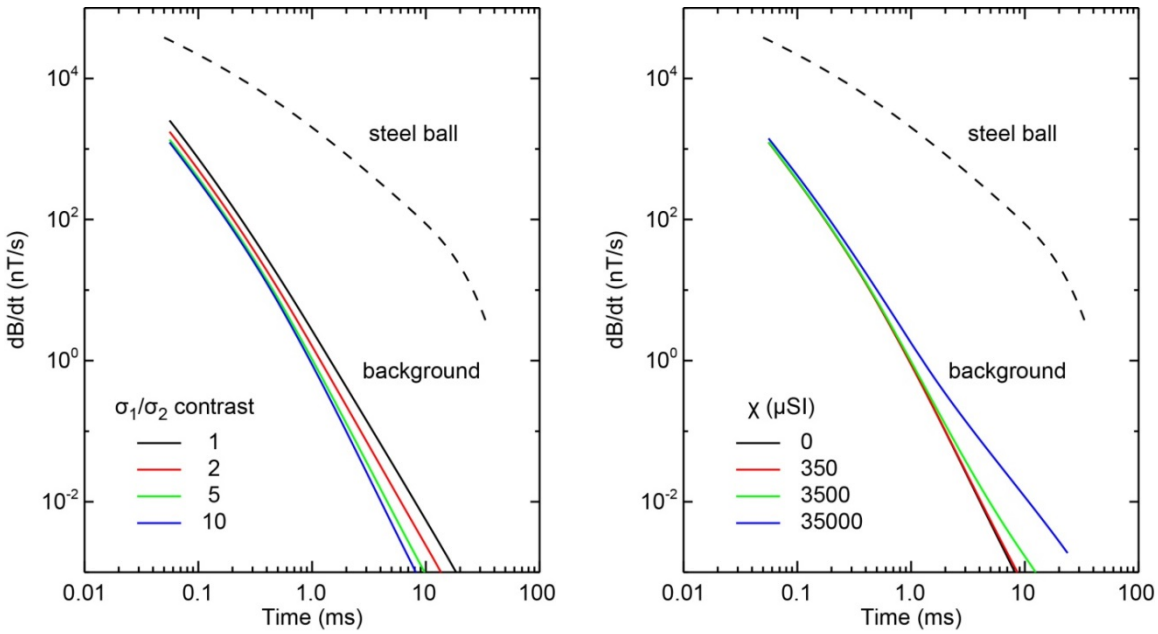

Figure 7. Left: Effect of variation in conductivity contract between seawater and underlying sediments on background signal levels; Right: Effect of sediment magnetic susceptibility.

So long as the background response is small compared to the target signal none of these effects are likely to cause problems. The response for our shotput-sized target is much larger than the background. For weaker targets the seawater response can be comparable to the signal from the target. Morrison [13] notes that the seawater response is an order of magnitude greater than the response from a 37 mm diameter steel ball suspended 75 cm below the sensor at 1 ms. The target response decays more slowly than the background and they are comparable in magnitude by about 15 ms. In discussing this somewhat extreme example, Morrison notes that on land this target would be beyond the detectability of the Lawrence Berkeley National Laboratory's advanced TEM sensor.

All of the effects considered above introduce background variations of at most 10-15%. By way of comparison **Figure 8** shows typical background and signal responses for the 2x2 man-portable TEMTADS system from the Camp Beale demonstration. The gray curves are monostatic background shots and the blue curve is the signal from a 105 mm projectile roughly 50 cm below the sensor (target BE-1). Shot-to-shot variability of the background response is a significant source of noise with advanced TEM sensors, and we typically use background subtraction to improve the signal-to-noise ratio for weaker targets. Comparing **Figure 8** with the figures showing seawater response and its variability we notice several things: the TEM sensors have an inherent background level which is comparable to the seawater return, and the background variations arising from operations in the marine environment are no worse than those encountered on land.

Key Finding: The seawater response is comparable to the inherent background response of current TEM sensors and background variations arising from operations in the marine environment are no worse than those encountered on land.

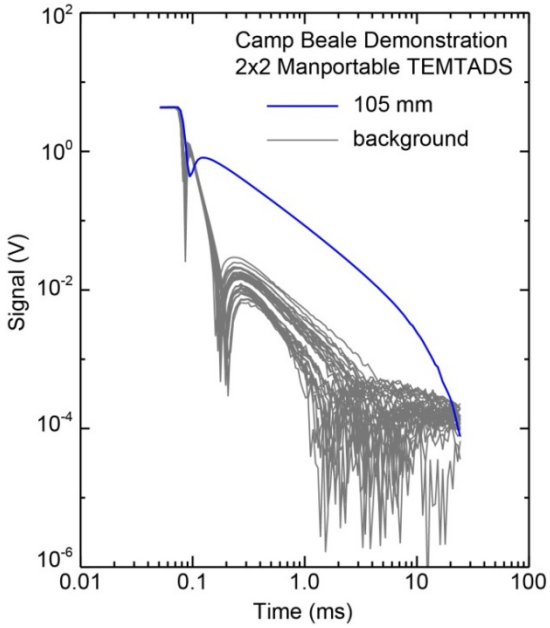

Figure 8. 2x2 man portable TEMTADS signal and background levels at the Camp Beale demonstration.

5. Summary and Conclusions

Two possible sensor array configurations were described in the proposal. Both were square planar arrays measuring two meters on a side. One was based on the TEMTADS concept, consisting of nine 67 cm square transmit loops paired with nine 3-axis receiver cubes. The other was based on the MetalMapper concept, but using only single-axis transmitters. This design consisted of four 100 cm square transmit loops, each paired with a constellation of five 3-axis receiver cubes. As it turns out, on the one hand the 3x3 TEMTADS array would introduce unacceptable complexity in the supporting electronics, while on the other hand in order to get better target illumination we need more transmitters than the 2x2 modified MetalMapper design includes. These considerations led us to a 2x2 m square modified TEMTADS array design comprising a staggered 2-3-2 array of 67 cm transmit loops with an outer transmit loop around the perimeter and eleven three-axis receive cubes. Our findings are that this array is compatible with our engineering constraints and will support good classification performance.

We have conducted a comprehensive analysis of the effects of the marine environment on TEM sensor performance. These effects include signal distortion due to propagation in a conducting medium, signal contributions from current channeling, and effects arising from EMI signals produced by the seawater and bottom sediments. Our findings here include:

1) Signal distortion due to propagation through seawater is restricted to very early times and the effects are negligible beyond a few 10^{th}s of a millisecond
2) The current channeling response will not have a noticeable effect on the target signal in situations of interest to this project

3) The seawater response is comparable to the inherent background response of current TEM sensors and background variations arising from operations in the marine environment are no worse than those encountered on land

The results indicate that the advanced TEM technology can be used to reliably classify targets in the marine environment, and our recommendation is to proceed to the Phase II Engineering Design and Construction.

6. References

1. Harry L. van Trees, *Detection, Estimation and Modulation Theory, Part 1*, John Wiley and Sons, 1968.

2. Stanley H. Ward and Gerald W. Hohmann, “Electromagnetic Theory for Geophysical Applications,” pp. 131-311 in *Electromagnetic Methods in Applied Geophysics, Vol. 1, Theory*, (Misac N. Nabighian, ed.), Society of Exploration Geophysicists, 1988.

3. Sven-Erik Hjelt, “The transient electromagnetic field of a two-layer sphere,” *Geoexploration 9*, 213-229, 1971.

4. J.D. McNeill, R.N. Edwards and G.M. Levy, "Approximate calculations of the transient electromagnetic response from buried conductors in a conductive half-space," *Geophysics 7*, 918-924, 1984.

5. J. Torquil Smith and H. Frank Morrison,"Approximating spheroid inductive responses using spheres," *Geophysics 71*, G21–G25, 2006.

6. James R. Wait and Kenneth P. Spies, “Quasi-static transient response of a conducting permeable sphere,” *Geophysics 34*, 789-792, 1969.

7. Thomas Bell, Bruce Barrow, Jonathan Miller and Dean Keiswetter, "Time and frequency domain electromagnetic induction signatures of unexploded ordnance," *Subsurface Sensing Technologies and Applications 2*, 153-175, 2001.

8. W. SanFilipo and I.J. Won, “Broadband Electromagnetic Detection and Discrimination of Underwater UXO,” Final Report, SERDP Project MR-1321, 2005.

9. Darrell R. Jackson and Michael D. Richardson, *High-Frequency Seafloor Acoustics*, Springer, 2007.

10. Leonard R. Pasion, Stephen D. Billings, and Douglas W. Oldenburg, "Evaluating the effects of magnetic soils on TEM measurements for UXO detection," SEG Int'l Exposition and 72nd Annual Meeting, Salt Lake City, October 6-11, 2002.

11. S.J. Watkins, B.A. Maher, "Magnetic characterisation of present-day deep-sea sediments and sources in the North Atlantic," *Earth and Planetary Science Letters 214*, 379-394, 2003.

12. Glenn R. Harbaugh, Daniel A. Steinhurst, Mark J. Howard, Bruce J. Barrow, Jonathan T. Miller and Thomas H. Bell, "Quantification of Noise Sources in EMI Surveys," Final Guidance Document, ESTCP Project MR-200508, 2012.

13. H. Frank Morrison, "Development and Testing of an Engineering Prototype for a Marine Version of the Berkeley Unexploded Ordnance Discriminator (BUD)," Final Report, SERDP Project MR-2228, 2013.

Page Intentionally Left Blank

APPENDIX C UNDERWATER ADVANCED TIME-DOMAIN ELECTROMAGNETIC SYSTEM DESIGN

Underwater Advanced Time-Domain Electromagnetic System Design

Prepared for

Environmental Security Technology Certification Program (ESTCP)

July 2015

ch2m
2411 Dulles Corner Park
Suite 500
Herndon, Virginia 20171

Contents

Underwater Advanced Time-Domain Electromagnetic System Design

Introduction

This document has been prepared under Environmental Security Technology Certification Program (ESTCP) Project MR-201313, titled Underwater Advanced Time-Domain Electromagnetic System, to present the preliminary system design of the proposed system. Based on the analysis conducted in Phase I (Initial Design and Modeling) of the project, documented in the white paper titled *Modeling for Underwater Advanced Time-Domain Electromagnetic System* (provided in June 2014), we have conducted a preliminary mechanical and electrical design meant to accomplish several objectives:

1. Achieve a configuration that employs the 2-3-2 staggered array design, shown as **Figure 1**, developed in the analysis outlined in the modeling white paper.

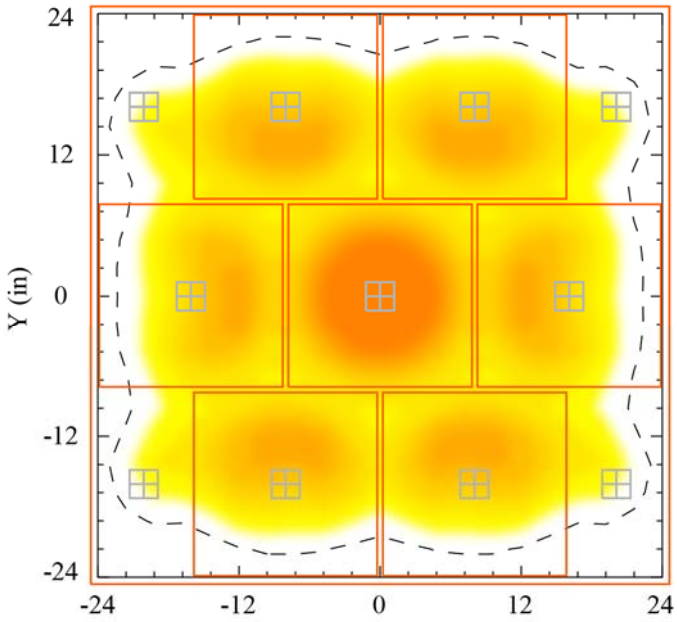

Figure 1. Modified TEMTADS array design with overlaid target sensitivity map. Darker colors correspond to higher target sensitivity.

2. Use materials and components that are ultraviolet (UV) and salt water resistant.
3. Incorporate parts that have been used by other Geometrics marine products to minimize the time required to test components.
4. Develop a design that is suitable for water depths in excess of 200 feet (ft) (60 meters [m]) to ensure sufficient margin for operation in the expected depths.
5. Attempt to reduce the weight of the transmitter/receiver array so that it can be hand deployed from a small boat. It is still expected that a winch will be required to raise and lower the system.
6. This system is intended to be a demonstration of the concept of a marine UXO characterization system and will currently require diver assistance to be placed at the correct location.
7. The current design will be limited to calm water conditions with minimal currents.
8. Allow the overall buoyancy of the system to be such that it will rest on the bottom without additional weight.

Electronics and Software

Digital Electronics

The electronics planned for use in the system are based on a new version of the MetalMapper electronics designed by engineers at Lawrence Berkeley National Laboratories based on the initial design, but incorporating modern components. (Prototype versions are currently being tested.) The main components of the electronics are:

- A Digital Main board that contains multiple field-programmable gate arrays (FPGAs) responsible for communicating with the Analog to Digital (A/D) boards, transmitter boards, preliminary data processing and the acquisition controller.
- A/D cards of eight channels each. The A/D converters operate at 1 megahertz (Mhz) sampling rate and have an 18 bit precision (current MetalMapper electronics use 16 bit A/Ds at 250 kilohertz [Khz].)
- A transmitter board that is capable of controlling up to 4 transmitters per board.
- Input/Output (I/O) interface board for routing signals coming from connectors
- Receiver board capable of providing pre-digitization filtering of the signals to reduce DC offsets and aliased noise and increase overall system dynamic range.

A schematic of the board setup is shown as **Figure 2**.

The current electronics are limited to 8 receiver cubes and 4 transmitter coils. For the proposed configuration of 8 transmitter coils and 11 receiver coils two sets of boards will need to be used and will thus require synchronization between the boards. This was anticipated in the original design and clock signals will be shared between the boards. Synchronization between the boards is anticipated to be on the order of 50 nanoseconds (ns), which will ensure that the merged data sets have sufficient timing accuracy.

Software

In order to accommodate communication with two boards, as opposed to one, the software will also require changes. The current plan is for both sets of boards to communicate independently with the acquisition controller. The communication between the boards and the acquisition controller is accomplished via User Datagram Protocol (UDP) transmission, which is less secure than then Transmission Control Protocol (TCP) transmission used in most Ethernet communications, and there is a risk of corruption of data when two boards are broadcasting data simultaneously over the same twisted pair. This may require a small interface system within the electronics package to receive data from each board set independently, buffer the data flow, and send it to the acquisition controller.

The remainder of the software will remain essentially the same, with the same navigational and QC displays of the terrestrial MetalMapper. It is expected that an inversion algorithm using the new array design will be incorporated into the software to provide feedback during operation on the interpreted location of any metallic objects so additional data can be collected if necessary.

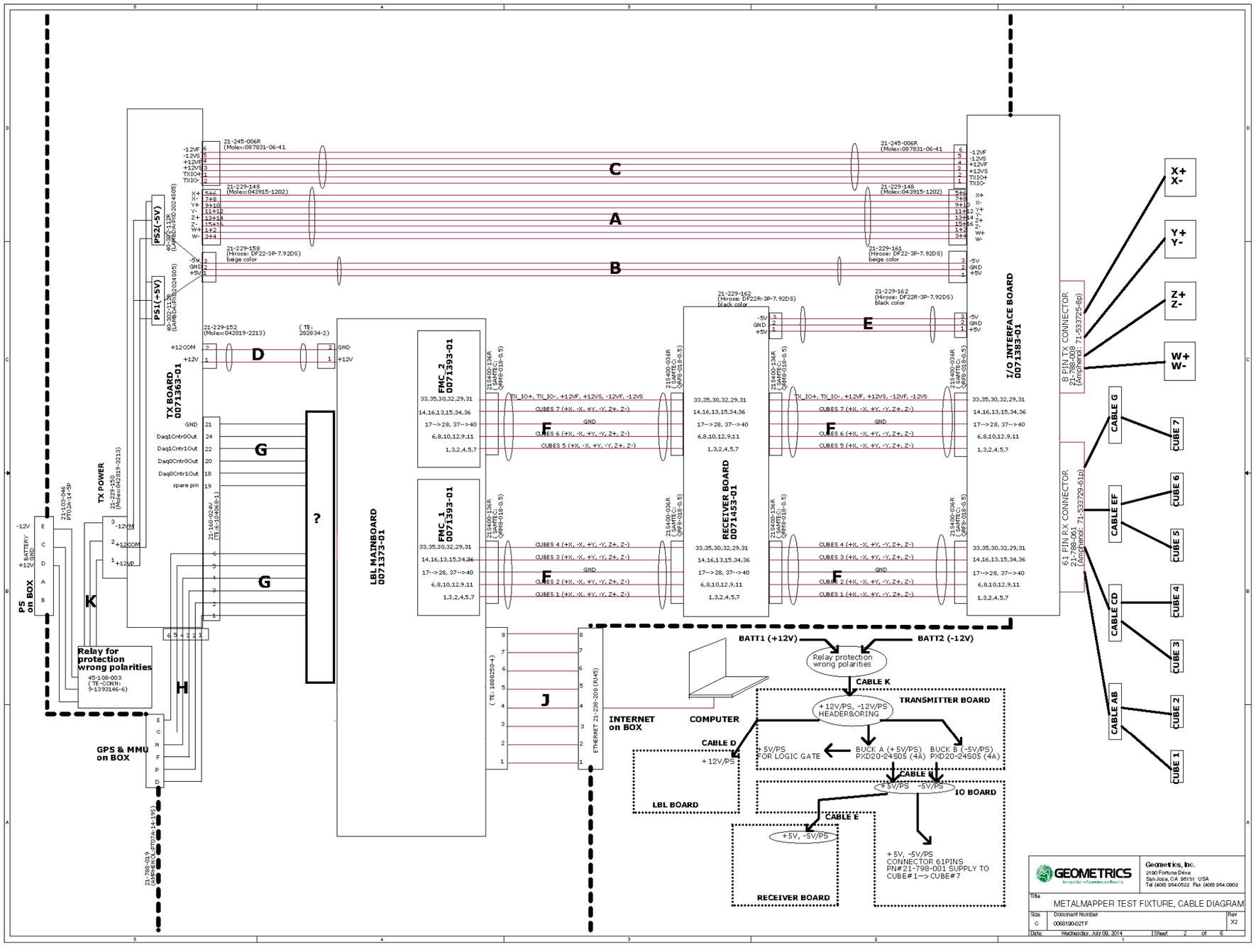

Figure 2 – Electronics interconnection diagram

Cable

The cable we have preliminarily chosen is used in Geometrics' marine seismic systems and has been selected for several reasons:

1. A Vectran strength member with a breaking strength of 10,000 pounds (lbs) so it can easily handle the weight of the array both in and out of the water.
2. A CAT5e Ethernet twisted pair to allow communications between acquisition board sets and the acquisition controller.
3. Sufficient wires for providing power from the surface.
4. Water blocking compound within the cable to reduce water penetration.
5. An existing design for the waterproof connector attached to the cable is already available and the selected connector can mate both the strength member and electronics connection; thus, only a single point of connection is required to the canister containing the electronics.
6. A bend radius of 12 inches (in.) (30.5 centimeters [cm]) so it can be run over commonly available sheaves and winches.

A cross-section of the cable is shown on **Figure 3**.

The connectors proposed for this cable are waterproof Glenair connectors that allow bonding of the strength member to the connector itself. Geometrics has deployed these connectors extensively in their marine systems and have found them to be reliable. The connectors are pressure rated up to 1,000 pounds per square inch (PSI), which corresponds to over 2,000 ft. (609.6 m) water depth. A cross-section of the connector is shown as **Figure 4**.

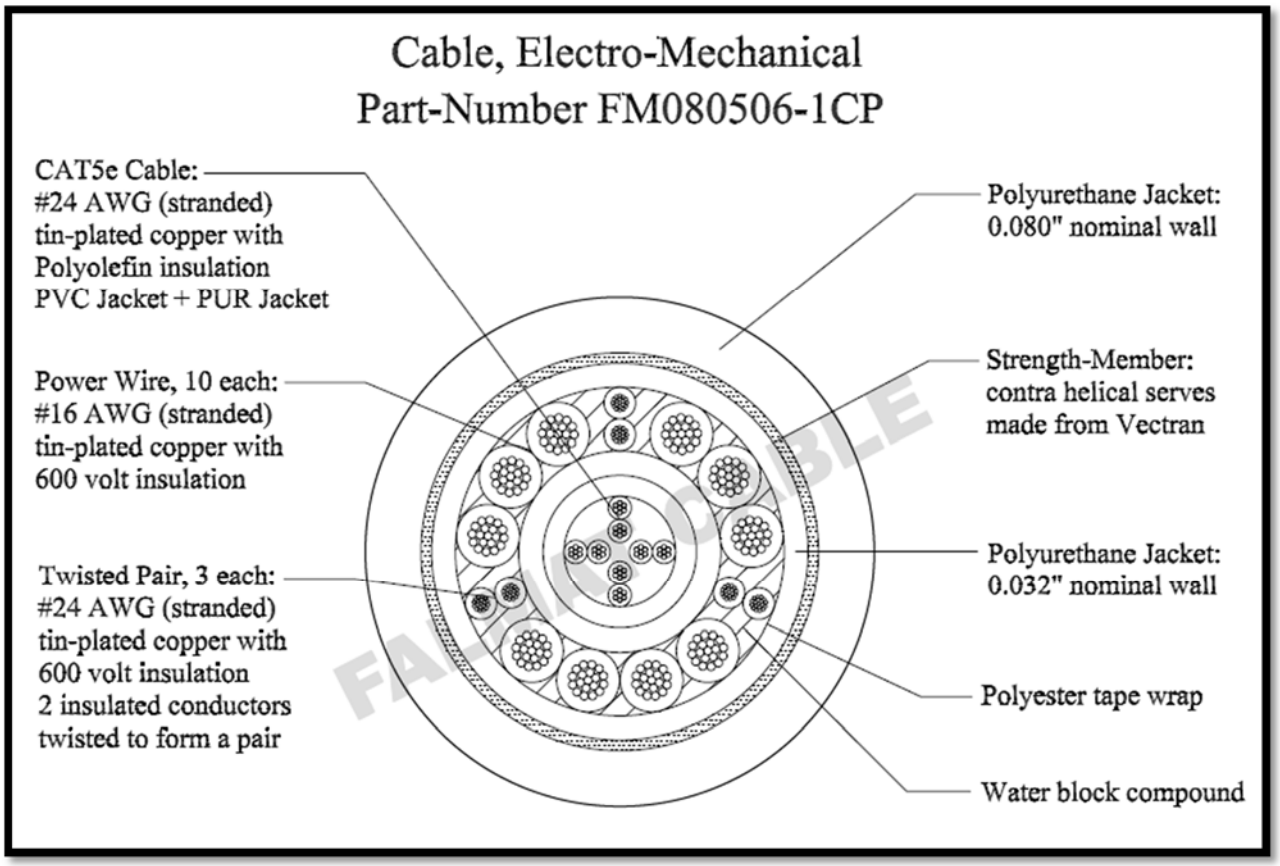

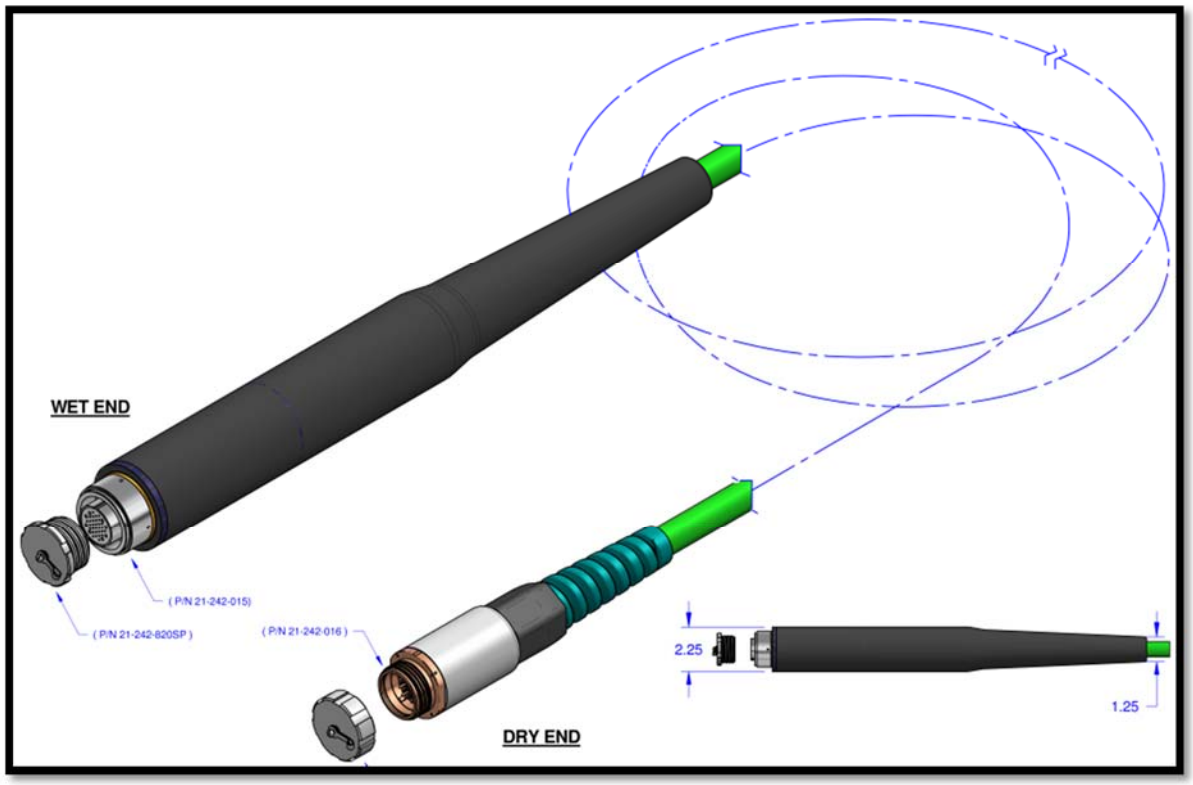

Figure 3 Cross-section of cable (TOP) and assembled cable with stress relief over-mold (BOTTOM)

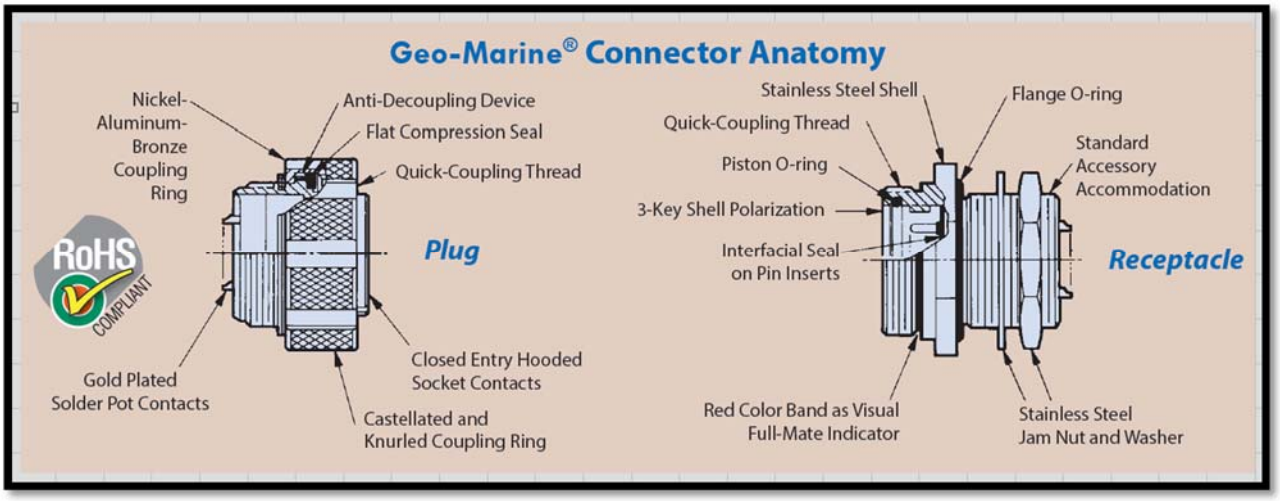

Figure 4 – Connector cross-section

Electronics Enclosure

The electronics will be housed in a 9 in (22.9 cm) diameter stainless steel metal cylinder 15 in (38.1 cm) long and will be constructed with a flat plate on either end. The flat plates will have the connectors for the receivers on the bottom and the transmitters and signal cable on the top. We have chosen to use separate connectors for each transmitter/receiver unit in order that defective parts can be easily swapped out.

The initial design for the electronics enclosure and the arrangement of the boards in the enclosure is shown by **Figure 5**. The transmitter boards will be thermally bonded to the enclosure walls to ensure adequate heat transfer.

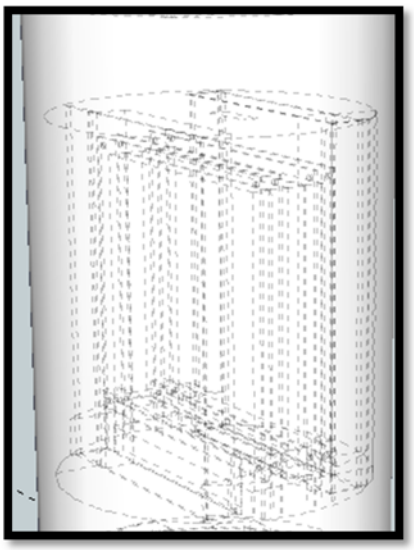

Figure 5 – Electronics enclosure

The end plates of the canister will be made out of an "L" shaped bracket in order to easily attach it to the frame of the instrument. The ends will be bolted onto the cylinder with 8 bolts that will seal the end cap onto the cylinder. The end-cap design is shown in **Figure 6**.

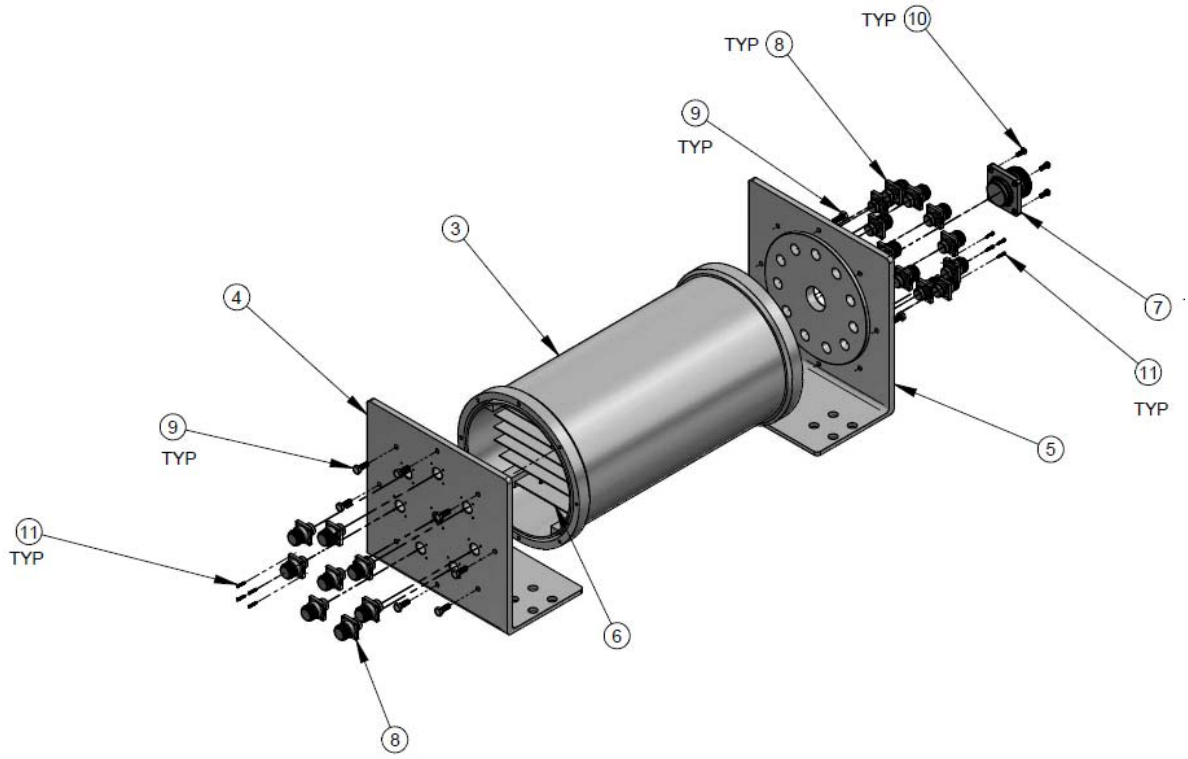

Figure 6 – Electronics Enclosure End Cap Detail

Array Construction

The array will be constructed of a combination of molded and extruded poly-vinyl chloride (PVC) parts with material composition selected for both resistance to salt water and UV degradation. The molded corners and extruded sides are constructed such that a portion of the corners fits into the hollow core of the sides, allowing for relatively quick assembly of a transmitter coil with minimal gluing and a simple modification to the length of the extruded side when a change in transmitter size is required. **Figure 7** shows an assembly of a corner and two sides as well as a cross-section of the extruded side. The wires carrying the transmitter current fit into the grooves on one side of the extrusion. (The flanges on the groove side are intended to be used for containing waterproofing material.) The interior of the sides will be hollow and will need to be open to the water. The receiver cubes are currently printed using a 3D plastic printer and there will be little modification to the coils, with the exception of a coating to provide waterproofing.

Coated wire will be used, providing water resistance in addition to application of a waterproof coating. The overall approach to waterproofing is to over-mold the cables onto the individual units as opposed to having connectors on the transmitters and receivers. The cables are not expected to have stress on them and therefore no strength members are required.

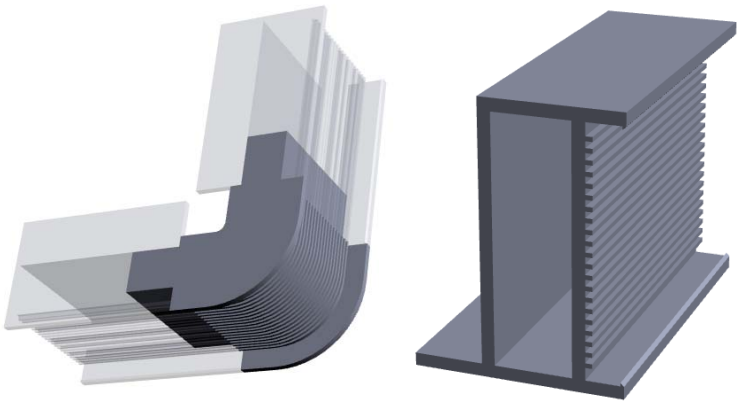

Figure 7 – Transmitter coil assembly

The proposed array is shown as **Figure 8** and, as designed, will weigh approximately 220 lbs on dry land. The cable weight for a 100 m cable is 90 lbs in air and 30 lbs in salt water. The dimensions (shown on the figure) and weight will require the use of an A-Frame or crane on the vessel to deploy it. There is an extension on one side of the array to hold the electronics package in a static position. Having a static location of the electronics array will accomplish several objectives:

1. The electronics canister will be in a static position relative the array so the currents induced in the canister can be removed from the measurement using a background subtraction.
2. There is no need for strain relief for the cables coming from the transmitter and receiver in the array as they can be fixed along the frame of the array.

The electronics canister will have a single cable that connects directly to the surface electronics and the antenna array will be suspended with ropes connected to each of the four corners. The weight of the platform will be transferred to the cable at the common point of the ropes with a Slack Pulling Grip (Kellums Grip). The section of the frame that the electronics enclosure is attached to will be detachable from the main part of the array with the transmitters and receivers to allow for easier shipping and moving onto the boat. It can be easily assembled on the deck of the vessel.

In order to provide sufficient distance from the sea floor, posts with rounded corners are used as shown in **Figure 9**. In the case that the bottom conditions are too irregular, then rails along the edges will be substituted. The rounded corners are to prevent the puncturing of the liners in the test pond.

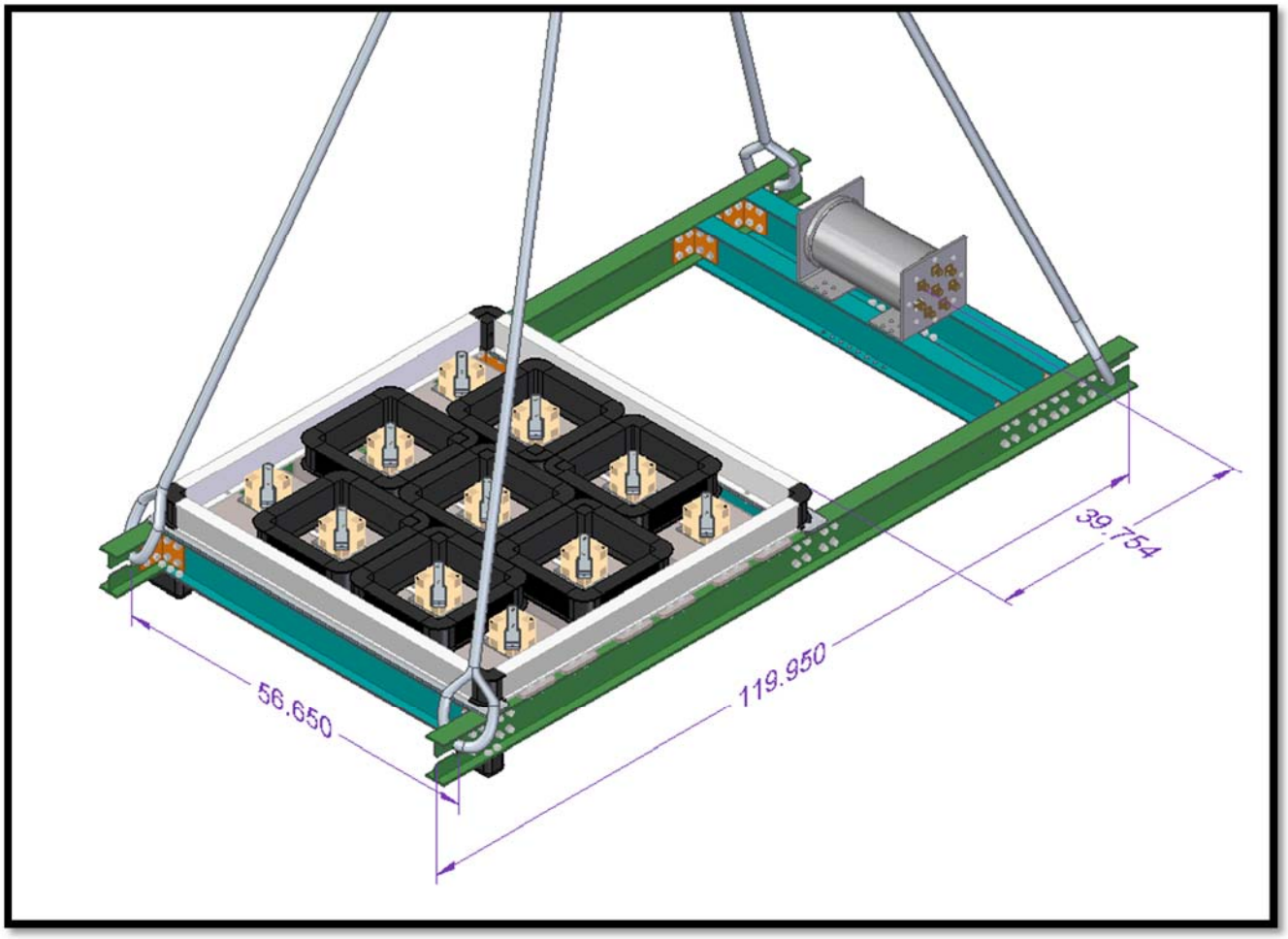

Figure 8 – Proposed array with fixed electronics package (dimensions in inches)

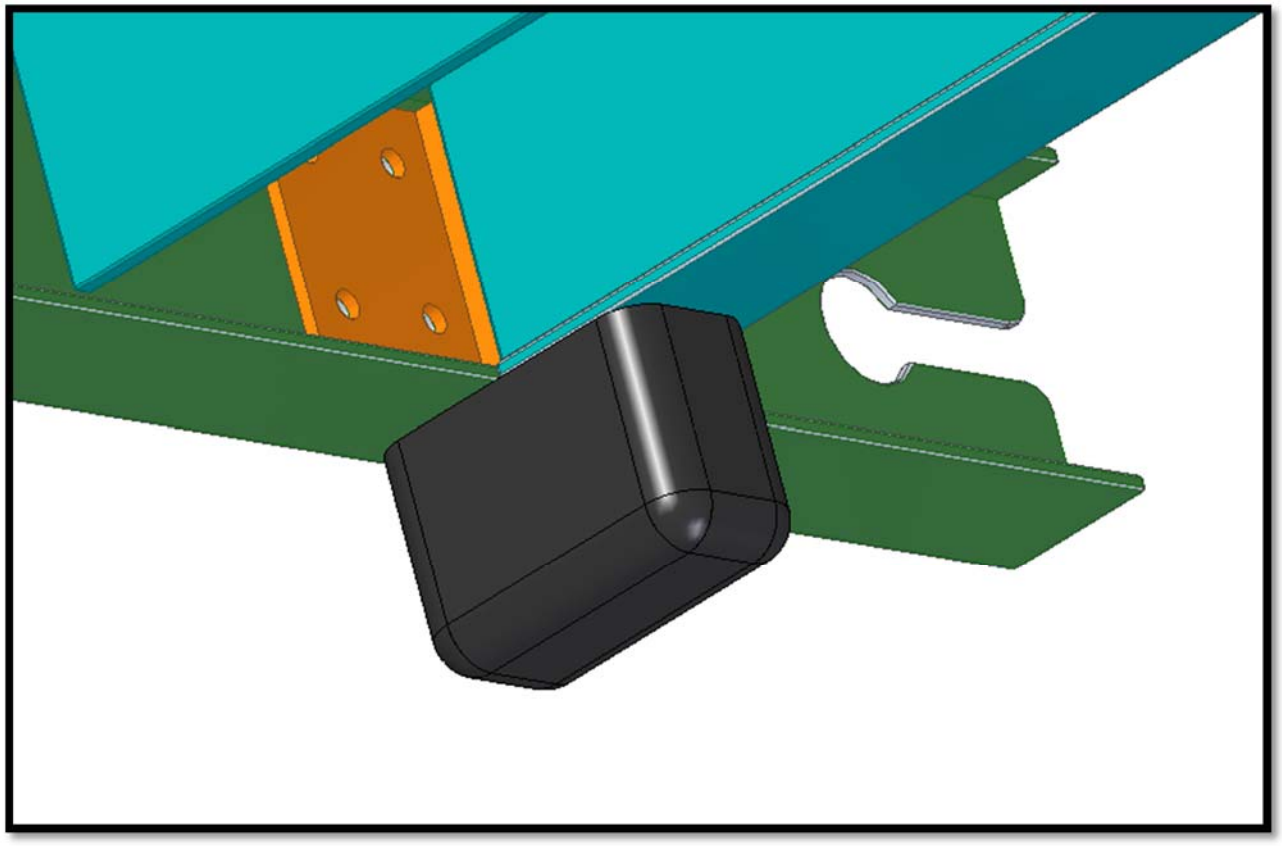

Figure 9– Rounded foot for elevation from sea floor.

Additional details of the array construction are shown on **Figure 10**, which illustrates how the receivers and transmitters will be fixed to the frame of the array. The pre-amplifiers on the receiver coils are highlighted in Yellow.

Figure 10 – Detail of coil assembly

In order to prevent the coil from draping over the array during measurements, as well as the potential for the deployment vessel to affect the measurement floats along the cable, a buoy will be used at the surface so that the cable remains suspended above the array. The size and buoyancy of the floats will be determined so the cable and floats combined are slightly positively buoyant just above the array. The buoy on the surface will allow the deployment vessel to offset from the array during the measurement. **Figure 11** shows a preliminary sketch of the proposed solution.

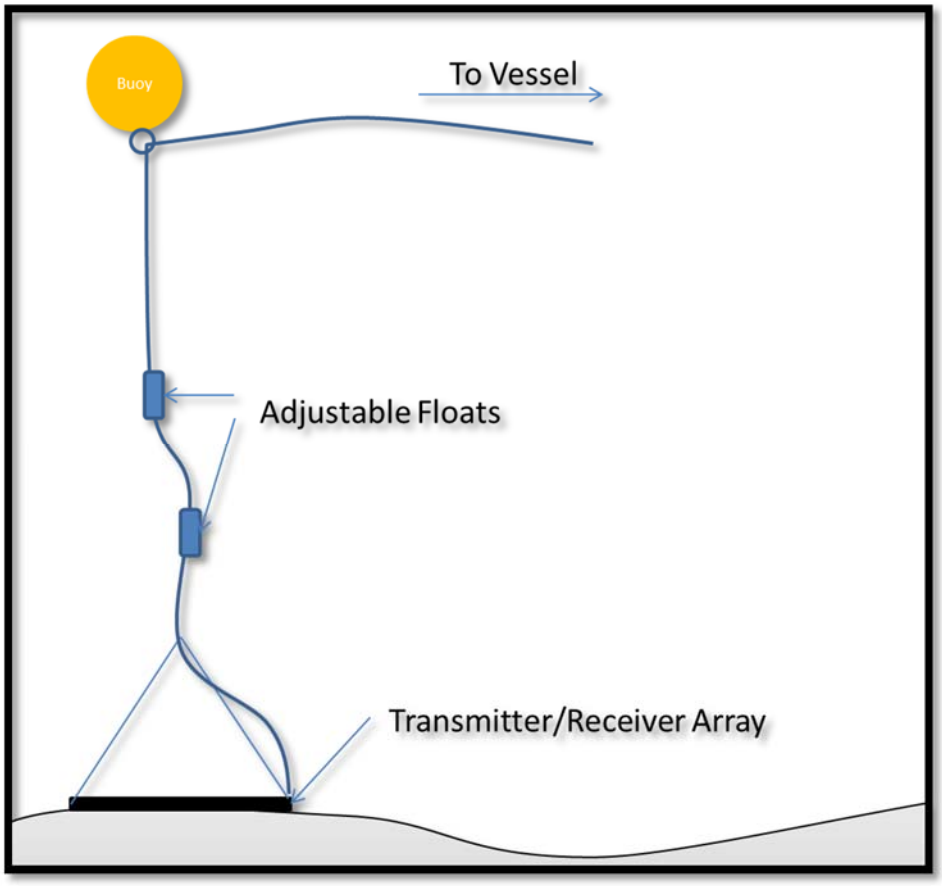

Figure 11 - Proposed cable, float and buoy design

Summary and Path Forward

The preliminary design of our proposed Underwater Advanced Time-Domain Electromagnetic System meant for shallow water use when characterizing sub-bottom metallic items in static mode is complete and the design meets the design goals of the system.

The next phase of the project, upon approval by ESTCP, is construction of an array using a single transmitter and receiver and testing the array with and without a known metal object suspended below the array. The test will provide information regarding:

1) The ability of all elements of the system to provide sufficient waterproofing to the desired depths.
2) The validity of the modeling conducted in the design phase.

Page Intentionally Left Blank

APPENDIX D FRESHWATER SYSTEM PERFORMANCE REPORT

FINAL

System Performance Report Underwater Advanced Time-Domain Electromagnetic System MR-201313

Prepared for

Environmental Security Technology Certification Program (ESTCP)

March 2017

ch2m:
2411 Dulles Corner Park
Suite 500
Herndon, Virginia 20171

Contents

Section **Page**

Figures

Figures (Cont.)

Tables

Acknowledgments

The CH2M project team for the underwater testing at the Naval Surface Warfare Center Panama City Division (NSWC-PCD) included the following Key Personnel who all played an integral role.

Name	Affiliation	Responsibilities
Tamir Klaff	CH2M	Principal Investigator
Kelsey Dubois	Geometrics	Project Engineer
Nick Odlum	Geometrics	Application Geophysicist
John Nichols	Geometrics	Project Engineer
Tom Bell	Leidos	Data Analysis and Reporting
Bruce Barrow	Acorn SI	Data Analysis and Reporting
Ray Lim	NSWC PCD	Site Coordinator

CH2M would also like to thank NSWC-PCD staff Lisa Arrieta and Russ Malcolm and the dive support team, led by Steve Lowe, for their fantastic support during the field operation.

System Performance Report

Introduction

This document has been prepared under Environmental Security Technology Certification Program (ESTCP) Project MR-201313, titled Underwater Advanced Time-Domain Electromagnetic System, to present results of the system evaluation performed by CH2M HILL, Inc. (CH2M) at the Naval Surface Warfare Center (NSWC) Panama City Division's (PCD's) freshwater pond facility in October 2016. The intent of the testing was to perform a field evaluation of the system designed and constructed in the initial phases of the project.

Project Description

The overall objective of the project is to design, build and demonstrate an underwater advanced time-domain electromagnetic (TEM) system for cued classification of munitions in the underwater environment. The phased approach consists of initial design and modeling (Phase 1 –completed), engineering design and construction (Phase 2 –completed), underwater evaluation of the system (Phase 3 – described in this document), and an optional Phase 4 demonstration of the system at a field site.

Technology

The system designed and constructed under this project has been described in detail in prior documents, titled *Modeling for Underwater Advanced Time-Domain Electromagnetic System* (June, 2014), *Underwater Advanced Time-Domain Electromagnetic System Design* (July, 2015), and in the *Underwater Advanced Time-Domain Electromagnetic System Evaluation Plan* (October, 2016). A diagram of the system, as tested, is provided as **Figure 1**. A photograph of the system is provided as **Figure 2**.

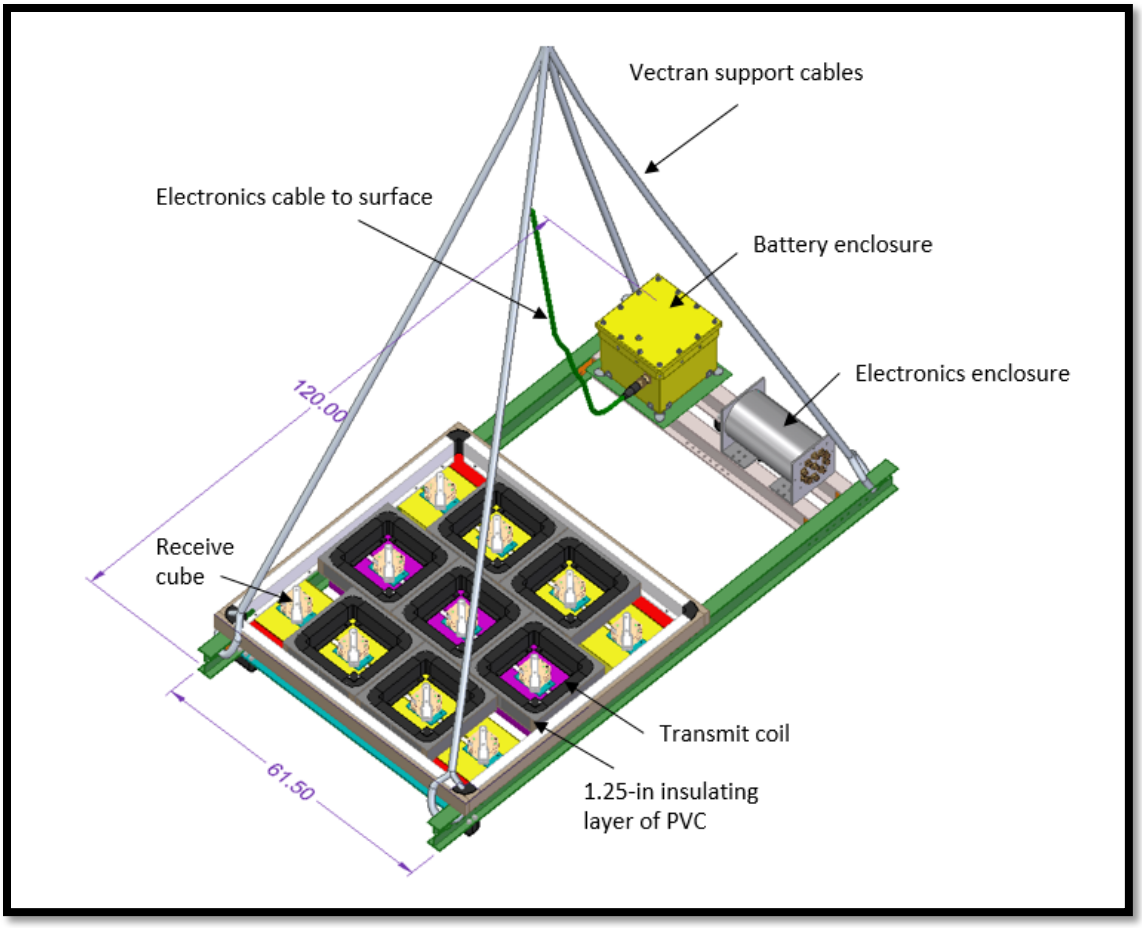

Figure 1. Underwater Advanced Time-Domain Electromagnetic System. Measurements are in inches.

Figure 2. Photograph of Underwater Advanced Time-Domain Electromagnetic System

Figure 3 presents a diagram identifying transmitter (Tx) and receiver (Rx) locations and nomenclature. The array consists of eleven 10 centimeter (cm) three-axis receive cubes, denoted by the cube identifier and an "r" indicating "receiver" (i.e. Ar-Kr), seven 40 cm square transmit coils, denoted by the cube identifier and a "t" indicating "transmitter" (i.e. At-Gt), and an outer 1.56 m square transmit coil (Ht). The resulting total number of data channels is 264. The raw sampling interval used for the evaluation was 0.004 ms and the recorded data were logarithmically averaged over 5% windows, resulting in 99 logarithmically spaced decay times ranging from 0.05 milliseconds (ms) to 8.124 ms. One hundred measurements were averaged for each recorded measurement.

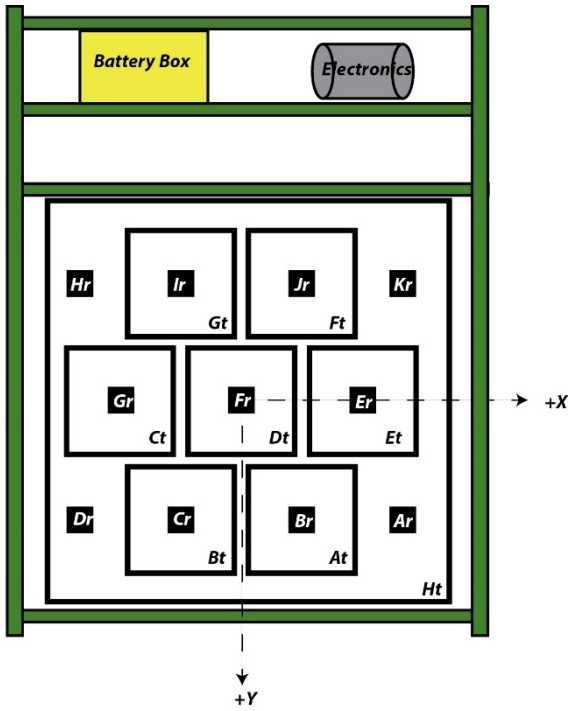

Figure 3. Transmitter and receiver locations and nomenclature.

Facility and Support

Dive operations, crane support, and general logistical support were provided by NSWCPCD. The NSWCPCD pond, shown by **Figure 4**, is 110 meter (m) wide by 80 m long and 13.5 m deep. A 30 m by 50 m bed of sand is located in the center of the pond. The pond was "shocked" on October 5, 2016 with 1800 pounds (lbs) of Calcium Hypochlorite followed by 12 cases of flocculent on October 7, 2016; however, by October 12 when the system was first introduced into the water the visibility was limited to a few feet and there was almost no visibility at times for the divers when the test bed sediment was disturbed by their activities.

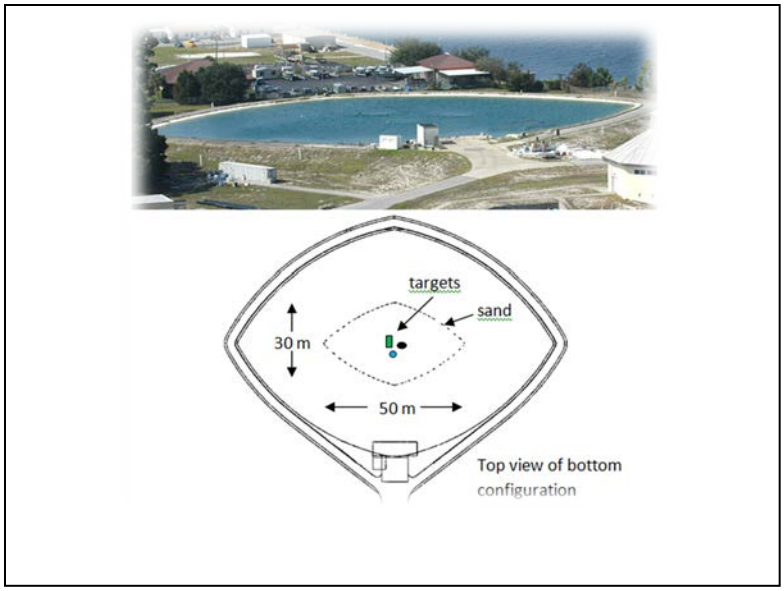

Figure 4. NSWCPCD's freshwater pond facility.

NSWCPCD provided a crane (see **Figure 5**), operator, and riggers for deployment of the system into and out of the pond, an inner-tube shallow water lift system with a 2500lb lift capacity crane (see **Figure 6**), and a team of divers to maneuver the inner-tube and the system.

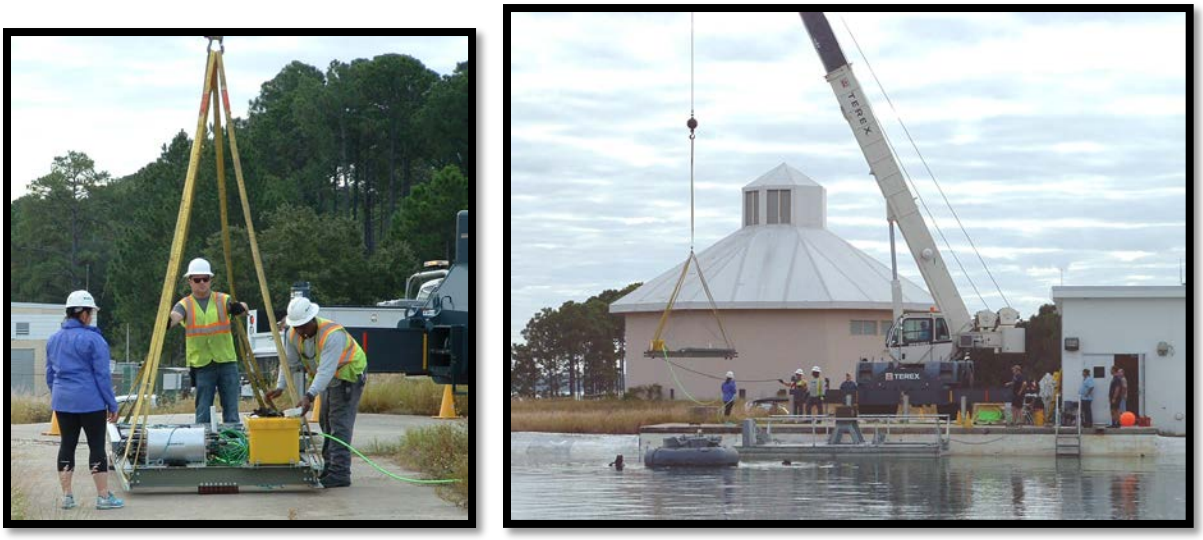

Figure 5. Crane provided by NSWCPCD for transfer of system from land into water.

Figure 6. Inner-tube shallow water lift system and dive team for maneuvering system from within the water.

System Setup and Testing

CH2M and its subcontractors, Geometrics Inc. (Geometrics) and Leidos, mobilized to NSWCPCD on October 10, 2016. System setup, initial sensor function tests, and establishment of an underwater test strip were performed on October 11, 2016. In-water tests on October 12 and 13 included background response measurements, board tests to check the accuracy of target locations and polarizabilities determined by inverting array data under controlled conditions, and buried target measurements.

Test Strip

A test strip, shown by **Figure 7**, was established by the dive team on October 11, 2016 along the north-south centerline of the pond using a rope and markers on the rope with objects buried at the marked locations beneath the surface of the sand. Objects were spaced at approximately 10 m increments to allow for enough space in between them for the collection of background measurements. The objects buried, photographs of which are shown in **Figure 8,** approximate depths, and their placement orientations consisted of:

1. Large industry standard object (ISO) (4-inch x 12-inch steel pipe[1]), approximately 1-2 foot depth, long axis approximately 30 degrees from the strip centerline
2. 105-millimeter projectile, approximately 1-2 foot depth, long axis oriented parallel to the strip centerline
3. 105-millimeter High Explosive Anti-Tank (HEAT) projectile, approximately 1-2 foot depth, long axis approximately 30 degrees from the strip centerline
4. 3-inch by 12-inch aluminum rod, approximately 6 inches depth, with its long axis approximately 30 degrees from the strip centerline
5. Medium ISO (2-inch x 8-inch steel pipe[2]), approximately 6 inches depth, with its long axis approximately 30 degrees from the strip centerline

[1] https://www.mcmaster.com/#44615k137/=155225y

[2] https://www.mcmaster.com/#44615k529/=15525a7

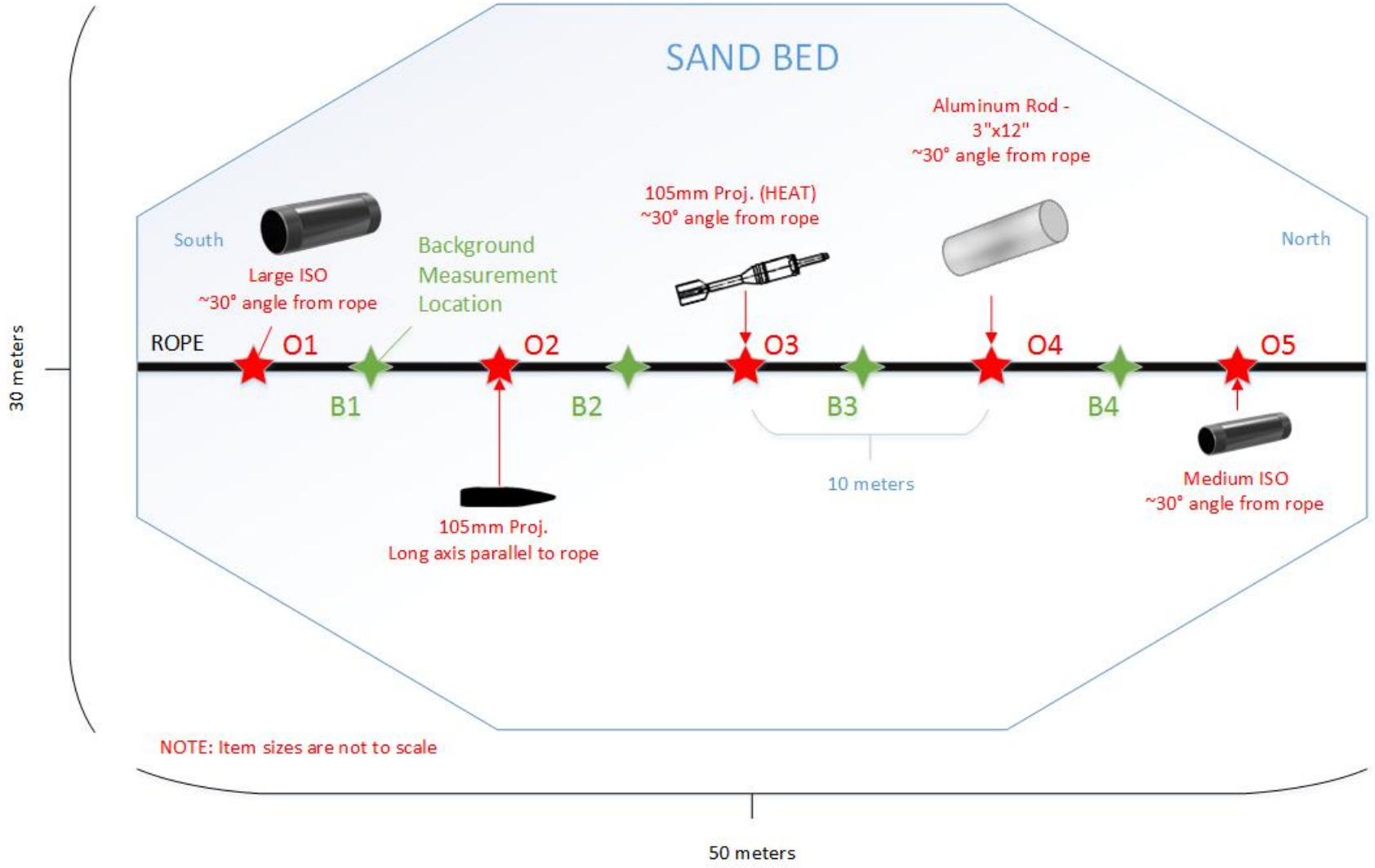

Figure 7. As-built diagram of test strip.

Object 1 (Large ISO)	Object 2 (105-mm Proj.)	Object 3 (105-mm Proj. HEAT)	Object 4 (Aluminum Rod)	Object 5 (Medium ISO)

Figure 8. Photographs of test objects prior to burial. (Intended burial depths and orientations relative to the centerline of the test strip were marked on the objects.)

Conductivity Measurements

After construction of the test strip, an Aqua Troll 200[3] was used to collect conductivity and other pond water parameter measurements directly above the burial locations of the objects, the results of which are shown in **Table 1**. The average values for actual conductivity and specific conductivity were 313 micro-siemens per centimeter (µS/cm) and 303 µS/cm, respectively. Typical seawater conductivity[4] is around 50,000 µS/cm and conductivity in most freshwater streams[5] is between 50 to 1500 µS/cm, thus the testing was performed in freshwater conditions.

[3] https://in-situ.com/products/water-level-monitoring/aqua-troll-200-data-logger/

[4] http://www.lenntech.com/applications/ultrapure/conductivity/water-conductivity.htm

[5] http://fosc.org/WQData/WQParameters.htm

Table 1. Pond water measurements

	OBJECT					
Parameter	**1**	**2**	**3**	**4**	**5**	**Average**
Temp (°C)	26.7	26.8	26.7	26.7	26.8	26.7
Pressure (PSI)	16.5	16.7	16.7	16.5	16.6	16.6
Depth (ft)	38	38.5	38.6	38.2	38.2	38.3
Actual Conductivity (µS/cm)	272.6	174.9	382.1	356.3	379.5	313.1
Specific Conductivity (µS/cm)	263.8	169.2	370.2	345.4	367.1	303.1
Resistivity (ohm-cm)	3668.7	5718.6	2617.1	2806.5	2635.1	3489.2
Salinity (PSU)	0.126	0.08	0.179	0.166	0.177	0.146
Total Dissolved Solids (ppt)	0.017	0.11	0.241	0.224	0.239	0.166
Water Density (g/cm^3)	0.997	0.997	0.997	0.997	0.997	0.997

NOTES
°C = degrees Celsius
PSI = pounds per square inch
ft = feet
µS/cm = microsiemen per centimeter
PSU = practical salinity unit
ppt = parts per thousand
g/cm^3 = grams per cubic centimeter

System Issue

Early in the data collection process it was determined that the signal was not being recorded properly for approximately 15% of the receiver cube channels from any particular measurement, but it was (for the most part) inconsistent which channels were affected. Troubleshooting in the field was not successful in identifying the cause of the issue, but the team determined that the data could still be used for classification. The electronics box was returned to Geometrics after completion of the pond testing and it was determined that the signal was being read in, but was extremely low and was not being recognized by the acquisition software. Further testing determined that the corrupt data were caused by incorrect delay values in the field-programmable gate array (FPGA) firmware that are affected by rising temperatures in the electronics canister, and this caused changes in the behavior of the serial lines on the analog-to-digital conversion hardware (specifically the FPGA Mezzanine Card [FMC] boards). The changes moved the converted digital signal partly out of the timing window during which the de-serialization hardware retrieves the data, resulting in mis-scaled or otherwise bad data. The host software controls the location of that hardware timing window by transmitting some FMC delays during startup and these delay values are determined empirically, during testing. Geometrics is in the process of determining the correct FMC delay values and their validity in varying thermal conditions, and developing tools to manage them during follow-up system work.

Sensor Function Test

A sensor function test was performed on the system after setup on October 11, 2016. The function test entailed measuring the response to a standard 4-inch diameter aluminum ball positioned above each of the receivers. **Figure 9** shows the aluminum ball above the array positioned over the A transmitter and B receiver (refer to **Figure 3** for transmitter and receiver nomenclature).

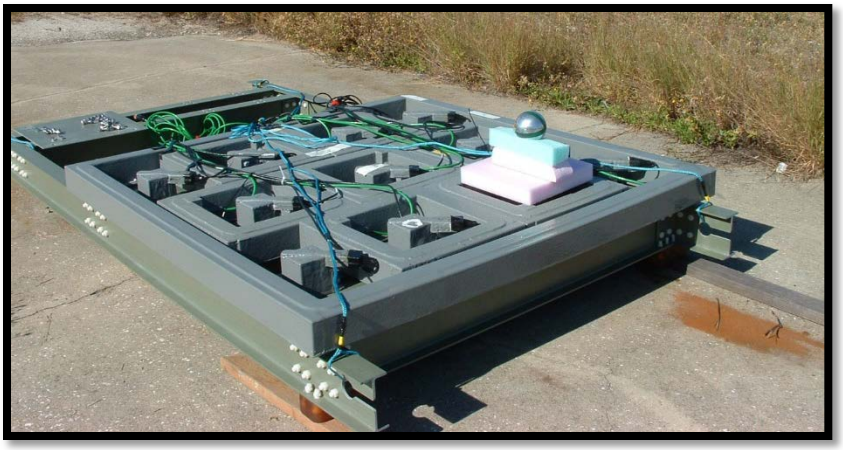

Figure 9. Aluminum ball over TxA/RxB during sensor function test.

Results for the sensor function test with the array on the deck (in air) on the first day are shown by **Figure 10**. Signal levels are in microTesla per Ampere-second (μT/As). Plot (a) (on the left) shows Z-axis responses for all of the monostatic transmit-receive TxRx pairs (the seven co-located transmitters and receivers). Negative signals are in red, positive in blue. All of the responses should be roughly identical. The odd blue curve is for the E receiver, which malfunctioned (see System Issue section above). The remaining six curves have a total spread in amplitude of ±2.8%. The middle plot (b) shows similar results for the ball over the corner receivers with the outer transmitter loop. By symmetry the responses should be identical. The observed spread was ±5.7%. The plot on the right (c) shows corresponding responses for the inner sets of receivers at the front and back of the array (B, C, I and J). Again, by symmetry they should have roughly identical responses. In this case the observed spread was ±2.9%. The sensor function test was not repeated with the array in the pond.

In-air and In-water Response Test

Identical in-air and in-water response measurements were made with the aluminum ball supported above the array on a PVC stand. The data were inverted using the UX-Analyze dipole fit algorithm and target locations calculated by inverting the in-air and in-water data were within 6 millimeters (mm) of each other. As shown by **Figure 11**, there was no discernable difference between the in-air and in-water polarizabilities; they were a near perfect match to each other based on the UX-Analyze classification algorithm. The PVC mounting broke after the first set of tests and the test was not repeated.

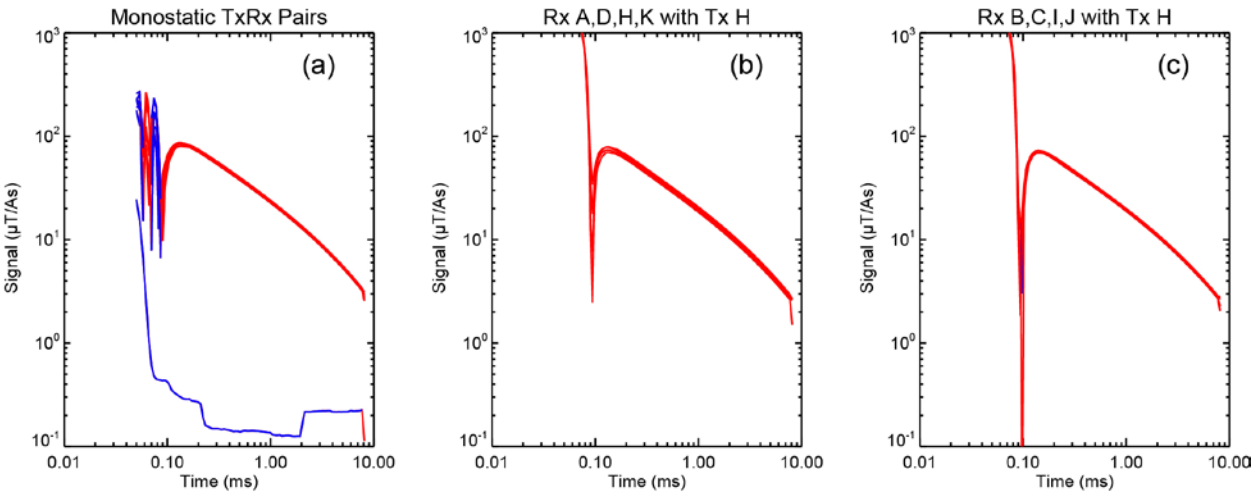

Figure 10. Sensor Function Test performance. (a) Measured Z-axis response to 4" aluminum ball for each monostatic TxRx pair. (b) Response for corner receivers with outer loop Tx. Response for inner front and back receivers with outer loop Tx.

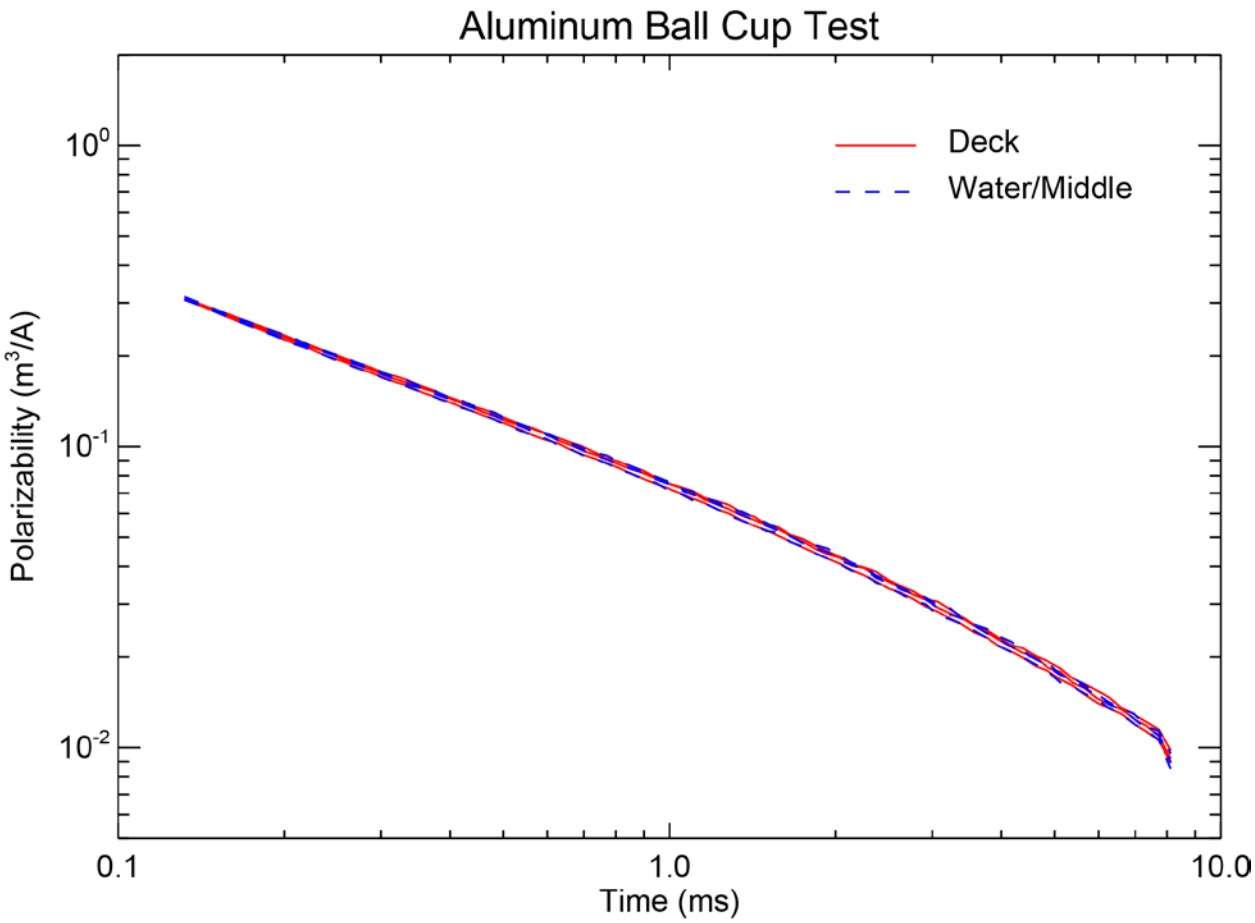

Figure 11. In-air (on deck) and in-water response measurements made with aluminum ball supported above the array on a PVC stand.

Background Response Test

Figure 12 shows the average background response for the monostatic TxC/RxG pair (Z-axis) at several locations. In the plot on the left (a) the array is in air on the deck. In the center plot (b) the array is on the bottom of the pond at background location B1 (see **Figure 7**), and on the right (**Figure 12c**) the array is in the pond at mid-depth (approximately 20 ft depth). Negative signals are plotted in red, positive in blue. In each plot the gray curves show the responses at the alternate locations for comparison. The monostatic background Z-axis responses are all similar, and are similar to background responses which have been observed with other TEM systems. Z-axis background responses with the outer loop transmitter (Ht) are similar to the monostatic background responses.

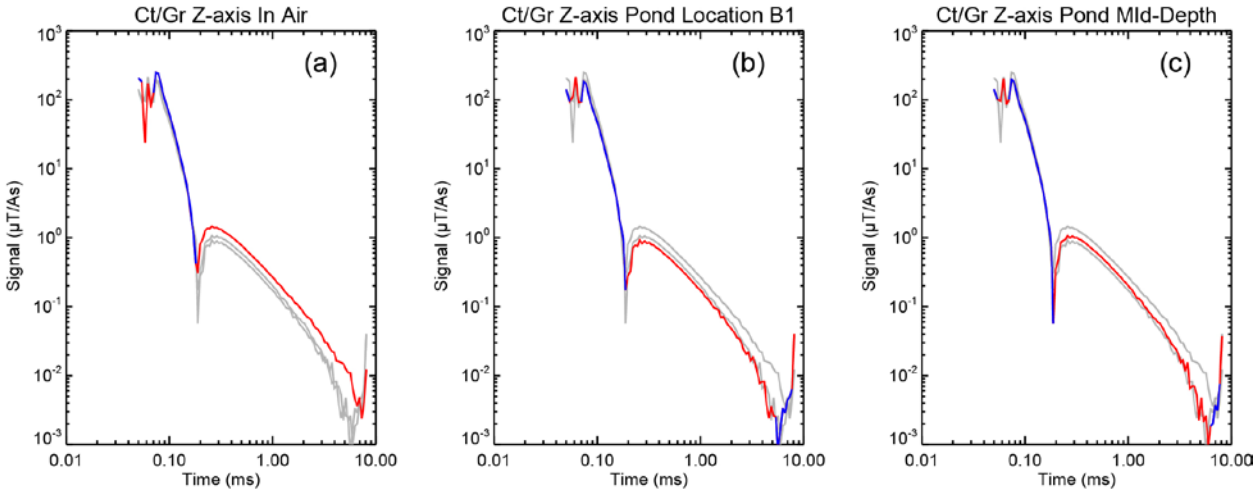

Figure 12. Average background response for monostatic TxC/RxG pair, Z-axis, at several locations. (a) Array in air on deck. (b) Array on the bottom of the pond at location B1. (c) Array in the pond at mid-depth. Negative signals in red, positive in blue. In each plot the gray curves show responses at the other locations for comparison.

Figure 13 compares the background responses for the different receiver axes (Z, Y and X for plots a, b and c respectively) using the monostatic TxC/RxG pair with the array in the pond at background location B1. As before, negative signals are plotted in red, positive in blue. In each plot the gray curves show the responses for the other receiver axes for comparison. Other Tx/Rx combinations (monostatic and bistatic) show similar X- and Y-axis responses. Bistatic Z-axis background responses are qualitatively different from monostatic Z axis responses. They are similar to the monostatic and bistatic X- and Y-axis responses.

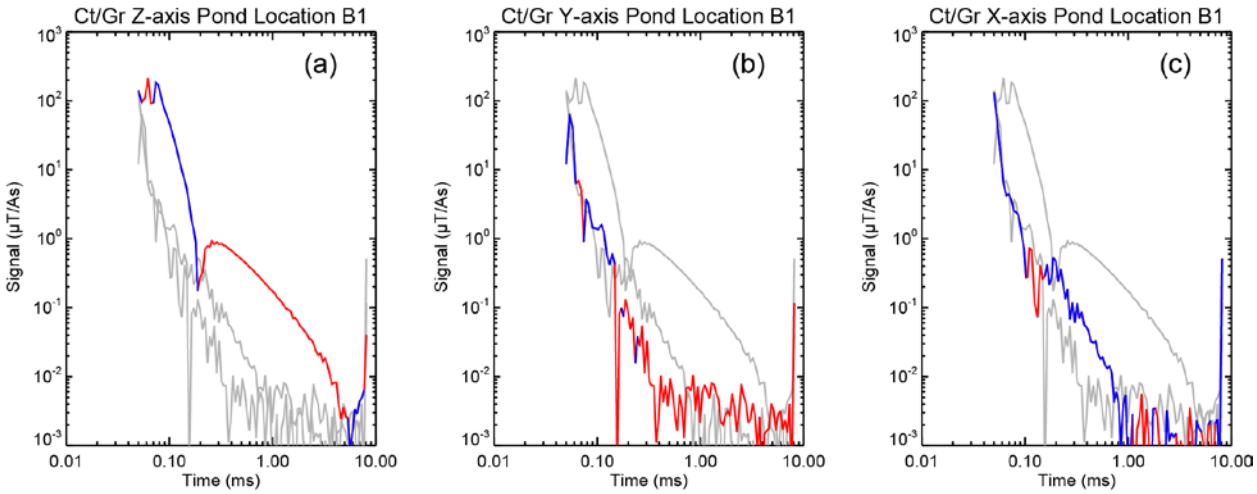

Figure 13. Average background response for monostatic TxC/RxG pair at background location B1. (a) Z-axis. (b) Y-axis. (c) X-axis. Negative signals in red, positive in blue. In each plot the gray curves show responses for the other axes for comparison.

Background response variability reflects the basic measurement noise for the array. **Figure 14** shows plots of the measurement-to-measurement background variability for the various transmit receive combinations with the array in the pond on the bottom at background location B1 (solid lines), suspended in the pond at mid depth (dashed lines) and in the air on deck beside the pond (chain dashed lines). The plots are arranged by row with monostatic combinations on the top, bistatic combinations in the middle and receivers paired with the outer transmit loop on the bottom, and by column with receiver Z-axis on the left, Y-axis in the middle and X-axis on the right. For each curve the root-mean-square (RMS) value was calculated for the measurement-to-measurement signal differences vs. decay time for each of the Tx/Rx pairs in the category. The plotted curve is the median of all of the RMS curves in the category (up to seven for monostatic combinations, seventy for bistatic combinations or eleven for outer loop combinations, depending on how many channels were operating properly). In **Figure 14** only measurements taken sequentially with the array stationary were used. The average time difference between measurements was 1½ minutes in all cases. The gray lines show the $t^{-1/2}$decay expected for logarithmically gated uncorrelated Gaussian noise:

$$\sigma_G(t) = \sigma_W \sqrt{2\delta t / Nwt}.$$

Here $\sigma_G(t)$ is the gated RMS variability as a function of decay time t, σ_W is the sensor white noise level, δt is the sampling interval (0.004 ms), N is the number of repeats in each measurement (100) and w is the gate width (5%). The factor of two accounts for differencing the lobes of the bipolar transmit waveform. In all cases beyond about 0.1 ms the gated white noise is apparent. The corresponding sensor white noise levels calculated from the gated noise curves are listed in **Table 2**.

Table 2. Sensor white noise levels (µT/As) (calculated from curves in Figure 14)

Location	Pond Bottom B1			Pond Mid Depth			Deck		
Axis	Z	Y	X	Z	Y	X	Z	Y	X
Monostatic	1.162	1.290	1.216	1.046	1.162	1.258	1.264	1.316	1.128
Bistatic	1.152	1.186	1.194	1.022	1.164	1.102	1.116	1.194	1.178
Outer Loop	1.948	1.790	2.030	1.772	1.770	1.868	1.906	1.880	2.098

The average white noise level was 1.18 µT/As with the 40 cm transmit coils and 1.92 µT/As with the large outer loop[6].

[6] It should be noted that the outer loop noise only differs because the raw receiver signal is normalized by transmit current. The raw receiver noise levels are pretty much equal.

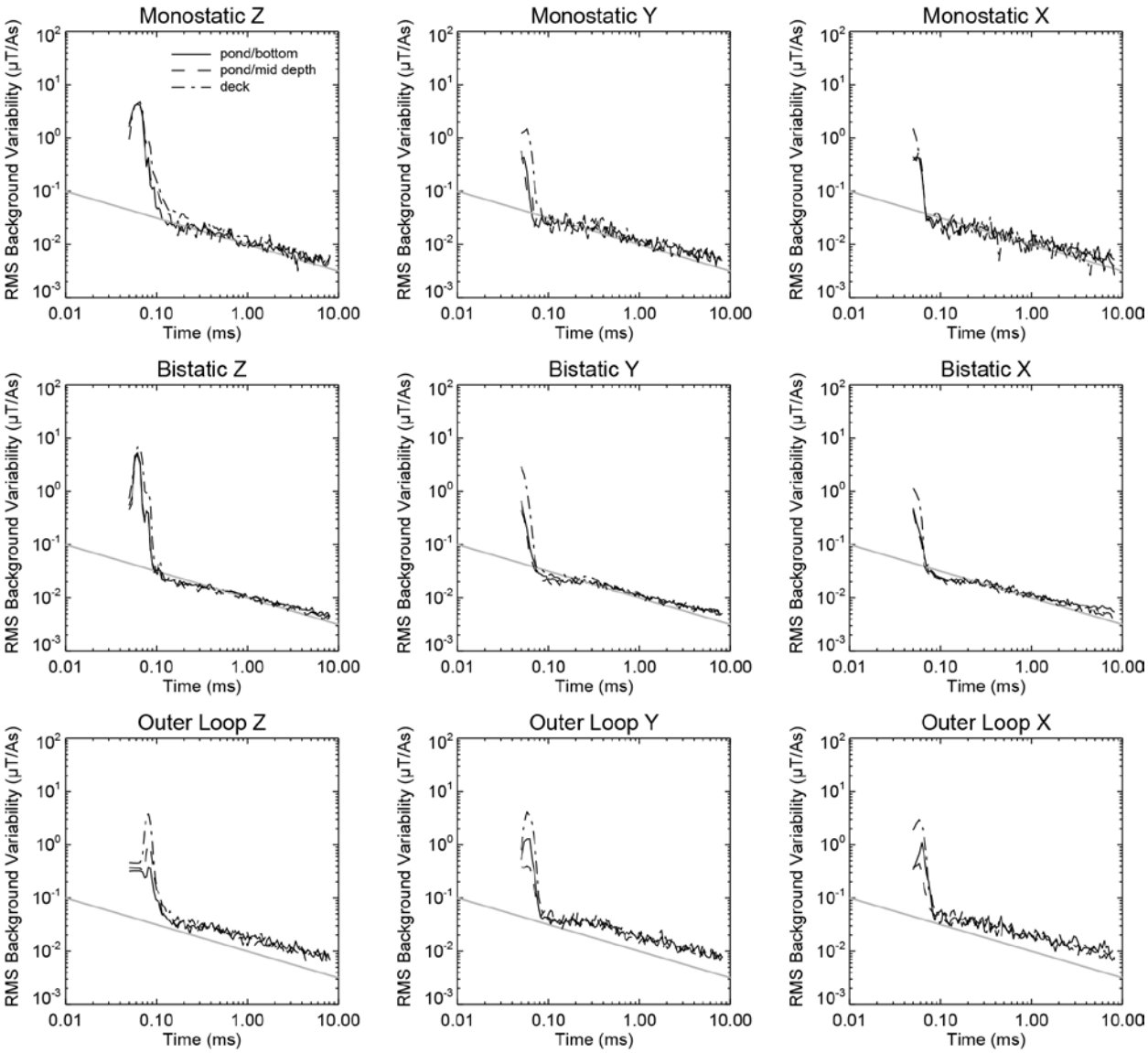

Figure 14. Median measurement-to-measurement background variability for various transmit/receive combinations. Top row, monostatic Tx/Rx pairs. Middle row, bistatic Tx/Rx pairs. Bottom row outer loop transmitter. Left column Z-axis receive, middle column Y-axis receive, right column X-axis receive. Solid curves are for successive measurements with the array on the bottom of the pond at background location B1. Dashed curves are for successive measurements with the array suspended in the pond at mid depth. Chain-dashed curves are for successive measurements with the array on deck beside the pond. The gray lines show the $t^{-1/2}$ decay expected for logarithmically gated white noise.

With longer time intervals and/or changes in the location of the array between measurements additional background variability is observed at early times, as illustrated in **Figure 15**. The layout of this figure is the same as **Figure 14**. Now the solid curves are for measurements as the array was moved from background locations B1 through B4 and back again. The average time interval between measurements was 37.7 minutes. The dashed curves are for measurements taken with the array suspended at mid depth with an average time interval between measurements of 14.9 minutes. A similar effect for successive measurements (average time interval 1½ minutes) is apparent with the array suspended at mid depth and held in position with rope by the divers. The chain dashed curves are for the array on deck with an average time interval between measurements of 18.4 minutes. The gray lines are the same as in **Figure 14**.

.

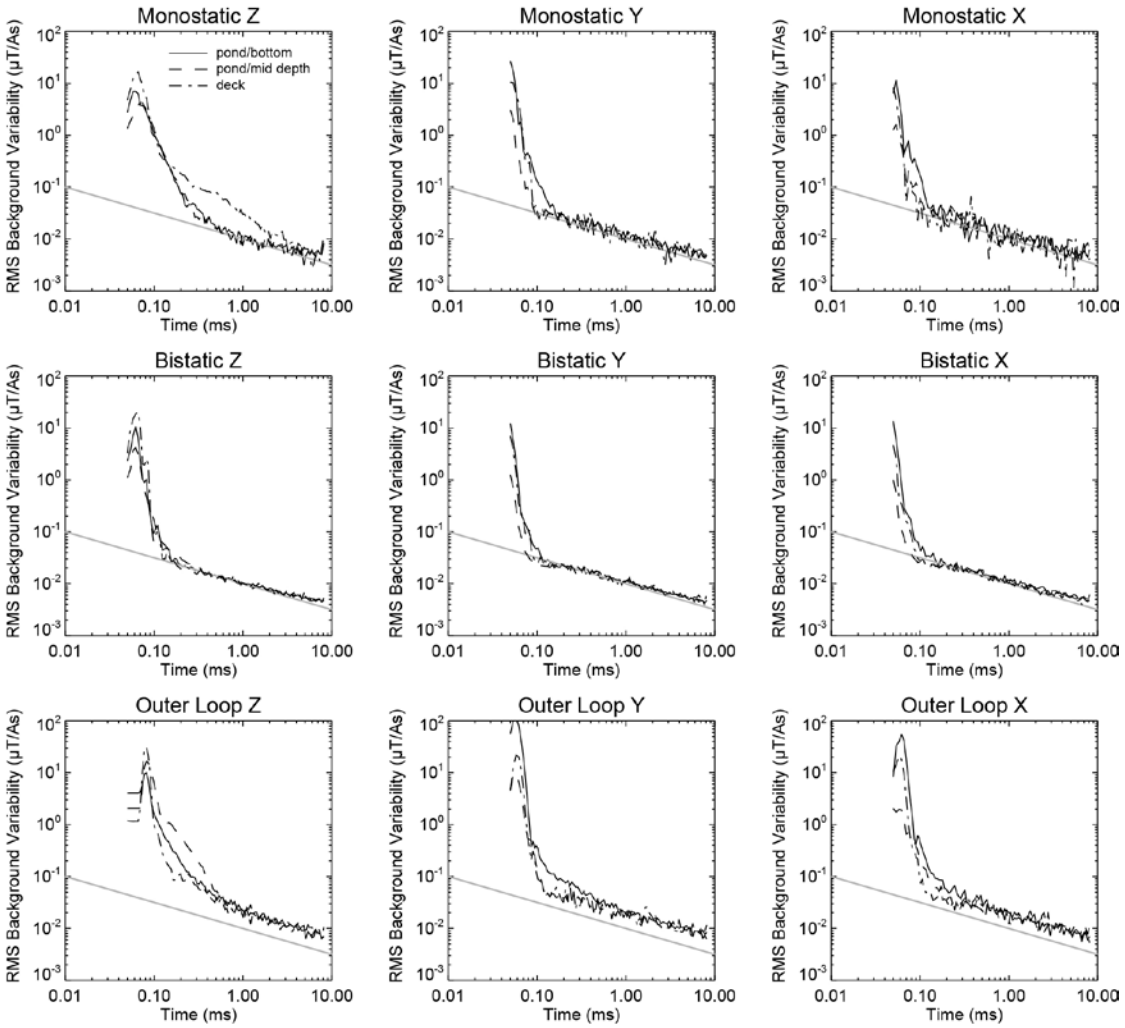

Figure 15. Background variability for various transmit/receive combinations for measurements spread out in time and/or space. Top row, monostatic Tx/Rx pairs. Middle row, bistatic Tx/Rx pairs. Bottom row outer loop transmitter. Left column Z-axis receive, middle column Y-axis receive, right column X-axis receive. Solid curves are for measurements with the array on the bottom of the pond at different background locations. Dashed curves are for measurements with the array suspended in the pond at mid depth with an average time between measurements of fifteen minutes. Chain-dashed curves are for measurements with the array on deck beside the pond with an average time between measurements of eighteen minutes. The gray lines show the $t^{-1/2}$ decay expected for logarithmically gated white noise.

Board Tests

The board tests were intended to check the accuracy of target locations and polarizabilities determined by inverting array data under controlled conditions. The basic UX-Analyze dipole inversion algorithm was used to fit the data. Malfunctioning data channels were not included and the first 18 time gates (t < 0.132 ms) were not used. The photograph on the left in **Figure 16** shows the test board mounted above the array. The board is a section of 6-inch I-beam with six sets of notches cut into the board for the targets. Medium and large ISO targets are shown resting in the notches. The drawing on the right shows dimensions of the board and its location relative to the array. The top of the test board was nominally 39.3 cm above the center of the array.

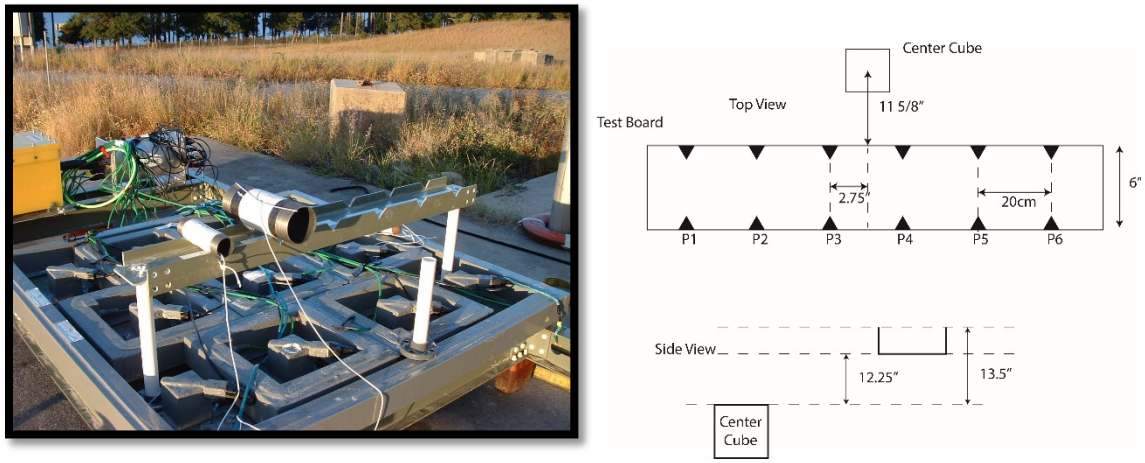

Figure 16. Left: Test board mounted above array, with medium and large ISO targets. Right: Drawing showing test board dimensions and location relative to array.

The board test was conducted with the array suspended at mid-depth (approximately 20 ft) in the pond. Three targets were tested: a medium ISO, a large ISO and a solid steel ellipsoid 6⅔ cm in diameter and 20 cm long. Each target was measured at each of the six notched locations on the board. The basic test procedure was to take a background measurement, measure the target at locations P1 through P3, then take another background followed by target measurements at locations P4 through P6, then a final background.
Figure 17 shows the board test results for the ellipsoid in the top row, the large ISO in the middle row and the medium ISO in the bottom row. The diagrams on the left compare dipole fit locations (◊) with nominal target locations (X). The diagrams in the middle compare dipole fit height above the center of the array with nominal target locations. The solid line is the top of the board and the dashed line shows the nominal distance to the center of the target resting on the board. The plots on the right compare calculated polarizabilities (solid curves) with library polarizabilities from ESTCP project MR-201424[7] for the large and medium ISO targets (dashed curves). The ellipsoid is not in the library.

[7] https://www.serdp-estcp.org/Program-Areas/Munitions-Response/Land/Enabling-Technologies/MR-201424

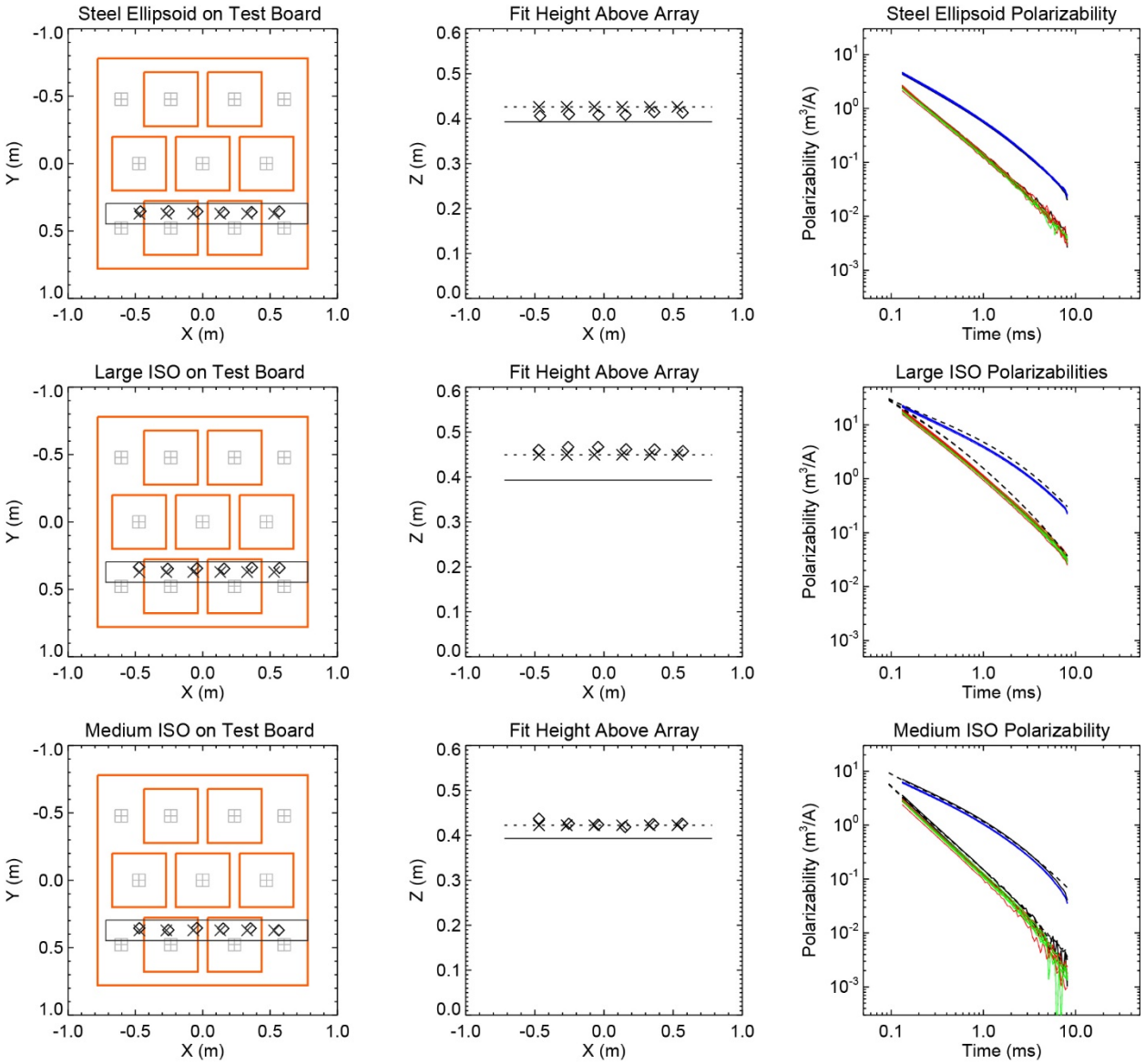

Figure 17. Board test results for the 6⅔ cm x 20 cm steel ellipsoid (top row), the large ISO (middle row) and the medium ISO (bottom row). The diagrams on the left compare dipole fit locations (◊) with nominal target locations (X). The diagrams in the middle compare dipole fit height above the center of the array with nominal target locations. The plots on the right compare calculated polarizabilities (solid curves) with library polarizabilities for the targets (dashed curves). The ellipsoid is not in the library.

Table 3 summarizes the results of the board tests. The dipole fit quality as determined by fit coherence (coh = squared correlation between data and dipole fit) was very good. Fit locations were generally within a few cm of the nominal target locations (Δxy, Δz). The ellipsoid dipole fit Z-locations are offset down a bit from the nominal Z-locations because the ellipsoid sits lower in the notches on the board than the ISOs. Classification metrics for matching to the library polarizabilities using the UX-Analyze classification algorithm are tabulated in the "library match" column. In all cases the polarizabilities determined by inverting the test board data are good matches to the library polarizabilities.

Table 3. Dipole fit parameters for targets on test board.

pos on board	Steel Ellipsoid				Large ISO				Medium ISO			
	Δxy (cm)	Δz (cm)	coh	library match	Δxy (cm)	Δz (cm)	coh	library match	Δxy (cm)	Δz (cm)	coh	library match
P1	1.9	-2.0	0.997	-	3.7	1.1	0.998	0.985	1.7	1.5	0.993	0.979
P2	2.6	-1.6	0.997	-	2.7	1.7	0.998	0.981	1.5	0.4	0.998	0.971
P2	3.4	-1.8	0.996	-	3.9	1.8	0.997	0.980	3.2	0.1	0.996	0.962
P4	2.7	-1.8	0.997	-	3.0	1.2	0.997	0.956	2.7	-0.4	0.998	0.932
P5	3.5	-1.2	0.997	-	4.9	1.2	0.998	0.981	3.0	0.3	0.987	0.987
P6	4.2	-1.3	0.997	-	5.1	0.8	0.998	0.984	3.4	0.4	0.956	0.956

Buried Target Measurements

As described previously, five targets were buried in the sand at the bottom of the pond and their locations are shown by **Figure 7**. Positions O1-O5 are target locations (large ISO, 105mm projectile, 105mm HEAT round, 4-inch x 12-inch aluminum rod, medium ISO) and B1-B4 are background locations where no objects were placed. During the first round of cued target measurements the array had 3-inch feet on it and it was positioned at each target location and moved[8] around over the nominal target locations for six different measurements (see **Table 4**). Background measurements were taken between each of the six-measurement target sequences at each of the five target locations.

For the second series of buried target measurements the 3-inch feet were switched out for 6-inch feet and three measurements (see **Table 4**) were subsequently performed at each target location with the array shifted slightly between measurements. The data were inverted using the UX-Analyze dipole fit algorithm. Malfunctioning data channels were not included, and the first 18 time gates ($t < 0.132$ ms) were not used. Several of the measurements on the large ISO required two-dipole fits, presumably because there were some metallic objects within the sand bed remaining from other operations conducted in the pond. The calculated polarizabilities were compared with polarizabilities from the ESTCP project MR-201424 library using the UX-Analyze classification algorithm and the results are summarized in **Table 4**. Anomalous early time signal behavior made it impossible to get good fits for the aluminum rod using single or multi-dipole models. This appears to be a problem with background removal rather than anomalous target signal content. Good fits were obtained using only late time ($t \geq 0.694$ ms) data. Observed signal variation with the aluminum rod relative to the apparent target locations based on late time data is not consistent with signal contributions from anomalous sources such as the electric field (current channeling) effects observed with aluminum targets in salt water in SERDP project MR-2409[9].

For the most part the measurements produced good fit quality and polarizabilities which were good matches to the library polarizabilities. The true target locations relative to the array are unknown; however, the board tests, discussed in the previous section, indicate an expected match of fit locations to within a few cm of the true target locations. To the extent that the fit locations reflect the actual target location, it appears that most of the time the array was positioned reasonably well over the target. With decent fit quality poor library matches typically occurred for targets outside the array footprint, as illustrated by **Figure 18**. The target locations in which the fit quality was okay but the match to the corresponding library item was less than 0.9, are circled on the figure. One of the medium ISO measurements (O5-6-1) did not converge to an acceptable fit using one or two dipole fit models and the library match failed; visual inspection of the data suggests that the array was not actually over the target and this is a bad

[8] The intent of moving the array between measurements was to compare classification with the object in various locations under the footprint of the array. The initial objective was to perform measurements in various locations within a single quadrant of the array but limited visibility in the pond resulted in a challenging environment within which the divers had difficulty precisely positioning the system.

[9] https://www.serdp-estcp.org/Program-Areas/Munitions-Response/Underwater-Environments/MR-2409

measurement. This measurement is represented by the red triangle at the center of the plot. Only two measurements (O1-3-1, O1-3-2) which fit to locations well outside the array footprint (near X = -0.4, Y = -1.2) had good (> 0.9) library matches. They are both measurements on the large ISO taken during the first sequence.

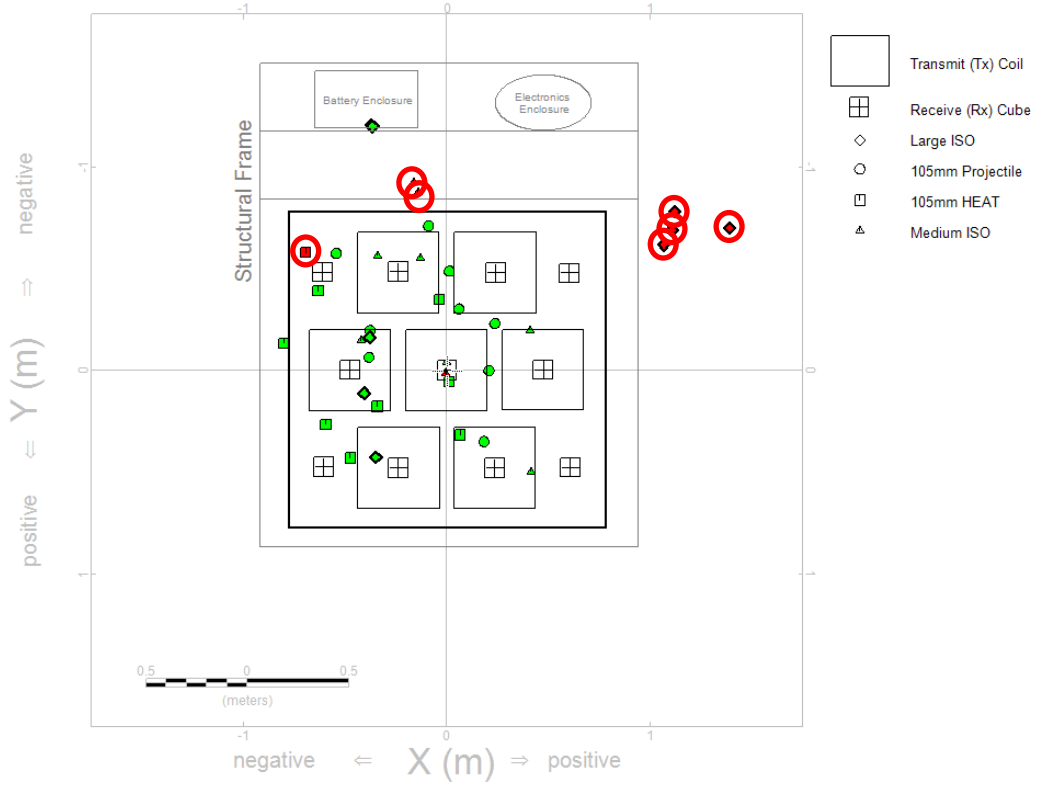

Figure 18. Buried target fit locations for ISOs and inert munitions. Green locations indicate >0.9 library match and red indicate <0.9. Circled locations indicate where the fit quality was good (>0.5) but the match to the corresponding library item was <0.9.

Table 4. Cued target fit parameters.

		Measurement with 3-inch feet						Measurement with 6-inch feet		
Large ISO (O1)	***Measurement ID:***	**O1-3-1**	**O1-3-2**	**O1-3-3**	**O1-3-4**	**O1-3-5**	**O1-3-6**	**O1-6-1**	**O1-6-2**	**O1-6-3**
	X (m)	-0.37	-0.37	*1.12*	*1.39*	*1.06*	*1.10*	-0.38	-0.41	-0.35
	Y (m)	*-1.21*	*-1.20*	-0.78	-0.70	-0.62	-0.69	-0.16	0.11	0.43
	Z (m)	0.39	0.38	0.30	0.12	0.33	0.29	0.45	0.44	0.41
	Fit Coherence	0.986	0.996	0.997	0.991	0.999	0.997	0.998	0.998	0.999
	Distance (m)	*1.26*	*1.26*	*1.36*	*1.56*	*1.23*	*1.30*	0.42	0.42	0.55
	Library Match	0.919	0.948	**0.861**	**0.630**	**0.866**	**0.816**	0.943	0.948	0.908
105mm Projectile (O2)	***Measurement ID:***	**O2-3-1**	**O2-3-2**	**O2-3-3**	**O2-3-4**	**O2-3-5**	**O2-3-6**	**O2-6-1**	**O2-6-2**	**O2-6-3**
	X (m)	-0.09	0.01	0.06	-0.39	-0.38	-0.55	0.24	0.21	0.18
	Y (m)	-0.71	-0.49	-0.30	-0.07	-0.20	-0.58	-0.23	0.00	0.35
	Z (m)	0.42	0.43	0.42	0.42	0.45	0.45	0.46	0.43	0.45
	Fit Coherence	0.999	0.996	0.989	0.993	0.991	0.998	0.992	0.992	0.997
	Distance (m)	0.72	0.49	0.31	0.39	0.43	0.79	0.33	0.21	0.39
	Library Match	0.957	0.969	0.993	0.952	0.970	0.964	0.997	0.943	0.971
105mm HEAT (O3)	***Measurement ID:***	**O3-3-1**	**O2-3-2**	**O2-3-3**	**O2-3-4**	**O2-3-5**	**O2-3-6**	**O2-6-1**	**O2-6-2**	**O2-6-3**
	X (m)	-0.60	-0.48	-0.34	*-0.80*	-0.63	-0.69	-0.04	0.01	0.07
	Y (m)	0.27	0.43	0.18	-0.13	-0.39	-0.58	-0.35	0.06	0.32
	Z (m)	0.41	0.39	0.43	0.42	0.44	0.46	0.51	0.48	0.50
	Fit Coherence	0.988	0.995	0.989	0.998	0.997	0.999	0.997	0.996	0.994
	Distance (m)	0.65	0.64	0.39	*0.81*	0.74	*0.90*	0.35	0.06	0.32
	Library Match	0.929	0.982	0.992	0.965	0.961	**0.697**	0.968	0.986	0.981
Aluminum Rod (O4)	***Measurement ID:***	**O4-3-1**	**O4-3-2**	**O4-3-3**	**O4-3-4**	**O4-3-5**	**O4-3-6**	**O4-6-1**	**O4-6-2**	**O4-6-3**
	X (m)	-0.02	0.08	0.29	-0.36	-0.53	-0.45	0.11	0.10	0.10
	Y (m)	-0.58	-0.30	0.16	0.08	0.17	-0.34	*-0.83*	-0.53	-0.10
	Z (m)	0.38	0.42	0.47	0.49	0.52	0.42	0.38	0.43	0.50
	Fit Coherence	0.997	0.995	0.990	0.997	0.996	0.995	0.991	0.997	0.994
	Distance (m)	0.58	0.31	0.33	0.36	0.55	0.56	*0.83*	0.54	0.14
	Library Match	-	-	-	-	-	-	-	-	-
Medium ISO (O5)	***Measurement ID:***	**O5-3-1**	**O5-3-2**	**O5-3-3**	**O5-3-4**	**O5-3-5**	**O5-3-6**	**O5-6-1**	**O5-6-2**	**O5-6-3**
	X (m)	-0.16	-0.13	0.00	-0.42	-0.34	-0.14	***[A]	0.41	0.42
	Y (m)	*-0.92*	-0.55	-0.04	-0.15	-0.57	*-0.88*	***	-0.20	0.50
	Z (m)	0.39	0.36	0.35	0.36	0.34	0.40	***	0.39	0.40
	Fit Coherence	0.990	0.999	0.996	0.998	0.980	0.653	***	0.988	0.992
	Distance (m)	*0.94*	0.57	0.04	0.45	0.66	*0.89*	***	0.45	0.65
	Library Match	**0.714**	0.968	0.917	0.938	0.957	**0.273**	***	0.936	0.937

Notes:

X, Y and distance values are relative to the center of the array and are *italicized and red* where greater than 0.8m.

Library match values below 0.9 are **bold and red**.

[A] Did not converge to acceptable fit. Review of the data suggests that this measurement was not collected over the object.

Performance Objectives

Results with respect to each of the performance objectives identified in the *Underwater Advanced Time-Domain Electromagnetic System Evaluation Plan* (CH2M, 2017) are discussed in the following sections and summarized in **Table 5**.

Objective: System is sufficiently waterproofed

The array remained underwater up to eight hours continuously and no leaks were discovered during field operations or indicated in the data collected.

Objective: Calibration method can be used both topside and underwater

Geometrics did not provide a baseline response plot in advance but a calibration test with an aluminum ball on a PVC pedestal was performed once on deck and once in the water. The pedestal broke after the initial measurements and could not be repeated, however, as shown by **Figure 11**, the results of the test showed an excellent match.

Objective: Classification can be achieved if item is anywhere within physical footprint of system

26 of 28 buried target measurements within the array footprint (initially considered as the entire 1.56 m x 1.56 m area within the outer coil) had a library classification match greater than 0.9. Visual inspection of the data for one of the two failures (medium ISO measurement O5-6-1) suggests that the target was not actually under the array. (An obvious lesson learned from this is that the individual performing the data collection must ensure that a response from a metallic object has been measured prior to moving to the next measurement location.) The remaining measurement that had a library classification match less than 0.9 was measurement O2-3-6 over the 105mm HEAT projectile, which had a match of 0.697. The projectile was within the footprint of the system but, as shown by the circled red square in **Figure 18**, it was at the outer edge (0.90m from the center) near a corner of the array. This result indicates that all objects will not necessarily be successfully classified if located within the footprint of the system if the footprint is considered the entire area within the outer coil. Until a revised footprint is determined, an alternative metric might be the distance of the object from the center of the array. **Figure 19** shows the relationship between the distance from the center of the array of each object (except the aluminum bar) when measured and its library match. Results indicate that all objects within 0.8m of the center of the array when measured were successfully classified (with the exception of medium ISO measurement O5-6-1 discussed earlier in this section.)

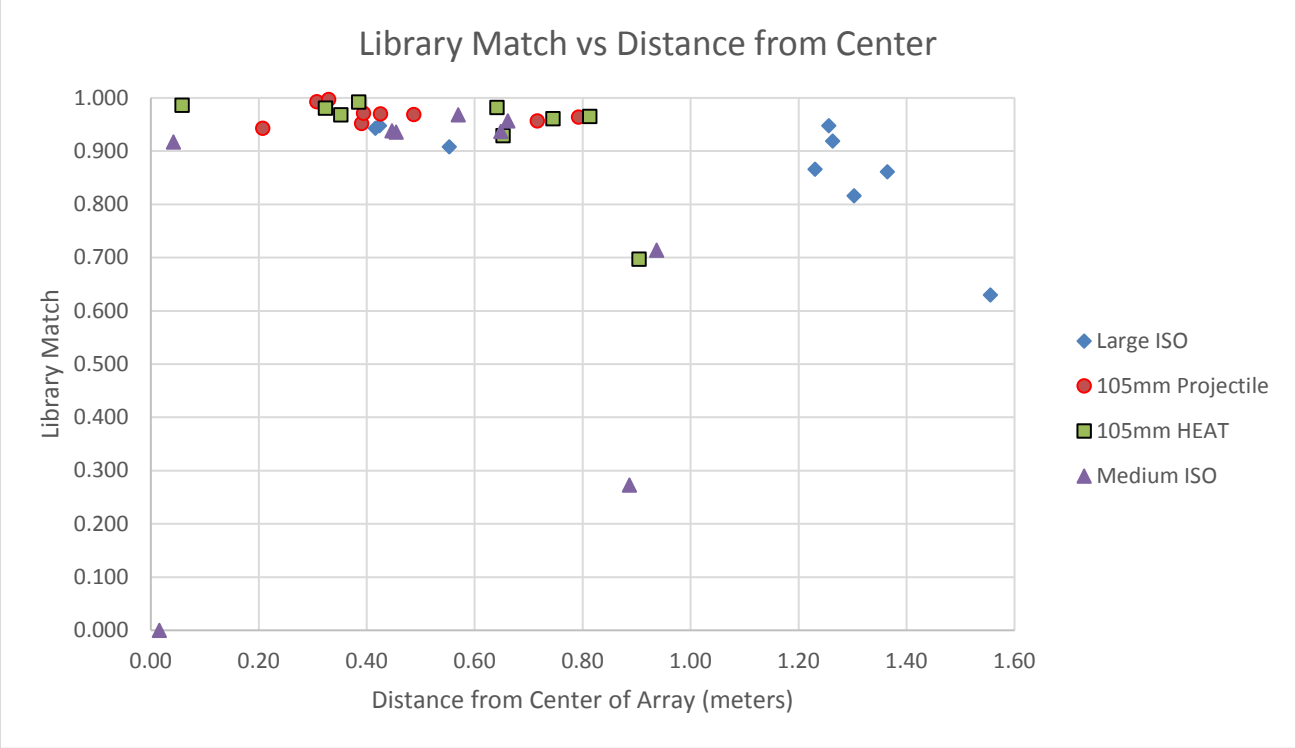

Figure 19. Graphs showing the relationship of the distance from the center of the array of each object during measurement to the library match.

Objective: Sensor response repeatability (cued surveys)

The intent of this objective was to record the response from a standard object at the same distance and orientation on a daily basis. As discussed previously, an aluminum ball on a PVC pedestal was to be used for this test but the pedestal broke after the initial day's measurements and was not repeated on the second day. However, multiple measurements over the same object at similar distances from the center of the array show good repeatability in terms of the library match. During the next phase of system evaluation, the sensor response repeatability will be further confirmed.

Objective: Sensor can be deployed using winch and donut approach

The array was easily deployed into the pond using the crane and maneuvered in the water using the inner-tube shallow water lift system (donut) and winch. The divers provided some feedback with respect to modifications, such as handles on the frame, holes in the base of the system for visibility to the bottom, cable management, and improvements to the attachment mechanism for the ropes used to deploy the system with the crane and winch.

Prior to the next deployment the team will attach handles, ensure that the harnesses cannot slip off of the system while being deployed, and a sleeve will be added around all cables to keep them together.

Objective: Sensor can be sufficiently maneuvered in underwater environment by divers such that the divers' safety is not compromised

Feedback from the divers indicated that there were no safety issues related to maneuvering the system underwater.

Objective: Sensor can be sufficiently maneuvered in underwater environment by divers such that the system can be placed satisfactorily on the desired cue location to collect classification data

The system was easily transported between measurement points in less than 10 minutes; however, as discussed previously, some improvements to the system would make it even easier to transport and effectively position the system over the intended target location. The divers had difficulty ensuring that the target location was under the array footprint in 9 out of the 45 measurements. While 3 of these were within 15 cm of the edge of the array, 6 were between 28 and 60 cm away; all 6 of these were measurements of the large ISO (O1-3-1 through O1-3-6), so clearly there was either an issue with movement of the rope marking the object location or some other factor specific to this set of measurements. (In other words, the inaccuracy may be related to the marking approach used as opposed to the divers' ability to maneuver and place the system.)

A Diver Proximity Test was performed near the end of the field operations to determine whether the procedure employed over the course of the testing of the divers moving 10-20 feet away from the system during measurements was necessary. For this test a measurement was collected at a background location with the divers away from the system and two separate measurements with a diver standing at the edge of the system where the battery and electronics boxes are located. **Figure 20** shows an overlay of the results, which indicates that the presence of the divers had little or no effect and that the time between measurements can be further reduced as the divers do not need to go as far away from the system as they did during the field evaluation.

During the next deployment the team will also employ additional markers and ropes on the sediment surface to assist the divers with appropriate reacquisition of the system for data measurements.

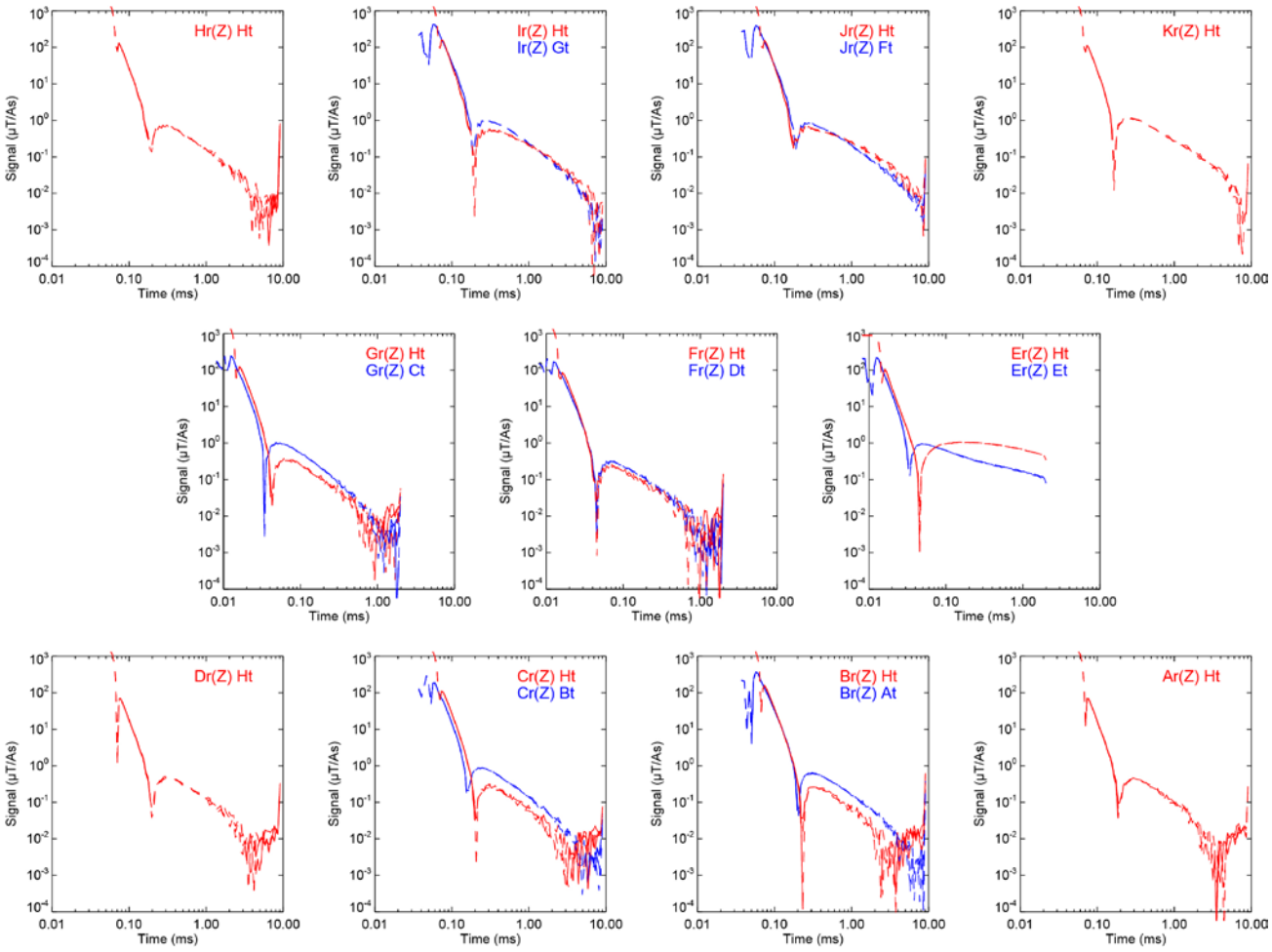

Figure 20. Overlay of monostatic Z-axis responses (blue) and Z-axis responses with outer (H) transmitter (red) for no diver and two measurements with a diver standing by the battery box. Solid portions are positive signal, dashed portions are when signal is negative.

Objective: Inversion results support classification

The Fit Coherence was greater than 0.8 for 43 of 45 cued measurements (see **Table 3**). One of the failures, medium ISO measurement O5-3-6, fit to a location 9 cm outside of the array footprint and 0.89 m from the center of the array. For the other failure, medium ISO measurement O5-6-1 discussed in previous sections, the dipole inversion failed and visual inspection of the data suggests that the array was not actually over the target.

Objective: Inversion result provides correct position

Fit locations were generally within a few cm of the nominal target locations for the board tests (see **Figure 9**, **Table 2**), with an average of 3.2 cm and a maximum of 5.1 cm. Exact locations relative to the array were not known for the buried target measurements.

Objective: Classification is valid

28 of 36 buried target measurements had a UX-Analyze classification metric greater than 0.9. All but one of the failures were outside of or near the edge of the array footprint. The other one was medium ISO measurement O5-6-1 (discussed in previous sections) which had a poor fit quality (0.264) and for which the library match failed; visual inspection of the data suggests that the array was not actually over the target.

Table 5. Performance Objectives and Results

Performance Objective	Metric	Data Required	Minimum Acceptable Criteria	Result
System is sufficiently waterproofed	No indications that water has leaked into system components	Data collected by system and visual observation	Data do not indicate water has entered system components.	No indications that water leaked into system components
Calibration method can be used both topside and underwater	Baseline response plots provided by Geometrics are similar to response in water and on land	Data collected by system and visual observation	Response plots of system are reasonably similar to baseline plots – qualitative measurement	Geometrics did not provide a baseline response plot in advance but a calibration test with an aluminum ball on a PVC pedestal was performed once on deck and once in the water. The pedestal broke after the initial measurements and could not be repeated, however, the results of the test showed an excellent match.
Classification can be achieved if item is anywhere within physical footprint of system	If classification is possible at a location under the physical footprint of the array it is possible at all other locations under the footprint as well	Response curve of metallic object placed at multiple locations under footprint, to include edges	If classification is possible at a single location under the physical footprint of the array it is possible at all other locations under the footprint as well	26 of 28 buried target measurements within the array footprint had a library classification match > 0.9. Visual inspection of the data for one of the 2 failures (medium ISO measurement O5-6-1) suggests that the target was not actually under the array. The remaining target (105mm HEAT measurement O3-3-6) that had a library classification match <0.9 had a match of 0.697. The projectile was within the footprint of the system but was at the outer edge (0.90m from the center) near a corner of the array. This result indicates that all objects will not necessarily be successfully classified if located within the footprint of the system. All objects within 0.8m of the center of the array when measured were successfully classified (with the exception of the erroneous medium ISO measurement and the aluminum bar.)
Sensor response repeatability (cued surveys)	Standard response to a known target in a known location	Amplitudes from daily testing over standard item at same distance and orientation	≤ 20% Root-Mean-Squared (RMS) variation in amplitude	An aluminum ball on a PVC pedestal was to be used for this test but the pedestal broke after the initial day's measurements and was not repeated on the second day. However, multiple measurements over the same object at similar distances from the center of the array show good repeatability in terms of the library match.

Table 5. Performance Objectives and Results

Performance Objective	Metric	Data Required	Minimum Acceptable Criteria	Result
Sensor can be deployed using winch and donut approach	System can be deployed using winch without compromising safety of test personnel, integrity of the system, or property damage	Visual observation of system and deployment components	Test personnel are not in danger of being injured and the system or property are not in danger of being damaged	The array was easily deployed into the pond using the crane and maneuvered in the water using the donut and winch.
Sensor can be sufficiently maneuvered in underwater environment by divers such that the divers' safety is not compromised	Divers are comfortable that their safety will not be compromised maneuvering the system	Verbal feedback from divers	Divers indicate they are comfortable that their safety is not compromised	Feedback from the divers indicated that there were no safety issues related to maneuvering the system underwater.
Sensor can be sufficiently maneuvered in underwater environment by divers such that the system can be placed satisfactorily on the desired cue location to collect classification data	Divers are able to effectively and efficiently maneuver the system to the desired cue location	Verbal feedback from divers Time to move system between cue locations	Divers indicate they are able to effectively and efficiently maneuver the system to the desired cue location. Time required to move system between cue locations is less than 10 minutes	The system was easily transported between measurement points in less than 10 minutes; however. The divers had difficulty ensuring that the target location was under the array footprint in 9 out of the 45 measurements. While 3 of these were within 15 cm of the edge of the array, 6 were between 28 and 60 cm away; all 6 of these were measurements of the large ISO (O1-3-1 through O1-3-6), so clearly there was either an issue with movement of the rope marking the object location or some other factor specific to this set of measurements. (In other words, the inaccuracy may be related to the marking approach used as opposed to the divers' ability to maneuver and place the system.)
Inversion results support classification	Modeled response match observed responses	Fit coherence from inversion	0.8 (using UX-Analyze fit coherence calculation)	The Fit Coherence was greater than 0.8 for 43 of 45 cued measurements. One of the failures, medium ISO measurement O5-3-6, fit to a location 9 cm outside of the array footprint and 0.89 m from the center of the array. For the other failure (medium ISO measurement O5-6-1) the dipole fit did not properly converge and visual inspection of the data suggests that the array was not actually over the target.

Table 5. Performance Objectives and Results				
Performance Objective	**Metric**	**Data Required**	**Minimum Acceptable Criteria**	**Result**
Inversion result provides correct position	Derived target positions match independent measured positions	Independent measurement of target in known position and inversion results	Offset < 40cm	Fit locations were generally within a few cm (average of 3.1cm, maximum of 5.1cm) of the nominal target locations for the board tests.
Classification is valid	Target polarizabilities for known items match library responses	Dipole inversion parameter values and polarizabilities for known, isolated targets (ISO's)	<25% difference between calculated and library reference polarizabilities UX-Analyze classification metric >0.9 (library match correlation)	28 of 36 buried target measurements had a classification metric >0.9. All but one of the failures were outside of or near the edge of the array footprint. The other one was medium ISO measurement O5-6-1 for which the dipole fit did not converge properly and for which the library match failed; visual inspection of the data suggests that the array was not actually over the target.

Summary and Path Forward

CH2M performed a system evaluation of the Underwater Advanced Time-Domain Electromagnetic System at NSWCPCD's freshwater pond facility in October 2016. With minor exceptions, the performance objectives were achieved and the system was demonstrated effective in collecting data used for the classification of munitions in a freshwater environment. The path forward, upon approval by ESTCP, is to prepare for and perform a saltwater evaluation of the full system. The following modifications will be made to the system prior to redeployment:

1. Handles will be attached to make the system more easily maneuverable for the divers
2. The attachment point for the ropes will be modified such that the ropes cannot slip off of the system while being deployed
3. A sleeve will be added around all cables to keep them together